Volume 10
Number 22
14 June 2022
Pages 8483–8882

Journal of Materials Chemistry C

Materials for optical, magnetic and electronic devices

rsc.li/materials-c

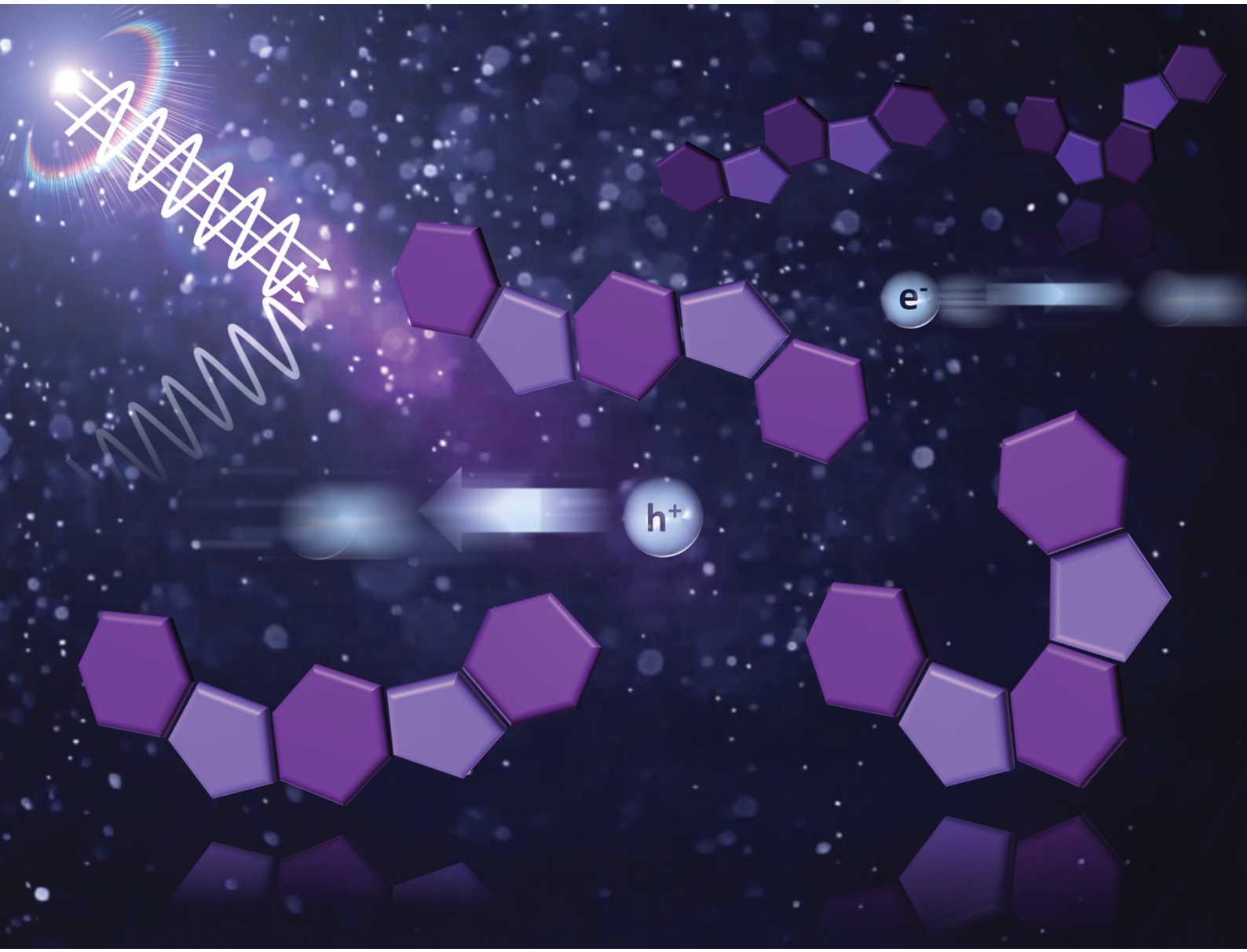

ISSN 2050-7526

ROYAL SOCIETY OF CHEMISTRY

REVIEW ARTICLE

Antonio Facchetti, Hakan Usta *et al.*
Indenofluorenes for organic optoelectronics: the dance of fused five- and six-membered rings enabling structural versatility

Journal of Materials Chemistry C

ROYAL SOCIETY OF CHEMISTRY

REVIEW

View Article Online
View Journal | View Issue

Cite this: J. Mater. Chem. C, 2022, 10, 8496

Indenofluorenes for organic optoelectronics: the dance of fused five- and six-membered rings enabling structural versatility

Ayse Can,[a] Antonio Facchetti *[bc] and Hakan Usta *[a]

Received 18th February 2022,
Accepted 28th April 2022

DOI: 10.1039/d2tc00684g

rsc.li/materials-c

Polycyclic π-conjugated hydrocarbons (PCHs), either unfunctionalized or structurally modified derivatives, have attracted tremendous interest in the past few decades as high-performance semiconductors for use in new generations of organic (opto)electronic devices. Among several PCHs realized to date, the 6-5-6-5-6 π-fused-ring backbone of indenofluorene (IF) stands out as a unique semiconducting architecture with great structural and property versatility affording six different regioisomers, diverse functionalization/substitution positions, π-conjugation/delocalization patterns, aromatic behaviors, and electronic structures. In this review, we summarize and analyze the historical and recent advances in the design and implementation of IF-based semiconductors in organic transistor and solar cell devices, as well as in understanding the chemical structure–molecular property–semiconductivity relationships. Following an introduction to the fascinating properties of an IF π-framework that distinguishes this core among PCHs, we present IF-based semiconductors and discuss their properties by classifying them into four main families (IF-diones, IF-DCVs/IF-TTFs, π-IFs, and (un)substituted DH-IFs) considering whether methylene or methine C-bridges are present and how these positions are functionalized or substituted. For each family, design and synthetic approaches, molecular properties, and transistor/solar cell device applicability and/or performance are reviewed and discussed. At the end, we conclude with a section discussing the challenges and opportunities for future progress of IF-based semiconductor materials and related (opto)electronic technologies.

1. Introduction

Elemental inorganic semiconductors undoubtedly represent one of the most prominent material families developed in the second half of the 20th century, which has led to unprecedented electronic, photovoltaic, and energy technologies. None of the major advancements realized in everyday life today would have been possible without the technologies enabled by these materials. By undertaking similar research-and-development directions, yet driven by the realization of unconventional technologies having mechanical flexibility, low material/fabrication costs, large area applicability, and efficient/inexpensive thin-film deposition (*e.g.*, printing), there has been tremendous interest in π-conjugated organic semiconductors.[1–10] Although early efforts made in investigating the electrical conductivity of organic compounds date back to the 1970s,[11] major breakthroughs have been achieved in the last two decades particularly regarding their design, synthesis, and integration into (opto)electronic devices.[1,3,12–15] The structural versatility of organic compounds has enabled the realization of organic semiconductors with diverse crystal packing,[16] and physicochemical, optoelectronic, and charge-transport properties,[17,18] enhancing the fundamental understanding[19–21] of organic semiconductor structure–property relationships and corresponding (opto)electronic device performances.[1,2,22–24] In particular, new-generations of (opto)electronic technologies such as circuits based on organic field-effect transistors (OFETs) and photovoltaic modules based on bulk-heterojunction organic solar cells (BHJ-OSCs) have greatly benefited from the charge transport characteristics and structural prosperity of several types of organic semiconducting small molecules and polymers.[1,25–27] In addition, dye-sensitized solar cells (DSSCs) have also emerged as an alternative photovoltaic device and mainly take advantage of the optical properties, reversible electrochemical doping, and electron-transfer characteristics, rather than thin-film charge transport ability, of organic π-conjugated semiconductors.[28]

[a] Department of Nanotechnology Engineering, Abdullah Gül University, Kayseri 38080, Turkey. E-mail: hakan.usta@agu.edu.tr
[b] Department of Chemistry and the Materials Research Center, Northwestern University, 2145 Sheridan Road, Evanston, IL, 60208-3113, USA. E-mail: a-facchetti@northwestern.edu
[c] Laboratory of Organic Electronics, Department of Science and Technology, Linköping University, SE-60174 Norrköping, Sweden

Regarding the structural versatility of materials for different (opto)electronic applications, while the most performing electron donors (hole-transporting semiconductors) in BHJ-OSCs have been low band gap donor–acceptor polymers,[29] efficient electron acceptors (electron-transporting semiconductors) are based on either fullerene or dicyanovinylene-functionalized (non-fullerene) π-architectures with fused hetero(aromatic) central cores.[27] Similarly, regarding hole-transporting (p-channel) OFETs, one of the best performing semiconductors relies on fused thienoacenes,[22,30] whereas functionalized rylenediimides enable the synthesis of excellent electron-transporting (n-channel) OFETs.[3,31]

Ayse Can

Ayse Can graduated with a bachelor's degree in chemistry from Bilkent University, Turkey, in 2016. She is currently pursuing a PhD degree at Abdullah Gül University under the supervision of Prof. Hakan Usta. Her research interests include theoretical design and synthetic development of novel molecular and polymeric π-conjugated materials for organic optoelectronic devices.

Among π-organic frameworks studied to date as organic semiconductors, polycyclic conjugated hydrocarbons (PCHs) have a long history going back to the first synthesis of artificial dyes in the late 19th century.[32] Specifically, aromatic PCHs could be considered as nanoscale cutout segments of graphene. Starting from aromatic PCH units such as those of *n*-acenes, a wide range of optoelectronic and charge-transport properties were tuned by incorporating heteroatoms, varying the number/position of ring atoms, and decorating the periphery with functional groups. For example, while, the benchmark acene pentacene has a very low solubility in common organic solvents and is prone to oxidative degradation, its triisopropylsilylethynyl-substituted derivative, TIPS-pentacene, could be processed from solution and shows much improved ambient chemical and charge transport stability when incorporated into OFETs.[33] Similarly, thienoacenes such as [1]benzothieno[3,2-*b*]benzothiophene (BTBT)[22] and dinaphtho[2,3-*b*:2′,3′-*f*]thieno[3,2-*b*]thiophene (DNTT)[34] show much lower highest occupied molecular orbital (HOMO) energies of −5.4 to −5.8 eV, as compared to acenes with the same number of fused rings ($E_{HOMO} > -5.0$ eV), greatly stabilizing charge transport in air. Among the PCHs realized to date, indenofluorene (IF) offers a unique 6-5-6-5-6 π-fused-ring architecture. Starting from this ring topology, five- and six-membered rings were arranged in different geometries affording six different regioisomeric backbones. These IF units have different π-conjugation/delocalization patterns (with 18, 20, or

Antonio Facchetti

Antonio Facchetti obtained his Laurea degree (cum laude) in chemistry and PhD in chemical sciences from the University of Milan (Italy). In 2002, he joined Northwestern University, where he is currently an Adjunct Professor of Chemistry. He is the Co-Founder and currently the Chief Technology Officer of Flexterra, Inc. He has authored over 550 research articles and 13 book chapters. He holds more than 120 patents. Dr Facchetti is a highly cited researcher in both Materials Science and Chemistry announced by Clarivate Analytics with an h-index of 109 (Web of Science). He has been elected as a Fellow of the American Association for the Advancement of Science (2012), Royal Society of Chemistry (2015), Materials Research Society (2013), ACS Polymeric Materials Science and Engineering (2016), National Academy of Inventors (2016), and the European Academy of Sciences (2021). He also received the ACS award for Creative Invention (2016) and the Natta gold medal of the Italian Chemical Society (2017). His research interests include organic/oxide semiconductors and dielectrics for thin-film transistors, conducting polymers, molecular electronics, organic second- and third-order nonlinear optical materials, and organic photovoltaics.

Hakan Usta

Hakan Usta obtained his PhD in Chemistry from Northwestern University under the supervision of Prof. Tobin J. Marks and Prof. Antonio Facchetti in 2008. He then joined Polyera Corporation (IL, USA), where he held Senior Research Scientist and Project Leader positions between 2008 and 2013. He then joined the faculty at Abdullah Gül University, where he is currently a full Professor in the Department of Nanotechnology Engineering. Dr Usta was the recipient of Young Investigator Awards from the Turkish Academy of Sciences (TÜBA) in 2015 and The Scientific and Technological Research Council of Turkey (TUBITAK) in 2020. Dr Usta has published more than 70 research articles, 3 book chapters, and holds 14 international patents on organic (opto)electronics. His current research interests include the development of novel π-systems, organic (opto)electronic materials and devices, micro-/nano-structured organic films, organic-SERS, and organic light-emitting-PUF applications.

22 π-electrons), different types of aromatic behaviors (*i.e.*, aromatic *vs.* antiaromatic) and ground state electronic structures (quinoidal/biradical)[35] leading to varied physicochemical–optical–electrochemical properties and device characteristics. The pictorial representations of five IF regioisomer scaffolds ([1,2-*a*], [2,1-*a*], [1,2-*b*], [2,1-*b*], and [2,1-*c*]) are shown in Fig. 1. Note that, to the best of our knowledge, a derivative based on the possible sixth regioisomer ([1,2-*c*]) has never been reported and we omitted it here. The structural arrangements of these 6-5-6-5-6 π-scaffolds could be seen as derived from two major structural combinations: (i) fusion of indene and fluorene units taking place between one of the fluorene benzene rings and indene five-membered ring, or (ii) annulation of *ortho*-, *meta*-, or *para*-terphenyl scaffolds by two bridge carbons in varied *anti*- or *syn*-arrangements. Quite different than most of the linear (hetero)acenes known in the literature, the presence of carbocyclic five-membered rings allows for efficient synthetic modifications and functionalization at these positions. Indenofluorenes show the following distinguished characteristics that make them quite attractive for (opto)electronics: (i) their synthesis relies on a bottom-up approach starting from the readily available (hetero)aromatic building blocks, and multi-gram scale intermediate compounds could be synthesized for structural screening; (ii) bridge carbons, in addition to central/peripheral aromatic carbons, offer excellent positions for functionalization/substitution in varied geometries to directly influence π-electronic structures and properties; (iii) the IF π-core is highly planar even when functionalized with sterically demanding substituents, thus preserving efficient intramolecular π-delocalization and promoting intermolecular π-interactions for efficient charge-transport; and (iv) bridge carbons could adopt sp^3 or sp^2 hybridizations to tune the aromatic characters and π-delocalization patterns.

The very first study of an indenofluorene compound could be traced back to the late nineteenth century, in which Gabriel *et al.* reported the synthesis of a dicarbonyl-functionalized [1,2-*a*] regioisomer.[36] After a silent period, several synthetic approaches to IF regioisomers were reported by several research groups from 1950s to 1970s,[37–40] however, with limited structural and optoelectronic characterization. Advances in structural and electrochemical/optical property characterization were reported by Gompper *et al.* in 1987,[41] Swager *et al.*[42] in 1994, and Scherf *et al.*[43] in 1996 using dicarbonyl-functionalized and fully-conjugated IF small molecules and polymers (*vide infra*, **IF-dione-1** and **IF-dione-2** in Fig. 3, and **π-IF-1**, **π-IF-2**, and **PIF** ↔ **PIF-Quinoid** in Fig. 18). Following these early studies and as a part of tremendous interest in organic semiconductors since the beginning of 2000s, IFs have embarked on an exciting journey in the field of organic (opto)electronics. Thus, the number of research articles investigating novel IF-based π-conjugated systems has increased exponentially in the last two decades. Although some of these studies do not investigate charge transport, our detailed literature analysis reveals that there are about 150 IF-based small molecules and polymers, all covered in this review, for which either transistor/solar cell device performance, or promising optoelectronic properties for use in these applications, is reported. Here, we note that realizing such a large number of semiconductor derivatives is purely the result of its 6-5-6-5-6 π-architecture enabling outstanding structural adaptability.

This review will provide an overview, including historical and recent approaches, on the design and development of IF-based organic semiconductors and their applications in organic transistors and photovoltaics. Considering that there are many review articles focusing on OFETs,[20,44] BHJ-OPVs,[27,29] and DSSCs,[45,46] we refer to them for details of the structures and operating principles of these devices. Here, IF semiconductors are presented and their properties are discussed by classifying them into four main families (Fig. 2) considering whether methylene (sp^3 hybridized) or methine (sp^2 hybridized) C-bridges are present and how these positions are functionalized/substituted. Specifically:

(1) IF-diones, where functionalization of the bridge carbon positions are carbonyl groups;

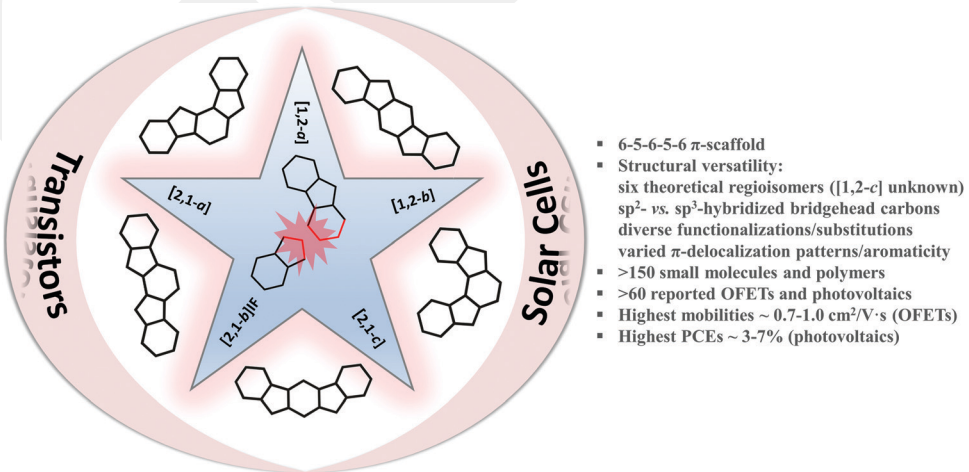

Fig. 1 Illustration of five ([1,2-*a*], [2,1-*a*], [1,2-*b*], [2,1-*b*], and [2,1-*c*]) indenofluorene (IF) regioisomeric π-scaffolds reported in the literature by fusion of one of the fluorene benzene rings and the indene five-membered rings (bonds are highlighted in red) and the key (opto)electronic properties of these semiconductors.

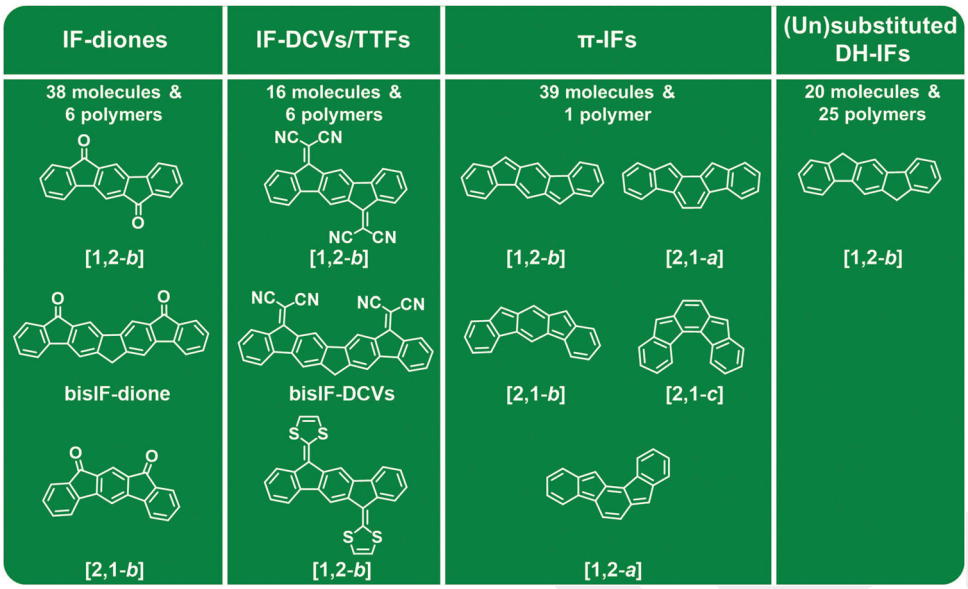

Fig. 2 Summary of the π-scaffolds of the IF-based semiconductor families divided into IF-dione, IF-DCVs/TTF, π-IF, and (un)substituted DH-IF families. These π-scaffolds are functionalized, substituted, and polymerized in different ways affording >150 semiconductors that are discussed in the Review.

(2) IF-DCVs/IF-TTFs, where the bridge carbon positions are dicyanovinylene or tetrathiafulvalene groups;

(3) Aromatic *vs.* anti-aromatic π-IFs, having sp^2 hybridized methine bridges for full π-conjugation and halogen/alkyl/aryl/ethynyl substitutions;

(4) (Un)substituted DH-IFs, having unsubstituted and substituted sp^3 hybridized methylene bridges.

In each of the sections where these families are reported, the most prominent IF regioisomers are discussed. At the end, we conclude with a section discussing challenges and opportunities for future progress of IF-based semiconductor materials and related (opto)electronic technologies.

2. Carbonyl functionalized indenofluorenes (IF-diones)

2.1. Brief introduction to IF-diones

The carbonyl (C═O) group is one of the most important electron withdrawing functionalities employed in the design of organic semiconductors, which provides a negative resonance effect (−*R*) to π-conjugated systems reducing the π-electron density.[47] It has been widely employed in IF π-scaffolds at the bridge methylene position resulting in numerous materials with lower π-electron density and frontier molecular orbital energy levels.[40,48] In this section, IF-based molecular structures functionalized with two bridge carbonyl units are named indenofluorenediones (IF-diones). Most of these IF-diones adopt highly coplanar conformations based on single-crystal structures and density functional theory (DFT) calculations. The structural and π-electronic effects of carbonyls at the molecular level are very crucial to realize favorable charge transport characteristics in thin-film (opto)electronic devices, especially in OFETs. To the best of our knowledge, IF-diones have never been studied in solar cells, and almost all of the IF-dione structures reported to date with reasonable OFET performance are based on the [1,2-*b*] regioisomeric form. The only example of a different IF-dione regioisomer is [2,1-*b*]IF-dione (**IF-dione-7**, Fig. 10), which is OFET inactive.[49] The chemical structures of the IF-dione-based semiconductors reviewed in this section are shown in Fig. 3 with the corresponding optoelectronic properties and device performance metrics listed in Table 1.

2.2. Early examples of IF-diones

Although the very first report of an IF-dione compound ([1,2-*a*] regioisomer) could be traced back to the late nineteenth century,[36] synthetic approaches to various IF-dione regioisomers (*e.g.*, [1,2-*a*], [1,2-*b*], and [2,1-*b*]) were reported from the 1950s to 1970s by several different research groups, yet with limited structural and optoelectronic characterization.[37–40] As an early example of an IF-dione with sufficient characterization, Gompper *et al.* synthesized **IF-dione-1** in 1987 as the precursor of **IF-DCV-1** (see Fig. 10, *vide infra*), which was developed as a promising molecular acceptor for charge-transfer complexes.[41] The authors also reported a four-step reversible reduction process for **IF-dione-1** with the first half-wave potential located at −0.69 eV (*vs.* SCE). In 1994, Swager *et al.* isolated **IF-dione-2** as the rapid oxidation product of a 20π electron system, indone[1,2-*b*]fluorene derivative (**π-IF-1** in Fig. 18, *vide infra*), under aerobic conditions in up to 95% yield (Scheme 1).[42] Later on, starting from the early 2000s, incredible advancements both in the structural diversity and (opto)electronic device applications of IF-diones have been realized, which have also contributed to the elucidation of the relationships between chemical structures, molecular properties, and charge transport relationships.[48,50–53]

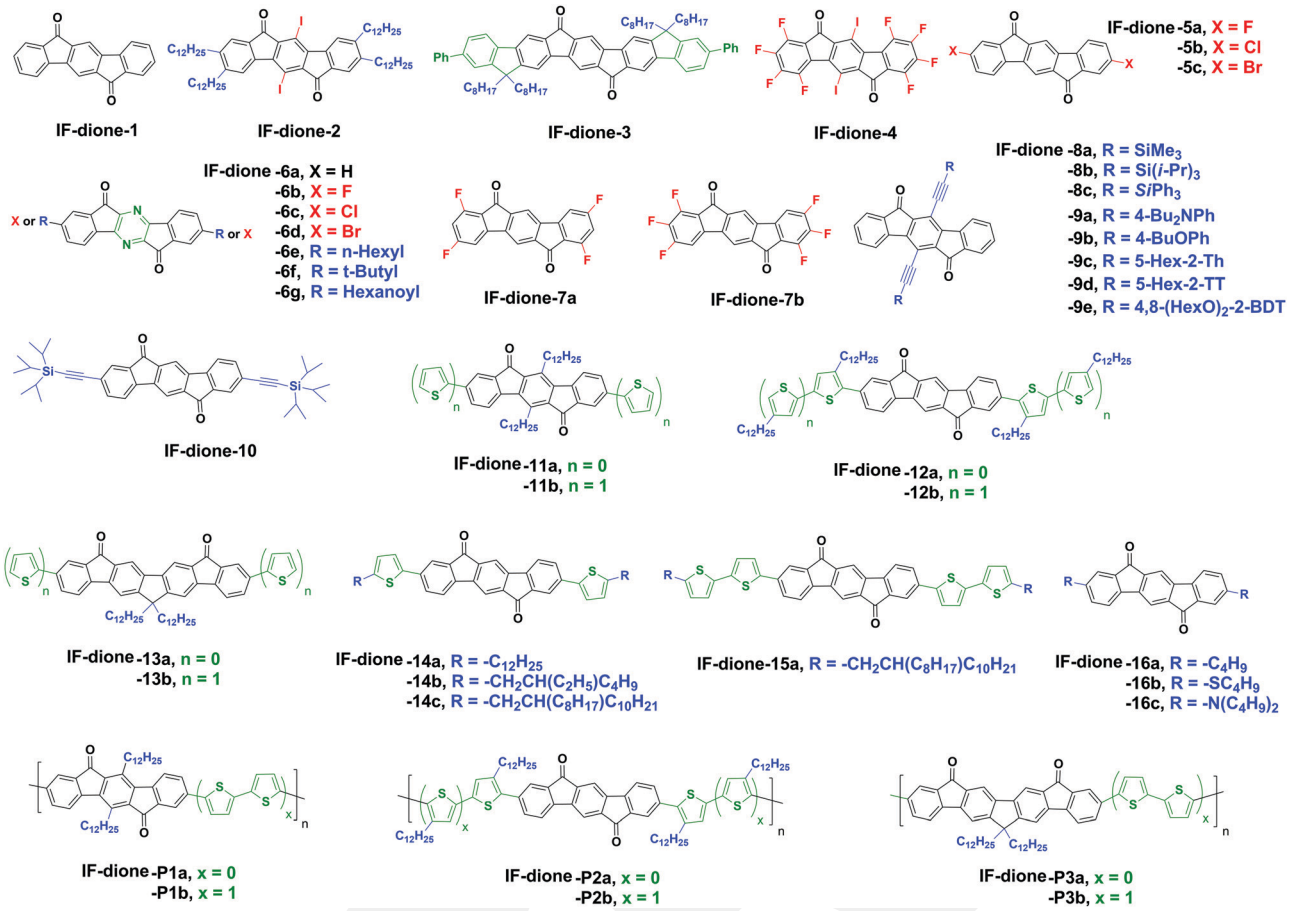

Fig. 3 Chemical structures of indenofluorenedione (IF-dione)-based semiconductors **IF-diones-1–16** and **IF-diones-P1–P3**.

Structures **IF-dione-1** and **IF-dione-5c** (Fig. 3) were originally reported in 2002 and 2005, respectively, as precursors to non-functionalized IF-based small molecules and polymers with fluorescence properties for light-emitting diodes.[54,55] As shown in Scheme 1 for **IF-dione-1**, very different from Swager's[42] original method, **precursor-1** was first synthesized using a modified Ebel method in water (98% yield), which was then oxidized using potassium permanganate in aqueous pyridine to yield **precursor 2** with carboxylic acid groups (96% yield). Finally, double intramolecular Friedel–Crafts acylations of **precursor-2** with concentrated sulfuric acid afforded **IF-dione-1** in high yields (90% yield). Despite the development of these early effective synthetic methods, the authors of these studies did not investigate the (opto)electronic properties of these IF-diones. The potential of an IF-dione structure for device applications was first reported by Müllen *et al.* in 2004.[56] In this study, an IF-dione was synthesized as a substructure of a ladder type pentaphenylene **IF-dione-3** (Fig. 3) exhibiting reversible electrochemical n-doping (electron-accepting) behavior and a LUMO energy level of −3.53 eV. Although charge transport and device characteristics were not reported in this study, the authors mentioned that a soluble electron accepting polymer employing **IF-dione-3** as a monomeric unit could be of great interest in OPVs. Following this report, Komatsu *et al.* developed the first IF-dione based organic semiconducting molecule **IF-dione-4** (Fig. 3) as an electron-transporting (n-channel) semiconductor in OFETs.[51] **IF-dione-4** has a perfluorinated indeno[1,2-*b*]fluorenedione π-core with –I substituents at the central 5,11-positions. This compound was synthesized *via* intramolecular cyclization, as previously depicted by Swager *et al.*,[42] by oxidizing a macrocyclic diacetylene molecule under aerobic conditions with I_2. The single-crystal structural analysis of **IF-dione-4** (Fig. 4) revealed a nearly coplanar conformation forming π-stacked (3.31 Å) columnar packing motifs with short intermolecular contacts (*e.g.*, F···I = 3.25 Å/C···F = 2.98 Å). Interestingly, a very short intramolecular I···O distance (3.08 Å ≪ r_{vdw}(I) + r_{vdw}(O) = 3.50 Å) was measured indicating an electronic interaction between these atoms. DFT molecular orbital computations indeed confirmed wavefunction mixing between I and O atoms in HOMO-8. Electrochemical measurements in solution showed the presence of two reversible reductions with the first half-wave potential of −0.91 V (*vs.* Fc/Fc^+), which is lower than that of unsubstituted IF-dione **IF-dione-1** (−1.14 eV). This was ascribed to the presence of electron withdrawing perfluoro substituents, and the low LUMO energy level of **IF-dione-4** was pointed out to be beneficial for electron transport. OFET devices based on **IF-dione-4** thin-films, which were deposited by thermal evaporation under

Table 1 Summary of experimental HOMO/LUMO energies (or oxidation/reduction potentials (E_{ox}/E_{red})), optical absorption maximum, and optical band gap values for IF-dione-based semiconductors, and the (opto)electronic device type and representative organic field-effect transistor (OFET)/bulk-heterojunction organic photovoltaics (BHJ-OPVs) performance values [field-effect mobility for electrons and/or holes (μ_e, μ_h), current on/off ratio (I_{on}/I_{off}), power conversion efficiency (PCE), and open-circuit voltage (V_{oc})] in the corresponding literature

Year	Semiconductor	HOMO/LUMO[a] [eV] or E_{ox}/E_{red}[a] [V]	λ_{max}^{abs} [b] [nm]	E_g^{opt} [c] [eV]	Opto(electronic) device type[d,e]	Performance (μ_e, μ_h [$cm^2\ V^{-1}\ s^{-1}$] (I_{on}/I_{off}) or PCE [%], V_{oc} [V])	Ref.
2007	IF-Dione-4	NR/−0.91 (*vs.* Fc/Fc^+)	505	NR	n-OFET (thermal evap.)	$\mu_e = 2.9 \times 10^{-5}$ (10^5)	51
2008 and 2011	IF-Dione-5a	NR/−1.02 (*vs.* Fc/Fc^+)	329	NR	n-OFET (thermal evap.)	$\mu_e = 0.17$ (10^7)	52 and 58
	IF-Dione-5b	NR/−1.05 (*vs.* Fc/Fc^+)	334	NR	n-OFET (thermal evap.)	$\mu_e = 0.02$ (10^7)	
	IF-Dione-5c	NR/−1.08 (*vs.* Fc/Fc^+)	335	NR	n-OFET (thermal evap.)	$\mu_e = 0.01$ (10^6)	
2008 and 2012	IF-Dione-6b	NR/−3.96	469	NR	n-OFET (thermal evap.)	$\mu_e = 0.17$ (10^7)	52 and 57
2009	IF-Dione-11b	−5.54/−3.54	537	2.02	p/n-OFET (thermal evap.)	$\mu_e = 0.01$ (10^6) $\mu_h = 6 \times 10^{-4}$ (10^7)	67
	IF-Dione-12a	−5.75/−3.70	525	2.05	p/n-OFET (thermal evap.)	$\mu_e = 0.006$ (10^4) $\mu_h = 0.006$ (10^4)	
	IF-Dione-12b	−5.53/−3.59	540	1.94	p-OFET (spin coat.)	$\mu_h = 1 \times 10^{-4}$ (10^4)	
	IF-Dione-13b	−5.50/−3.19	472	2.31	p-OFET (thermal evap.)	$\mu_e = 0.001$ (10^5)	
	IF-Dione-P1b	−5.42/−3.64	497	1.70	p-OFET (spin coat.)	$\mu_h = 0.001$ (10^4)	
	IF-Dione-P2b	−5.42/−3.62	560	1.55	p-OFET (spin coat.)	$\mu_h = 0.01$ (10^5)	
	IF-Dione-P3b	−5.34/−3.54	514	2.06	p-OFET (spin coat.)	$\mu_h = 3 \times 10^{-4}$ (10^4)	
2011	IF-Dione-7a	−6.67/−3.43	337	3.24	n-OFET (thermal evap.)	$\mu_e = 0.07$ (10^6)	58
	IF-Dione-7b	−6.73/−3.53	334	3.20	n-OFET (thermal evap.)*	$\mu_e = 0.16$ (10^5) $\mu_e = 0.07$ (10^5)*	
2012	IF-Dione-6g	NR/−3.93	440	NR	n-OFET (thermal evap.)	$\mu_e = 9.2 \times 10^{-3}$ (10^6)	57
2016	IF-Dione-14b	−5.60/−3.65	556	1.95	p/n-OFET (solution shear.)	$\mu_e = 0.12$ (10^6) $\mu_h = 0.02$ (10^3)	68
	IF-Dione-14c	−5.57/−3.63	560	1.94	p/n-OFET (solution shear.)	$\mu_e = 0.04$ (10^5) $\mu_h = 3.3 \times 10^{-4}$ (10^5)	
2017	IF-Dione-15a	−5.47/−3.61	568	1.89	p/n-OFET (solution shear.)	$\mu_e = 0.02$ (10^5) $\mu_h = 0.01$ (10^6)	69
2017	IF-Dione-16b	−5.60/−3.70	554	1.90	p/n-OFET (thermal evap.)	$\mu_e = 0.65$ (10^4) $\mu_h = 0.71$ (10^5)	71
	IF-Dione-16c	−5.00/−3.40	721	1.40	p-OFET (thermal evap.)	$\mu_h = 1.03$ (10^5)	
2018	IF-Dione-10	−5.77/−3.65	514	2.12	n-OFET (spin coat.)	$\mu_e = 4 \times 10^{-5}$ (10^4)	66

NR: the corresponding value is not reported in the reference. [a] Measured *via* cyclic voltammetry and estimated based on using the vacuum energy level of the reference electrode. [b] Measured in solution as the low-energy optical absorption maximum. [c] Measured in solution from the low-energy optical absorption edge. [d] Active layer deposition method is given in parentheses. [e] The n-OFET devices measured in an ambient environment are shown with an asterisk (*).

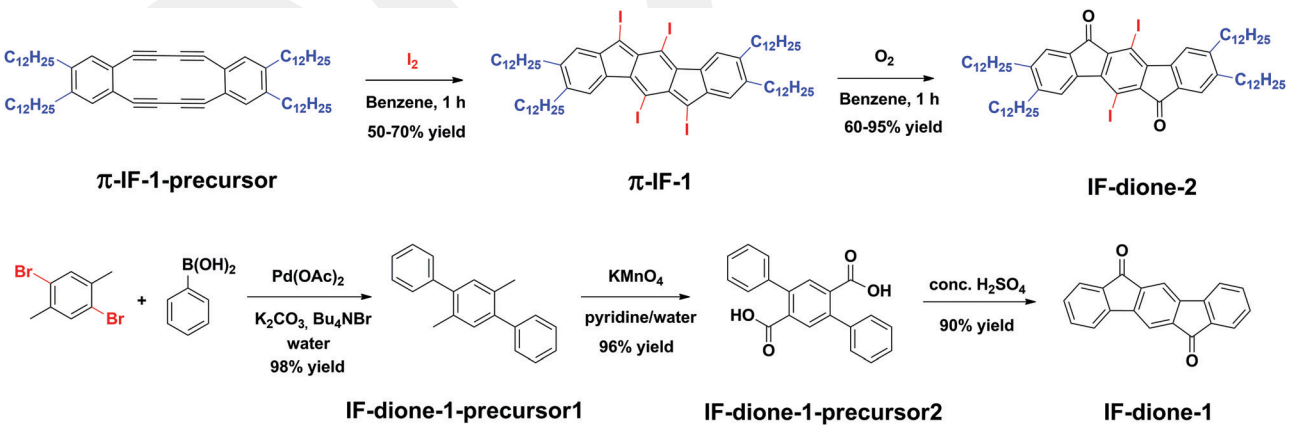

Scheme 1 Early synthetic routes to **π-IF-1**, **IF-dione-1**, and **IF-dione-2**.[42,54]

vacuum, exhibited electron transport behavior; however, electron mobility (μ_e) values were very low ($\mu_e = 10^{-6}$–10^{-5} $cm^2\ V^{-1}\ s^{-1}$), which was attributed to the poor semiconductor film morphology.

2.3. 2,8-Disubstitution approach

Yamashita *et al.* synthesized a series of disubstituted IF-dione derivatives, **IF-diones-5a–c** and **IF-diones-6a–g** (Fig. 3), having central benzene and pyrazine rings in which the electronic and

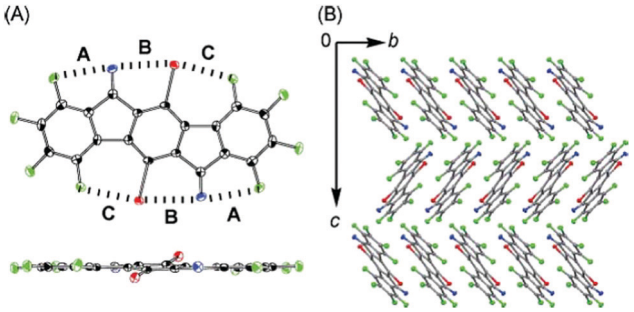

Fig. 4 (A) The top view and side view of **IF-dione-4** in ORTEP drawings. Thermal ellipsoids are drawn with the probability level of 50%. Selected distances (Å) of dotted lines **A**: F···O, 2.87; **B**: I···O, 3.08; **C**: F···I, 2.97. (B) Packing structure within the *bc* plane of **IF-dione-4**. Fluorine, oxygen, and iodine atoms are displayed in green, blue and red, respectively.[51] Reprinted with permission from ref. 51. Copyright 2007, The Royal Society of Chemistry.

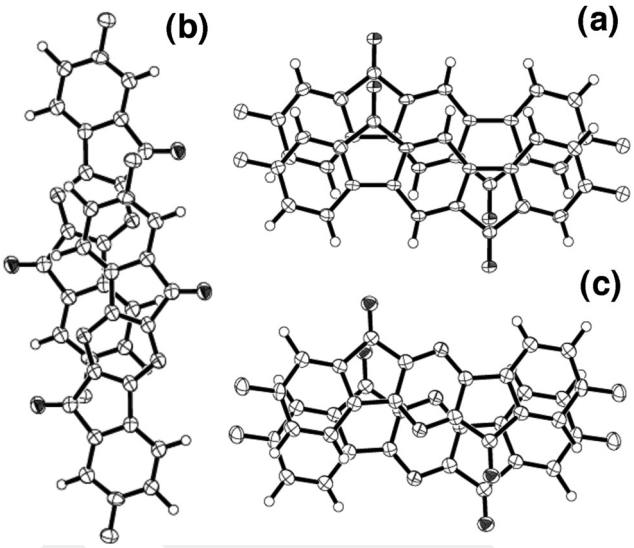

Fig. 5 Dimeric packing motifs of **IF-dione-5a** (a) and **IF-dione-6b** (b: red-crystal and c: black-crystal) in single crystals.[52] Reprinted with permission from ref. 52. Copyright 2008, American Chemical Society.

structural properties are finely tuned.[52,57] These compounds were substituted at the 2,8-positions with halogens (–F, –Cl, and –Br) or hexyl, *t*-butyl, and hexanoyl groups, with the goal of tuning electron affinity and enhancing the electron transport characteristics. While halogens were employed to improve electron injection/transport, alkyl groups were used to provide solubility in common organic solvents. This was the first systematic study addressing the semiconducting properties of IF-dione π-cores. The electrochemical characterization of F-substituted derivatives **IF-dione-5a** and **IF-dione-6b** revealed good electron accepting abilities with the first half-wave potentials of −1.02 V and −0.75 V (*vs.* Fc/Fc^{+}), respectively. This indicates relatively lower LUMO energies for these compounds, as compared to those of (> −3 eV) non-functionalized PCHs, as a result of the presence of electronegative –F substituents. As expected, the other halogen-substituted derivatives with –Cl (**IF-dione-5b**) and –Br (**IF-dione-5c**) substituents showed reduction potentials at more negative values. The more positive reduction potential measured for **IF-dione-6b**, as compared to **IF-dione-5a**, was attributed to the presence of a more electron deficient pyrazine central unit. As shown in Fig. 5, the single-crystal structures of **IF-dione-5a** and **IF-dione-6b** revealed completely planar molecular backbones forming columnar cofacial π-stacks (∼3.2–3.3 Å) with different molecular overlapping offsets. Interestingly, the pyrazine derivative **IF-dione-6b** showed polymorphism forming two kinds of crystals *via* sublimation, which differed in their dimeric molecular overlap patterns (Fig. 5b and c) and crystal colors (*i.e.*, red *vs.* black).

Among all IF-dione derivatives studied in this research, fluorine-substituted **IF-dione-5a** and **IF-dione-6b** molecules stand out as high mobility n-type semiconductors. Top- and bottom-contact OFETs fabricated with these semiconductors (vapor-deposited) showed μ_e values of up to 0.17 $cm^2\ V^{-1}\ s^{-1}$ with a high I_{on}/I_{off} of $\sim 10^7$. The other IF-diones with –Br and –Cl substituents showed lower electron mobilites of ∼0.01 $cm^2\ V^{-1}\ s^{-1}$, indicating that the halogen type is also crucial to the performance. The authors also investigated the semiconducting behavior of unsubstituted **IF-dione-1** in the same OFET architectures, however, these devices were inactive. This result pointed out the importance of terminal halogens to induce electron transport in OFETs. The θ–2θ X-ray diffraction (XRD) patterns of **IF-dione-5a** and **IF-dione-6b** films indicated that the molecules adopt a very favorable edge-on orientation on the HMDS-treated SiO_x dielectric surface with 0–35° tilting angles from the surface normal, which explains the observed high electron mobilities since this is known to favor in-plane π–π charge transport from the source to the drain electrodes. Due to the presence of alkyl substituents, **IF-dione-6f** and **IF-dione-6g** are soluble in common organic solvents. Although similar reduction potentials were observed for **IF-dione-6e** (−0.63 V *vs.* SCE) and **IF-dione-6f** (−0.62 V *vs.* SCE), a more positive reduction potential of −0.43 V (*vs.* SCE) was observed for **IF-dione-6g** due to the presence of additional electron withdrawing carbonyl units on the peripheral benzene rings. The single-crystal structures of **IF-dione-6c** and **IF-dione-6d** showed that these compounds are completely planar and only a half of the planar backbone is face-to-face π-overlap with another molecule at interplanar distances of 3.37–3.44 Å. Bottom-contact OFETs with vapor-deposited **IF-dione-6c** and **IF-dione-6d** on HMDS-treated p^{++}/n^{++}-Si/SiO_2 showed poor electron mobilities (1.4×10^{-6} $cm^2\ V^{-1}\ s^{-1}$–2.2×10^{-4} $cm^2\ V^{-1}\ s^{-1}$) compared to **IF-dione-6b**. The OFETs based on **IF-dione-6e** and **IF-dione-6f** also exhibited poor electrical performances. On the other hand, the OFETs based on **IF-dione-6g** (vapor-deposited on p^{++}/n^{++}-Si/SiO_2/HMDS) showed an electron mobility of 9.2×10^{-3} $cm^2\ V^{-1}\ s^{-1}$ with a high I_{on}/I_{off} of 10^6.

2.4. Tetra- and hexa-fluorination approach

Following this study and seeing the advantageous structural/electronic effects of –F incorporation for efficient electron transport, Park *et al.* investigated IF-dione structures with an increased number of –F substituents on the peripheral benzene

rings.[58] In this study, tetra- and hexa-fluorinated compounds **IF-dione-7a** and **IF-dione-7b** (Fig. 3) were developed, which showed lower LUMO energies of −3.43 eV and −3.53 eV, respectively, when compared with the non-fluorinated or di-fluorinated IF-diones. The optical band gaps (3.43 eV → 3.20 eV) were found to decrease upon increasing the number of –F substituents, and the electrical stability of the corresponding OFETs was found to improve with the number of fluorine substituents. In this study, the authors quantified the electrical stability of hexa-fluorinated **IF-dione-7b**, as compared to di-fluorinated **IF-dione-5a**, by measuring the device threshold voltage as a function of time under bias stress (V_G = 50 V applied over a period of 90 min). When the threshold voltage shift is modeled using a stretched exponential equation, a higher activation energy for the formation of charge trap states during electrical bias was calculated for **IF-dione-7b** (0.63 eV *vs.* 0.48 eV for **IF-dione-5a**). This was ascribed to the more electron-depleted π-structure of **IF-dione-7b** as a result of hexa-fluorination, which stabilizes the charge carrier electrons and reduces the possibility to be trapped. As shown in Fig. 6a–d, the OFETs fabricated with vapor-deposited films of fluorinated IF-diones **IF-dione-5a**, **IF-dione-7a**, and **IF-dione-7b** on polystyrene-treated n^{++}-Si/SiO_2 functioned as efficient n-type semiconductors with μ_e values of 0.05–0.16 $cm^2\ V^{-1}\ s^{-1}$ (I_{on}/I_{off} = ∼10^5–10^6). Considering that **IF-dione-1** is inactive as a semiconductor, the observed n-type semiconductivities are a direct result of fluorination on the IF-dione π-framework. In this study, OFETs were fabricated with both Au and LiF/Al source–drain electrodes, and lower contact resistances (for Au–semiconductor contact) and better device performances were recorded with the Au electrodes. The LUMO energy of the hexa-fluorinated **IF-dione-7b** was found to be the lowest among those of all fluorine-substituted IF-diones, thus, OFETs fabricated with **IF-dione-7b** showed good electrical (low V_{th} shift under an electrical bias stress) and ambient storage (μ_e = 0.07 $cm^2\ V^{-1}\ s^{-1}$ and I_{on}/I_{off} > ∼10^5 after 3 months) stabilities (Fig. 6f) with the highest initial μ_e of 0.16 $cm^2\ V^{-1}\ s^{-1}$ (I_{on}/I_{off} = ∼10^5–10^6) among all fluorinated IF-diones. As shown in Fig. 6f, when **IF-dione-7b** is compared with **IF-dione-5a**, the effect of fluorination-based LUMO stabilization on the air stability of OFET devices appears to be very significant. On the other hand, the stabilized LUMO energy level for **IF-dione-7b** enabled for the first time a low threshold voltage of only ∼9 V for an indenofluorene-based n-OFET. It is noteworthy that improved OFET ambient stability as a result of stabilized frontier molecular orbitals and improved thin-film hydrophobicity has recently been demonstrated for other semiconducting families upon fluorination of the π-backbone.[59]

2.5. 5,11- and 2,8-bis(ethynylation) approach

Another substitution strategy employed with IF-diones introduced rigid ethynyl units (–C≡C–) with terminal tri(alkyl/aryl)silyl groups and finely tunes solubility, frontier molecular orbital energetics, and crystal packing. In this approach, while terminal tri(alkyl/aryl)silyl groups govern solid-state molecular packing and solubility of the π-core for convenient synthesis/purification and film processing/microstructure, the rigid ethynyl spacers could allow for the formation of favorable π-stacked molecular arrays. This substitution approach was originally introduced for (hetero)acenes by Anthony *et al.* in the early 2000s prior to IF-diones.[60,61] Anthony *et al.* demonstrated that bis(trialkylsilylethynylation) on the short molecular axes of p-type pentacene/anthradithiophene semiconductors could enhance solubility in common organic solvents (>100 mg mL^{-1} in chloroform), decrease the HOMO energy level (>300 meV) for oxidative stability, and yield an extensive degree of intermolecular π-stacking for high hole mobilities (μ_h > 0.4–1 $cm^2\ V^{-1}\ s^{-1}$). During 2011–2014, Haley *et al.* utilized a similar substitution approach for IF-diones at the 5,11-central benzene ring positions. In their first study,[62] 5,11-bis(tri(alkyl/aryl)silyl)ethynyl-IF-diones with six different tri(alkyl/aryl)silyl groups were synthesized. Different than diethynylated (hetero)acenes, as shown in Scheme 2, these compounds were synthesized *via* Sonogashira cross-coupling reactions of the appropriate (tri(alkyl/aryl)silyl)acetylene with 5,11-diodo-IF-dione **I_2-IF-dione-1**. Among these compounds, the single-crystal structure analysis of **IF-diones-8a–8c** (Fig. 3) revealed that the nature of the alkyl/aryl substituents in 5,11-bis(tri(alkyl/aryl)silyl)ethynyl-IF-diones drastically alters the solid-state packing motifs and, thus, the degree of the corresponding intermolecular π–π interactions (Fig. 7). Consistent with the prior results on (hetero)acenes, triisopropylsilyl (TIPS) groups (**IF-dione-8b**) yielded the most favorable solid-state packing (*i.e.*, 2-D bricklayer arrangement shown in Fig. 7c and d) with the largest number of intermolecular π–π interactions at a short distance (3.40 Å). Note that this distance becomes much larger (3.77 Å) in **IF-dione-8c** when the substituents are changed from triisopropylsilyl to phenylene (Fig. 7b). The favorable packing observed in **IF-dione-8b** was previously attributed to the suitable diameter size of the TIPS group (∼7.5 Å), since two of these groups could occupy the same in-plane area as one π-core unit (∼14 Å for pentacene) allowing for a bricklayer packing arrangement.[63] The electrochemical data suggested excellent electron accepting behaviors for these molecules with the first half-wave reduction potentials located at ∼−0.8 eV (*vs.* SCE). Later, Haley *et al.* developed an improved synthetic route to 5,11-bis(tri(alkyl/aryl)silyl)ethynyl-IF-diones using relatively more robust –Br substituents (instead of labile –Is) and avoiding problematic transannular cyclization.[64] As shown in Scheme 2, a stable 5,11-dibromo-IF-dione compound **Br_2-IF-dione-1** was prepared in the multigram scale by intramolecular double Friedel–Crafts acylations starting from ambient stable and commercially available compounds, and it was cross-coupled with (tri(alkyl/aryl)silyl)acetylenes.

In a separate study during the same year, Haley *et al.* developed a series of donor–acceptor–donor 5,11-bis(ethynylated)-IF-dione triads **IF-diones-9a–e** (Fig. 3) that were substituted with various arylethynyl donors (4-Bu_2Nphenyl, 4-BuOphenyl, 5-hexyl-2-thienyl, 5-hexyl-2-thieno[3,2-*b*]thienyl, and 4,8-$(HexO)_2$-2-benzo[1,2-*b*:4,5-*b*′]dithienyl).[65] These compounds utilize ethynyl groups as both π-bridges between donor aryl units and IF-dione acceptor unit and electron withdrawing functionalities to increase the core electron

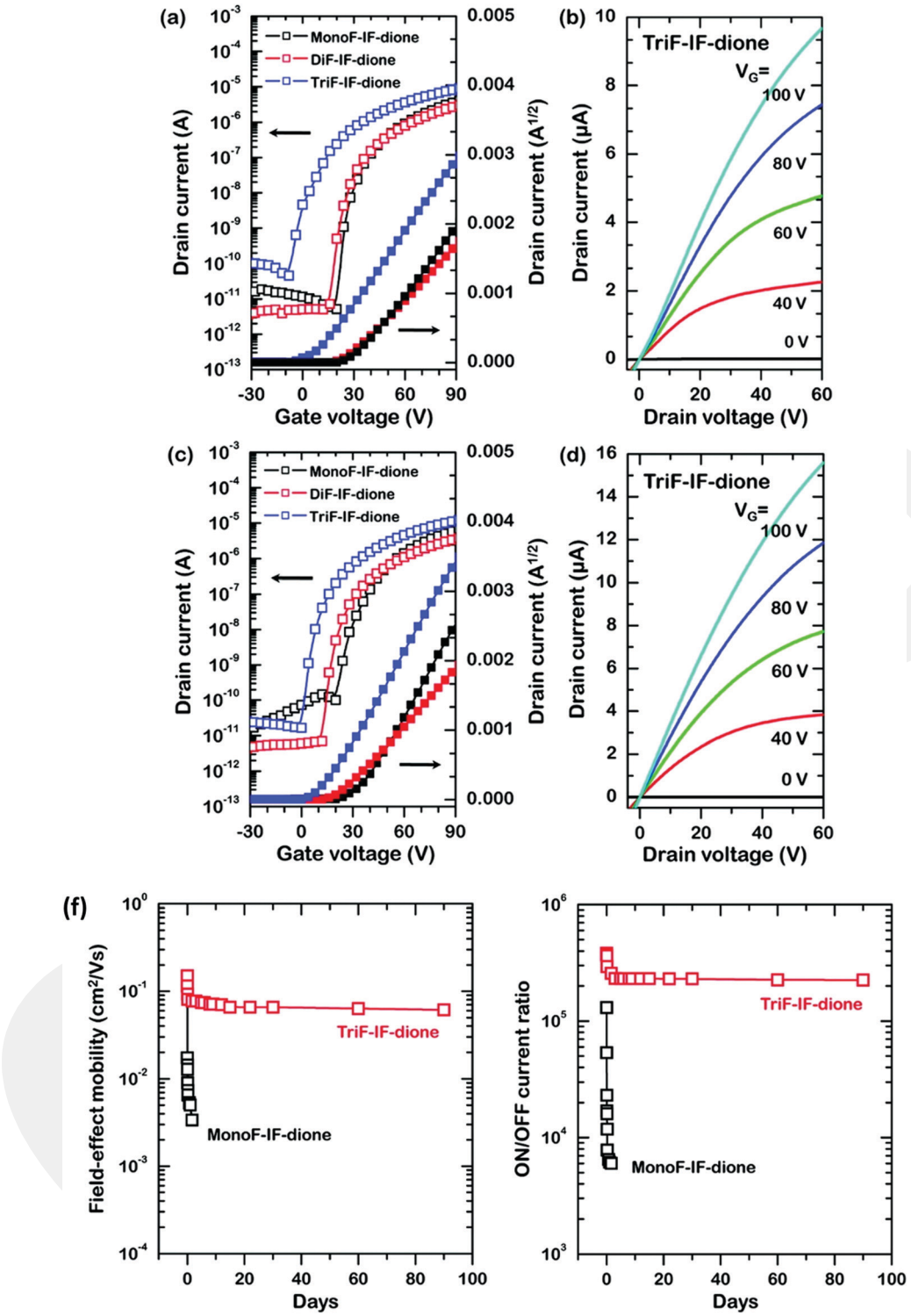

Fig. 6 Transfer (I_{DS} *vs.* V_G) and output (I_{DS} *vs.* V_{DS}) curves of OFETs based on **IF-dione-5a** (MonoF-IF-dione in the figure), **IF-dione-7a** (DiF-IF-dione in the figure), and **IF-dione-7b** (TriF-IF-dione in the figure) semiconductors, and LiF/Al (a and b) or Au source–drain electrodes (c and d). (f) Long-term air stability of OFETs (with Au source–drain electrodes) based on **IF-dione-7b** (TriF-IF-dione in the figure) and **IF-dione-5a** (MonoF-IF-dione in the figure) semiconductors stored in air in the dark for 100 days.[58] Reprinted with permission from ref. 58. Copyright 2011, American Chemical Society.

deficiency. On the basis of UV-Vis absorption and photoluminescence measurements, intramolecular charge transfer characteristics of **IF-diones-9a–e** were evident with extended electronic transitions in the low-energy spectral region of 600–700 nm. When **IF-dione-9a** was treated with trifluoroacetic acid, the low-energy absorption peaks were found to disappear as a result of

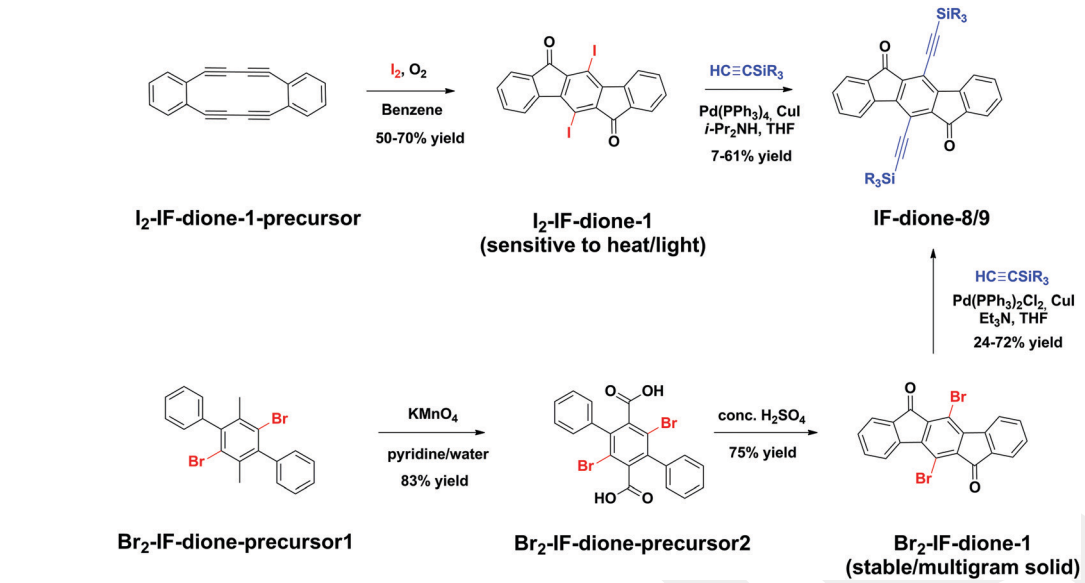

Scheme 2 Synthetic routes to **IF-dione 8/9**.[64]

protonation of the dibutylamino nitrogen atom disrupting intramolecular charge transfer. Despite the presence of donor end groups on the ethynyls, **IF-diones-9a–e** showed similar or more positive reduction potentials (−0.64 to −0.82 V *vs.* SCE) as compared to bis(trialkylsilyl)ethynyl-IF-diones. Although great progress was reported in the synthesis and characterization of ethynylated IF-dione molecules, the charge transport characteristics were not investigated in these studies. Very recently, Usta and Kim *et al.* employed a different ethynylation strategy and prepared an IF-dione derivative (**IF-dione-10** in Fig. 3) with triisopropylsilylethynyls along the long molecular axis (2,8-positions).[66] This molecule showed stabilized (ΔE = 50–100 meV) HOMO/LUMO energies of −5.77 eV/−3.65 eV as compared to the thiophene terminated IF-diones (*e.g.*, **IF-diones-11b** and **-12a** in Fig. 3), reflecting the higher electron deficiency of the new π-backbone due to the presence of ethynyl acceptor units and the absence of thienyl donor units (Fig. 8). Single-crystal structural analysis revealed a slightly S-shaped highly coplanar π-backbone for **IF-dione-10** forming slipped π-stacked one-dimensional (1-D) columnar motifs at 4.04 Å both in the single-crystal and in the solution-sheared thin-films. Because of poor thin-film crystallinity, a relatively low μ_e of 4×10^{-5} cm^2 V^{-1} s^{-1} ($I_{on}/I_{off} \sim 10^3$–10^4) was measured in the corresponding solution-processed OFETs. Despite the poor charge transport behavior, as of today **IF-dione-10** remains the only known ethynylated IF-dione semiconductor characterized in OFETs. Note that using this ethynylated IF π-scaffold, the modification of the carbonyl functional groups into dicyanovinylenes was found to increase the electron mobility by three orders of magnitude ($\mu_e \sim 0.02$ cm^2 V^{-1} s^{-1} and $I_{on}/I_{off} \sim 10^7$–10^8 for **IF-DCV-6** in Fig. 10, *vide infra*).[66]

2.6. Donor–acceptor–donor molecules and donor–acceptor copolymers

Introduction of electron donating alkyl, alkylthio, and dialkylamino substituents, or thiophene-based heteroaryl units, into the outer phenylenes of the IF-dione π-acceptor system has yielded donor–acceptor–donor (D–A–D) type molecular or D–A type polymeric π-backbones with favorable π-electronic structures and charge transport characteristics. To this end, Marks and Facchetti *et al.* first synthesized a series of D–A–D type molecular (**IF-diones-11a,b–13a,b** in Fig. 3) and D–A type polymeric (**IF-diones-P1a,b–P3a,b** in Fig. 3) IF-dione materials with systematically changed chemical structures.[48,67] Note that although the majority of these structures include the IF-dione π-core, **IF-diones-13a,b** and **-P3a,b** incorporate extended indenofluorene π-structures, namely bisIF-dione, with carbonyls separated by a fluorene unit. All thiophene-containing small molecules (**IF-diones-11b**, **-12a,b**, and **-13b**) and copolymers (**IF-diones-P1b**, **-P2b**, and **-P3b**) were synthesized *via* Stille cross-couplings, and were found to be solution processable; however, homopolymers **IF-diones-P1a**, **-P2a**, and **-P3a**, which were synthesized *via* Yamamoto polycondensations, were found to have limited solubilities preventing their purification/characterization. The IF-diones reported in this study showed low optical band gaps of 1.5–2.3 eV as a result of the D–A–D/D–A type π-electronic structures. According to cyclic voltammetry measurements, multiple reversible reductions were observed for all compounds with the first half-wave potentials ranging from −0.74 V to −1.25 V (*vs.* SCE). This indicates that the LUMO energies of these compounds vary from −3.19 eV to −3.70 eV while the HOMO energies were found to vary between −5.50 eV and −5.95 eV. The single crystal structure of **IF-dione-13b** revealed a substantially planar molecular conformation with minimal plane-to-plane twists (<1.5°) in the bisIF-dione π-core and between bisIF-dione and thiophene π-units (0.6°/7.3°) (Fig. 11, *vide infra*). The OFETs fabricated by spin-coating (bis)IF-dione-thiophene copolymers **IF-diones-P1b**, **-P2b**, and **-P3b** showed p-type charge transport with hole mobilities of up to 0.01 cm^2 V^{-1} s^{-1} ($I_{on}/I_{off} \sim 10^4$–10^5). However, the OFETs fabricated with molecular (bis)IF-dione-thiophene π-structures

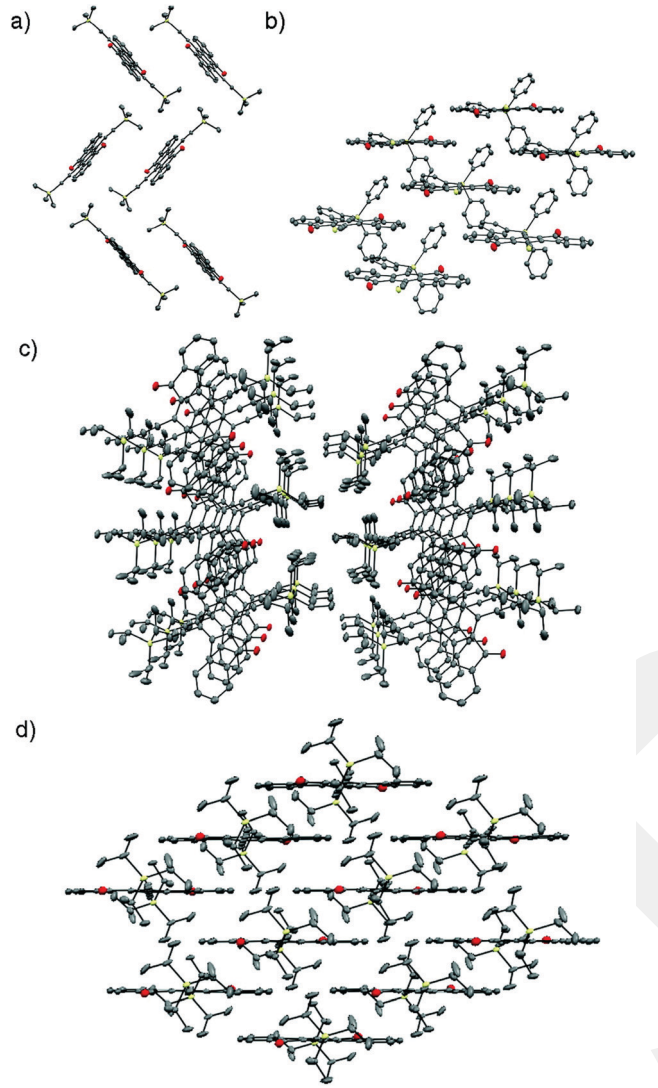

Fig. 7 Crystal packing of **IF-dione-8a** (a), **IF-dione-8b** (c and d), and **IF-dione-8c** (b) illustrating (a) herringbone, (b) 1-D columns without π–π interactions, and (c) coplanar slip stacking, respectively. (d) A side view of **IF-dione-8b** displays the favorable brick and mortar stacking pattern. Thermal ellipsoids drawn with a probability level of 30%.[62] Reprinted with permission from ref. 62. Copyright 2011, American Chemical Society.

IF-diones-11b, **-12a,b**, and **-13b** (**IF-diones-11a** and **-13a** were inactive) showed different semiconducting behavior depending on the alignment of the frontier molecular orbital energies with respect to the Au work function (−5.1 eV) – the magnitudes of hole (Φ_h) *vs.* electron (Φ_e) injection barriers. While **IF-diones-12b** and **-13b** were p-type semiconductors with μ_h values of $\sim 10^{-3}$–10^{-4} cm^2 V^{-1} s^{-1} ($I_{on}/I_{off} \sim 10^4$–10^5), **IF-diones-11b** and **-12a** were found to be exhibit ambipolarity with electron and hole mobilities of up to 0.01 cm^2 V^{-1} s^{-1} and 0.006 cm^2 V^{-1} s^{-1}, respectively. The induction of electron transport in **IF-diones-11b** and **-12a** is the direct result of their reduced LUMO energies (down to −3.7 eV) as compared to **IF-diones-12b** and **-13b**. Remarkably, the charge carrier mobilities for electron *vs.* hole transport in ambipolar **IF-dione-12a**-based OFETs were found to be highly balanced ($\mu_e/\mu_h \sim 1$) as a result of finely tuned FMO energies.

In later studies, Usta and Kim *et al.* designed and synthesized ambipolar thiophene and bithiophene terminated IF-dione molecules **IF-diones-14a–c** and **-15a** (Fig. 3) *via* alkyl chain engineering.[68,69] The design strategy in their first study was to develop a planarized D–A–D molecular π-scaffold for efficient ambipolar charge transport by repositioning the alkyl substituents from β to α,ω positions.[68] In contrast to the β-dodecyl substituted **IF-dione-12a** (Fig. 3), the α,ω-dodecyl substituted **IF-dione-14a** was found to have very limited solubility in common organic solvents as a result of molecular π-backbone planarization. However, the swallow-tailed 2-ethyhexyl and 2-octyldodecyl substitutions yielded the entirely solution processable molecules **IF-diones-14b** and **-14c**, which showed low thin-film optical band gaps of ∼1.8 eV with HOMO and LUMO energies of −5.6 eV and −3.6 eV, respectively. These balanced frontier molecular orbitals are favorable to provide simultaneous injection of both charge carrier types (*i.e.*, electrons and holes) from the Au electrode. 2-Ethylhexyl substitution in **IF-dione-14b** was found to provide the finest balance of solubility, favorable physicochemical/optoelectronic properties, and good thin-film crystallinity, which leads to high electron and hole mobilities of 0.12 cm^2 V^{-1} s^{-1} and 0.02 cm^2 V^{-1} s^{-1}, respectively, with I_{on}/I_{off} ratios of 10^5–10^6 in solution-processed top-contact/bottom-gate OFETs (solution-sheared semiconductors on an n^{++}-Si/SiO$_2$/PS-brush). This resulted in two/three orders of magnitude charge carrier mobility enhancement relative to the β-substituted **IF-dione-12a** due to rational alkyl chain engineering. In a following study,[69] the same researchers developed a π-extended D–A–D IF-dione molecule (**IF-dione-15a**) by introducing bithiophene units on each side of the IF-dione π-core. In this design, 2-octyldodecyl-bithiophenes were employed to extend the π-conjugation length, enhance the D–A–D π-electronic structure, and ensure good solubility. The solid-state optical band gap was measured to be as low as 1.65 eV. The electrochemical properties indicated the coexistence of reversible oxidation and reduction processes with the first half-wave potentials of +1.07 V and −0.79 V (*vs.* Ag/AgCl), respectively. The HOMO/LUMO energies were estimated as −5.47 eV/−3.61 eV that were very favorable for the concurrent electron and hole injection/transport in the corresponding films. The top-contact/bottom-gate OFETs based on **IF-dione-15a** (solution-sheared semiconductors on an n^{++}-Si/SiO$_2$/PS-brush) exhibited highly balanced ambipolar behavior with an electron mobility of 0.02 cm^2 V^{-1} s^{-1} and a hole mobility of 0.01 cm^2 V^{-1} s^{-1} (I_{on}/I_{off} = 10^5–10^6). Complementary-like inverters were demonstrated to show sharp signal switching with high gains of 80. It is noteworthy that the same authors used soluble **IF-diones-14c** and **-15a** compounds as precursors in the synthesis of lower LUMO (<−4 eV) dicyanovinylene-functionalized liquid-crystalline semiconductors **IF-DCVs-5a,b** (*vide infra*, Fig. 10).[69,70]

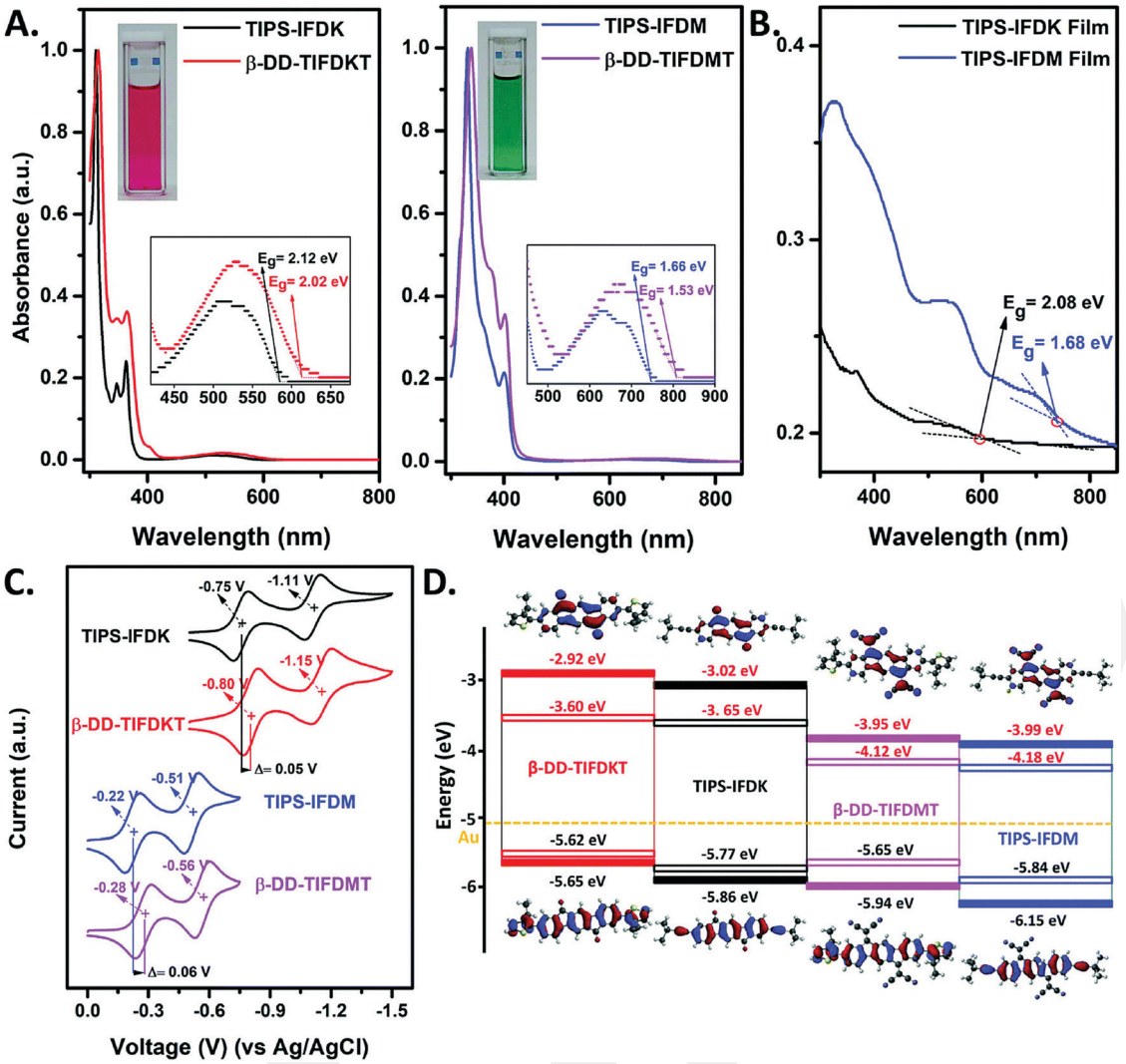

Fig. 8 For **IF-dione-10** (**TIPS-IFDK** in the figure) and **IF-DCV-6** (**TIPS-IFDM** in the figure) and the reference molecules **IF-dione-12a** (**β-DD-TIFDKT** in the figure) and **IF-DCV-4a** (**β-DD-TIFDMT** in the figure), optical absorption spectra in dichloromethane solution (insets show the images of the corresponding **IF-dione-10** and **IF-DCV-6** solutions) (A), optical absorption spectra in thin films (B), cyclic voltammograms in dichloromethane (0.1 M $Bu_4N^+PF_6^-$, scan rate = 50 mV s^{-1}) (C), and topographical orbital representations of calculated (solid blocks; DFT/B3LYP/6-31G**) and experimental (hollow blocks) HOMO and LUMO energy levels (D).[66] Reprinted with permission from ref. 66. Copyright 2018, The Royal Society of Chemistry.

2.7. Alkylthio and alkylamino substituents for high mobility in OFETs

In a recent study by Zhang *et al.*, the [1,2-*b*]IF-dione regioisomer **1**, which did not shown any appreciable charge carrier mobility in prior studies, was substituted at the 2,8-positions with electron donating alkyl, alkylthio, and dialkylamino substituents to yield **IF-diones-16a–c** (Fig. 3).[71] When compared with the alkyl-substituted [1,2-*b*]IF-dione **IF-dione-16a**, butylthio and dibutylamino substituents in **IF-diones-16b** and **-16c** were found to significantly change the optical band gaps, frontier molecular orbital energies/topographies, and solid-state packings. The optical band gaps were found to be 2.2 eV for **IF-dione-16a**, 1.9 eV for **IF-dione-16b**, and 1.4 eV for **IF-dione-16c**, and the HOMO/LUMO energies were −6.0/−3.5 eV, −5.6/−3.7 eV, and −5.0/−3.4 eV, respectively. While the strongly electron donating nitrogen atom of dialkylamino substitution increases both HOMO and LUMO energies in **IF-dione-16c**, resulting in exclusively p-type charge transport, the weakly electron donating sulfur atoms of the alkylthio group, having some π-acceptor ability ($p_\pi(C)$–$d_\pi(S)$), in **IF-dione-16b** lowers the LUMO and increases the HOMO energies leading to ambipolar semiconductor behavior. The sulfur and nitrogen heteroatoms were found to induce two-dimensional (2D) molecular packing motifs for **IF-diones-16b** and **-16c** with π–π stacking distances of 3.22–3.39 Å, while the alkyl substituted **IF-dione-16a** showed one-dimensional (1D) columnar packing with π–π stackings of 3.45 Å. While top-contact/bottom-gate OFETs (vacuum deposited semiconductors on p^{++}-Si/SiO_2/OTMS) fabricated with **IF-dione-16a** exhibited no field effect characteristics, as a result of large charge injection barriers and 1D molecular packing, **IF-diones-16b** and **-16c** showed ambipolar (μ_e = 0.65 $cm^2\ V^{-1}\ s^{-1}$ ($I_{on}/I_{off} \sim 10^3$–10^4) and μ_h = 0.71 $cm^2\ V^{-1}\ s^{-1}$ ($I_{on}/I_{off} \sim 10^4$–10^5)) and

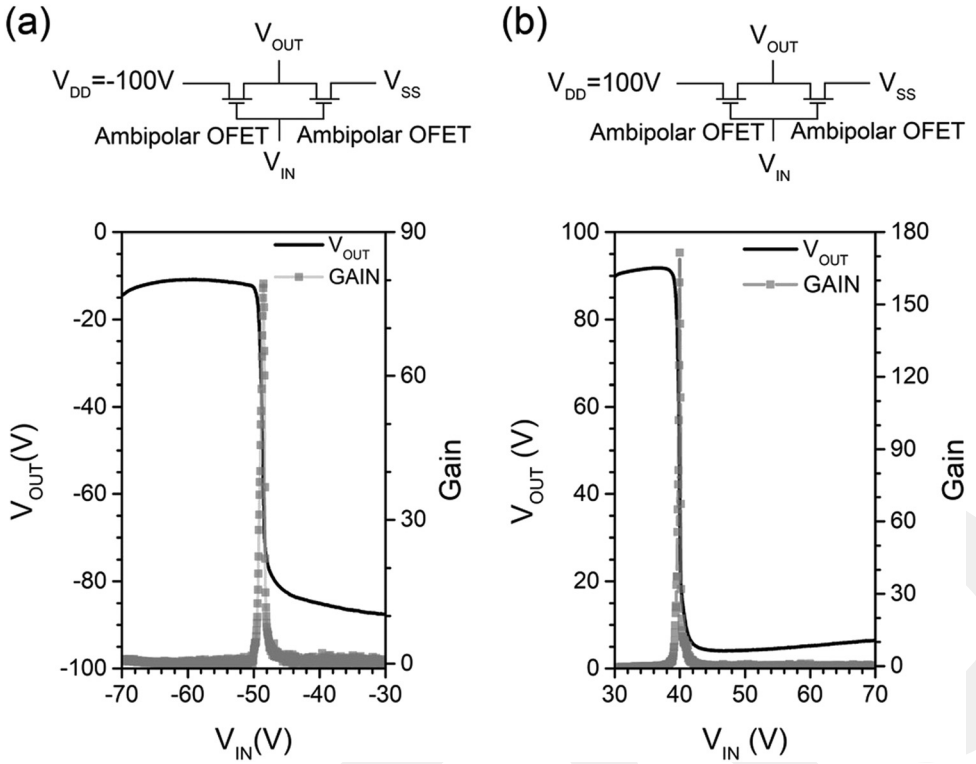

Fig. 9 CMOS-like inverter structures fabricated with **IF-dione-16b**-based OFETs and input/output characteristics for negative (a) and positive (b) supply biases (V_{DD}).[71] Reprinted with permission from ref. 71. Copyright 2017, Wiley-VCH.

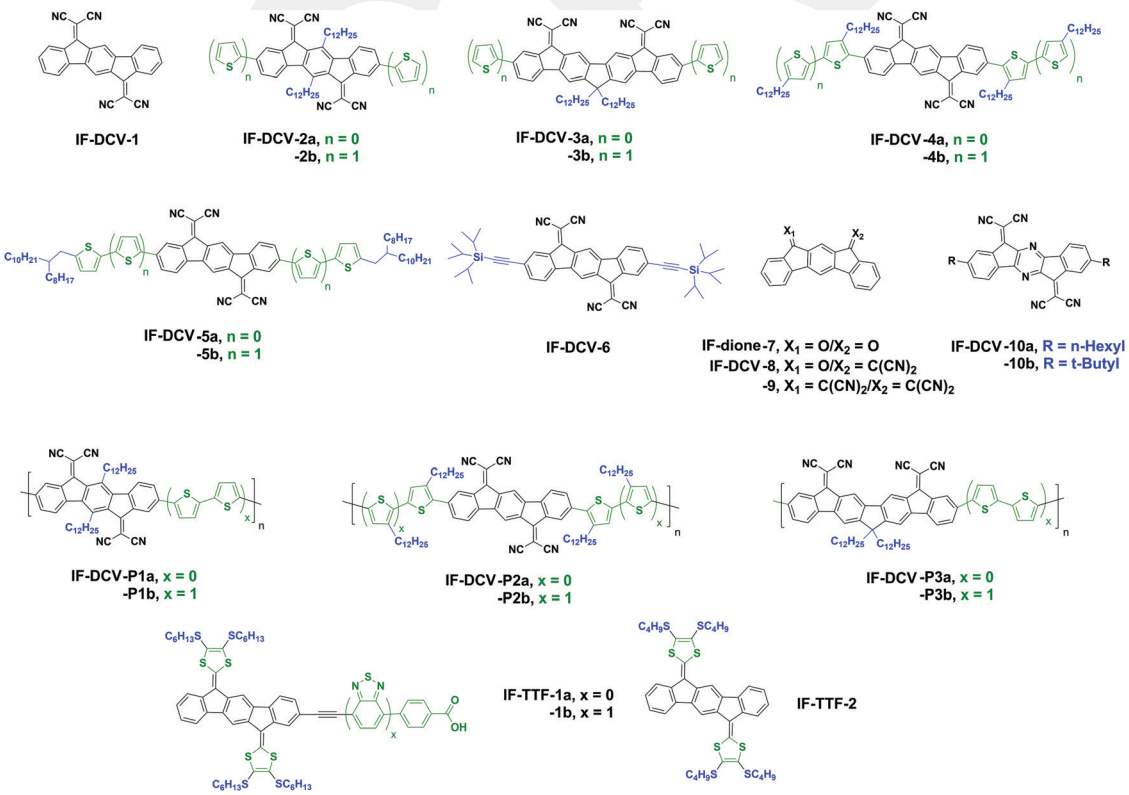

Fig. 10 Chemical structures of indenofluorenedicyanovinylene (IF-DCV)-based semiconductors **IF-DCVs-1-10** and **IF-DCVs-P1**-**P3**, and indenofluorenetetrathiafulvalene (IF-TTF)-based molecules **IF-TTFs-1a,b** and **-2**.

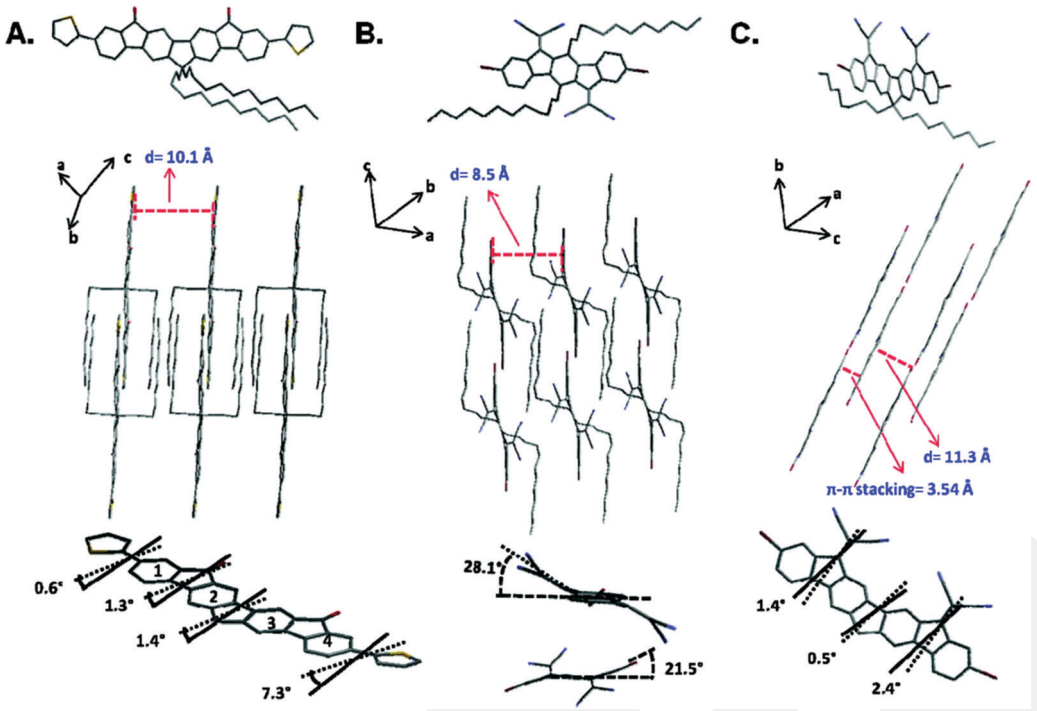

Fig. 11 Single-crystal structures and packings of (A) **IF-dione-13b**, (B) **Br_2-IF-DCV-2a**, and (C) **Br_2-IF-DCV-3a**.[67] Reprinted with permission from ref. 67. Copyright 2009, American Chemical Society.

p-type (μ_h = 1.03 $cm^2\ V^{-1}\ s^{-1}$ ($I_{on}/I_{off} \sim 10^4$–10^5)) semiconductor behavior, respectively. The highly balanced electron/hole mobilities for **IF-dione-16b** are remarkable, which enabled the fabrication of high performance CMOS-like inverters with a maximum gain value of 173 (for V_{DD} = 100 V and V_{IN} = 40 V, Fig. 9b). In the semiconductor class of IF-diones, the charge carrier mobilities reported for **IF-diones-16b** and **-16c** are the highest reported to date. The findings presented in this study revealed that the incorporation of heteroatom-linked side chains could be a widely applicable strategy for the development of high performance IFs.

3. Dicyanovinylene and tetrathiafulvalene functionalized indenofluorenes (IF-DCVs and IF-TTFs)

3.1. Brief introduction to IF-DCVs and IF-TTFs

Indenofluorene-based π-scaffolds functionalized with dicyanovinylene (DCV) groups on the bridge methylenes of the five-membered rings exhibit excellent electron transport characteristics particularly under ambient conditions. Dicyanovinylene is one of the strongest electron-withdrawing functional group and can greatly stabilize the frontier molecular orbitals of a π-conjugated system to induce electron injection/transport characteristics. DCV has been used in the structure of the first reported metallic charge transfer complex, tetrathiofulvalene:tetracyano-*p*-quinodimethane (TTF:TCNQ).[72] The solid-state structure of this charge transfer complex consists of quasi-one-dimensional segregated stacks of TTF and TCNQ molecules. In the corresponding electronic structure of this charge transfer complex, electrons from the HOMO of the π-electron rich TTF are transferred to the low-lying LUMO of the π-electron deficient TCNQ, which increases the carrier density in the solid-state. As a result, electrical conductivities (1.47×10^6 S m^{-1}) approaching those of metals were measured. A later study by Morpurgo *et al.* demonstrated that stable and reproducible interfacial charge transfer and a high electrical conductivity could be achieved even by mechanically laminating TTF and TCNQ single crystals.[73] Motivated by these discoveries, extensive research addressed the synthesis of new molecules with strong electron accepting/transport properties, during which the first example of a DCV-functionalized IF π-conjugated system was developed in 1987.[41] Despite being less investigated compared to IF-DCVs, the IF π-system could also be extended through the sp^2-hybridized bridge carbons in the lateral molecular direction to extend the redox-active tetrathiafulvalene (TTF) π-system yielding so-called indenofluorene-extended TTFs (IF-TTFs). These molecules have been recently used in DSSCs and OFETs.[74] The chemical structures of the IF-DCV/TTF-based semiconductors reviewed in this section are shown in Fig. 10 with the corresponding optoelectronic properties and device performance metrics listed in Table 2. Here, we note that, although the functional groups in this subclass of indenofluorenes are indeed dicyanomethylidene and 1,3-dithiol-2-ylidene groups, the acronyms "IF-DCV and IF-TTF" are preferred considering the structure of the functional groups (*i.e.*, dicyanovinylene and tetrathiafulvalene) in the final semiconducting π-backbones.

Table 2 Summary of experimental HOMO/LUMO energies (or oxidation/reduction potentials (E_{ox}/E_{red})), optical absorption maximum, and optical band gap values for IF-DCV/TTF-based semiconductors, and the (opto)electronic device type and representative organic field-effect transistor (OFET)/bulk-heterojunction organic photovoltaics (BHJ-OPVs) performance values [field-effect mobility for electrons and/or holes (μ_e, μ_h), current on/off ratio (I_{on}/I_{off}), power conversion efficiency (PCE), and open-circuit voltage (V_{oc})] in the corresponding literature

Year	Semiconductor	HOMO/LUMO[a] [eV] or E_{ox}/E_{red}[a] [V]	λ_{max}^{abs} [b] [nm]	E_g^{opt} [c] [eV]	Opto(electronic) device type[de]	Performance (μ_e, μ_h [$cm^2\ V^{-1}\ s^{-1}$] (I_{on}/I_{off}) or PCE [%], V_{oc} [V])	Ref.
2008	IF-DCV-4a	−5.84/−4.32	653	1.52	n-OFET (spin coat.)*	μ_e = 0.16 $cm^2\ V^{-1}\ s^{-1}$ (10^8)	48
	IF-DCV-P2b	−5.51/−4.15	810	1.38	p/n-OFET (spin coat.)	μ_e = 2 × 10^{-4} $cm^2\ V^{-1}\ s^{-1}$ (10^4) μ_h = 2 × 10^{-4} $cm^2\ V^{-1}\ s^{-1}$ (10^4)	
2009	IF-DCV-2b	−5.74/−4.20	661	1.54	n-OFET (thermal evap.)*	μ_e = 0.001 $cm^2\ V^{-1}\ s^{-1}$ (10^5)	67
	IF-DCV-3a	−5.86/−3.91	513	1.95	n-OFET (thermal evap.)	μ_e = 0.006 $cm^2\ V^{-1}\ s^{-1}$ (10^6)	
	IF-DCV-3b	−5.52/−3.72	576	1.80	n-OFET (thermal evap.)	μ_e = 0.02 $cm^2\ V^{-1}\ s^{-1}$ (10^6)	
	IF-DCV-4b	−5.64/−4.20	711	1.44	p/n-OFET (spin coat.)*	μ_e = 0.001 $cm^2\ V^{-1}\ s^{-1}$ (10^5) μ_h = 1 × 10^{-4} $cm^2\ V^{-1}\ s^{-1}$ (10^5)	
	IF-DCV-P3a	−5.75/−4.07	577	1.99	n-OFET (spin coat.)	μ_e = 5 × 10^{-5} $cm^2\ V^{-1}\ s^{-1}$ (10^4)	
	IF-DCV-P3b	−5.56/−3.84	661	1.57	p/n-OFET (spin coat.)	μ_e = 5 × 10^{-5} $cm^2\ V^{-1}\ s^{-1}$ (10^4) μ_h = 5 × 10^{-5} $cm^2\ V^{-1}\ s^{-1}$ (10^4)	
2012	IF-DCV-10a	NR	581	NR	n-OFET (thermal evap.)	μ_e = 0.01 $cm^2\ V^{-1}\ s^{-1}$ (10^6)	57
	IF-DCV-10b	NR/−4.15	346	NR	n-OFET (thermal evap.)	μ_e = 3.3 × 10^{-4} $cm^2\ V^{-1}\ s^{-1}$ (10^4)	
2015	IF-DCV-8	−5.90/−3.93	505	2.16	n-OFET (thermal evap.)	μ_e = 5 × 10^{-6} $cm^2\ V^{-1}\ s^{-1}$ (10^4)	49
	IF-DCV-9	−5.91/−3.81	542	2.13	n-OFET (thermal evap.)	μ_e = 0.001 $cm^2\ V^{-1}\ s^{-1}$ (10^6)	
2017	IF-DCV-5a	−5.64/−4.19	721	1.45	n-OFET (spin coat.)*	μ_e = 0.11 $cm^2\ V^{-1}\ s^{-1}$ (10^8)	70
2017	IF-DCV-5b	−5.49/−4.23	755	1.31	p/n-OFET (spin coat.)*	μ_e = 0.13 $cm^2\ V^{-1}\ s^{-1}$ (10^4) μ_h = 0.01 $cm^2\ V^{-1}\ s^{-1}$ (10^4)	69
2017	IF-TTF-2	−4.64/−2.09	475	2.48	p-OFET (single crystal)	μ_h = 1.44 $cm^2\ V^{-1}\ s^{-1}$ (10^5)	88
2018	IF-DCV-6	−5.84/−4.18	625	1.66	n-OFET (spin coat.)*	μ_e = 0.02 $cm^2\ V^{-1}\ s^{-1}$ (10^8)	66
2020	IF-TTF-1a	NR/−0.32 (*vs.* Fc/Fc^+)	487	2.36	DSSC (solution dep.)	PCE = 4.8–5.0% V_{oc} = 0.81 V	74
	IF-TTF-1b	+1.68/−0.32 (*vs.* Fc/Fc^+)	479	2.36	DSSC (solution dep.)	PCE = 6.4–7.1% V_{oc} = 0.81 V	

NR: the corresponding value is not reported in the reference. [a] Measured *via* cyclic voltammetry and estimated based on using the vacuum energy level of the reference electrode. [b] Measured in solution as the low-energy optical absorption maximum. [c] Measured in solution from the low-energy optical absorption edge. [d] Active layer deposition method is given in parentheses. [e] The n-OFET devices measured in an ambient environment are shown with an asterisk (*).

3.2. Early examples of IF-DCVs

Gompper *et al.* synthesized the first IF-DCV molecule **IF-DCV-1** (Fig. 10) by reacting **IF-dione-1** (Fig. 3) with malononitrile and titanium tetrachloride.[41] **IF-DCV-1** showed a high melting temperature > 330 °C indicating the presence of strong solid-state cohesive interactions, and the electrochemical characterization in DMF revealed four reversible reduction processes with the first reduction potential located at a very low voltage of −0.04 V (*vs.* SCE). This result indicated that **IF-DCV-1** is a very strong electron acceptor with a low-lying LUMO energy level (<−4 eV), and could be a promising acceptor candidate for use in charge transfer complexes. After this initial study, the development of IF-DCVs stalled for almost two decades. Starting from the early 2000s, DCVs again attracted interest in the field of organic optoelectronics, which was emerging at that time to develop ambient stable n-channel semiconductors for OFETs. The early DCV-functionalized organic semiconductors were quinoidal oligothiophenes exhibiting electron mobilities of 0.005–0.16 $cm^2\ V^{-1}\ s^{-1}$ (I_{on}/I_{off} ~ 10^4–10^5).[75]

3.3. Donor–acceptor–donor molecules and donor–acceptor copolymers

In 2008–2009, Marks and Facchetti *et al.* demonstrated for the first time that DCVs could be employed in (bis)IF π-scaffolds (*e.g.*, structures **IF-DCVs-2a,b–4a,b** and **IF-DCVs-P1a,b–P3a,b** in Fig. 10) to yield remarkable semiconductor performances in OFETs.[48,53,67] The lack of understanding of ambient-stable electron transport and the scarcity of n-channel/ambipolar OFETs that could operate under ambient conditions in the early 2000s had motivated these studies. The authors developed a structural library of several functionalized (bis)IF-based small molecules and polymers (including carbonyl-functionalized precursors) and investigated their physicochemical, optoelectronic, single-crystal, and OFET device characteristics in detail.[67] This study demonstrated one of the early examples of a low-LUMO organic semiconductor library in the optoelectronics literature, in which LUMO energies were tuned over 1 eV to identify the energetic window for ambient stability. The IF-DCV small molecules (**IF-DCVs-2a,b–4a,b**) and their dibrominated monomers were synthesized *via* Knoevenagel condensations from their carbonyl-functionalized counterparts by using excess malononitrile and an organic base (*i.e.*, pyridine or piperidine) in ~50–70% yields. The (bis)thiophene-based terminal units were introduced into the molecular and polymeric π-backbones *via* Stille cross-couplings. As depicted in Scheme 3, while the Knoevenagel condensations for the bis-IF compounds **IF-DCVs-3a,b** proceeded well with CH_2CN_2 and piperidine in the absence of a Lewis acid, IFs **IF-DCVs-2a,b** and **-4a,b** required $TiCl_4$ as the strong Lewis acid and pyridine base to form the

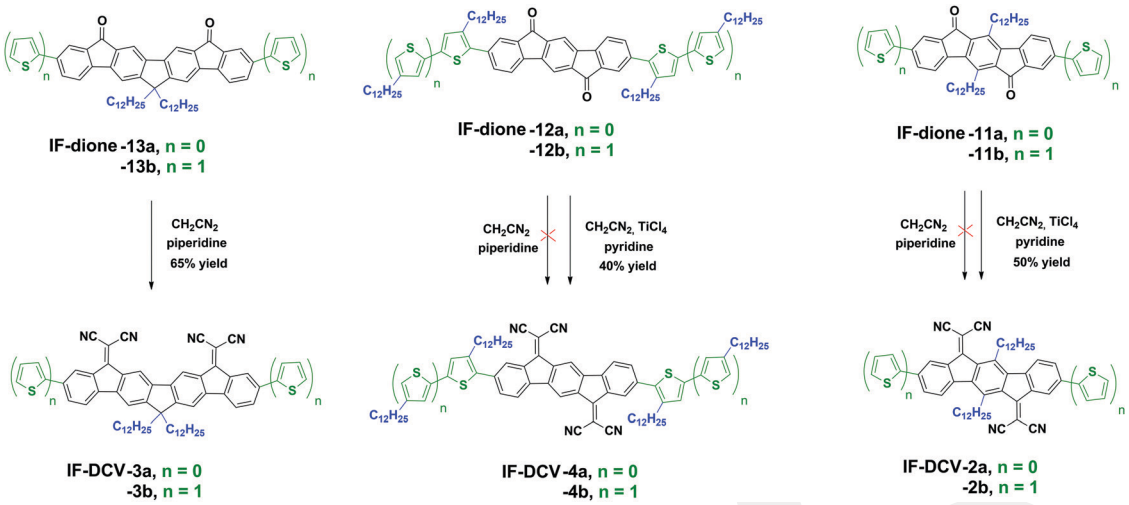

Scheme 3 Synthesis of **IF-DCVs-2a/b**, **3a/b**, and **4a/b** *via* Knoevenagel condensations. The reactions that do not yield the desired products are shown with a red cross.[48,53,67]

IF-DCV π-core. The LUMO comparisons of **IF-DCV-3a** (−3.91 eV) *vs.* **IF-DCV-2a** (−4.30 eV) and **IF-DCV-3b** (−3.72 eV) *vs.* **IF-DCV-2b** (−4.20 eV)/**IF-DCV-4a** (−4.32 eV) clearly revealed that IF-DCV is a much more electron deficient π-core than bisIF-DCV (ΔE_{LUMO} up to −0.6 eV), which explains the synthetic difficulty of forming this π-core.

With respect to its electronic structure, IF-DCV is indeed one of the most electron deficient π-systems reported to date. When the electron accepting properties of the (bis)IF-DCVs were compared with those of their carbonyl-functionalized counterparts, the dicyanovinylene units provided both π-extended conjugation and the negative resonance (−*R*) effect. These favorable electronic features of dicyanovinylene functional groups enabled LUMO stabilizations by ∼600–700 meV and LUMO wavefunction delocalization. The electrochemical characterization studies of **IF-DCVs-2a,b–4a,b** and **IF-DCVs-P1a,b–P3a,b** showed multiple reversible reductions revealing very low LUMO energies from −4.0 eV to −4.3 eV. In addition, as a result of the presence of strong donor–acceptor π-electronic structures, these compounds showed low optical band gaps of 1.35–1.80 eV in the solid state. As shown in Fig. 11B and C, the single-crystal structures of dibrominated IF-DCVs **Br$_2$-IF-DCV-2a** and **Br$_2$-IF-DCV-3a** showed that the positions of the alkyl chains on the central six- and five-membered rings, respectively, of the (bis)IF π-system impede effective π–π interactions (intermolecular distances ∼8.5–11.3 Å).[67] Only in **Br$_2$-IF-DCV-3a**, partial π–π interactions with a distance of ∼3.54 Å were evident. While the DCVs were found to be displaced out of the cyclopentadienyl planes (by ∼28.1°) in the IF-DCV π-core of **Br$_2$-IF-DCV-2a**, a highly coplanar π-backbone with in-plane DCVs was observed in the bisIF-DCV π-core of **Br$_2$-IF-DCV-3a**. This difference was ascribed to the significant steric hindrance between the 5,11-dodecyl chains and 6,12-DCV units in **Br$_2$-IF-DCV-2a**. A later single crystal report by Usta and Kim *et al.* confirmed that the IF-DCV π-core (**IF-DCV-6** in Fig. 15, *vide infra*) could be highly coplanar when alkyl substituents are removed from the central benzene ring.[66] The single crystals of **IF-DCVs-2a-Br$_2$**, **3a-Br$_2$**, and **IF-DCV-6** are the only (bis)IF-DCV structures reported to date.

3.4. DCV functionalization for ambient stable electron transport in OFETs

Among the semiconductors, top-contact/bottom-gate OFETs (p^{++}-Si/SiO_2/OTS/semiconductor/Au) fabricated by spin-coating an **IF-DCV-4a** solution in chloroform exhibited an ambient stable electron mobility of 0.16 $cm^2\ V^{-1}\ s^{-1}$ with a very high I_{on}/I_{off} of 10^7–10^8 and a very low threshold voltage of ∼0 V. **IF-DCV-4a** with excellent performance was one of the early examples of truly ambient-stable, solution-processed n-type semiconductors, and it was mentioned to reflect a combination of enhanced intra/inter-molecular π-orbital overlaps, edge-on molecular orientation on the dielectric surface, and highly textured thin films with micron-sized grains. The solution-processed thin films of low band gap (E_g = 1.3–1.4 eV) semiconductors **IF-DCV-4b** and **IF-DCV-P2b** were reported to exhibit ambient stable ambipolar semiconductor behaviors with electron and hole mobilities of 10^{-4}–10^{-3} $cm^2\ V^{-1}\ s^{-1}$ (I_{on}/I_{off} = 10^4). These compounds were also the first examples of highly soluble ambipolar organic semiconductors in the optoelectronics literature that could operate under ambient conditions. As shown in Fig. 12, based on the analysis of the operational ambient stabilities for the large library of OFETs fabricated in this study, the authors suggested that the ambient stability for thermodynamically predicted (*i.e.*, no kinetic barrier contribution) organic semiconductors was mainly governed by LUMO energetics with minimal contribution from thin-film microstructures, and the onset LUMO energy for carrier electron stabilization was precisely predicted to be −4.1 eV. These results were consistent with previous studies[76,77] and had been critical to the development of new ambient-stable n-type semiconductors over the years in the past decade.

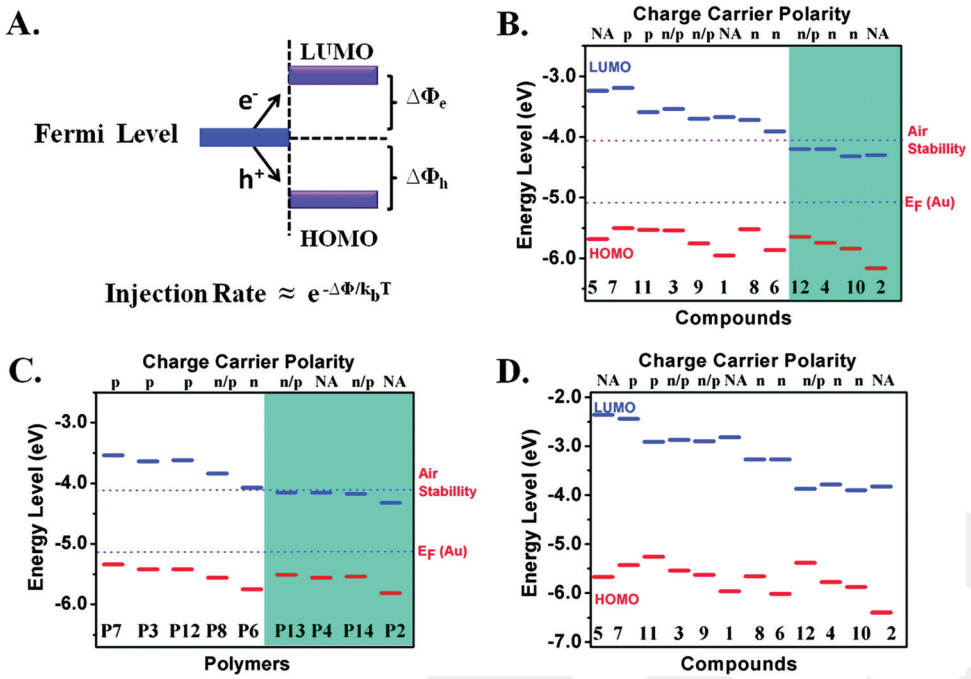

Fig. 12 (A) Illustration of a Schottky-type injection barrier for metal–organic semiconductor contacts and the corresponding electron ($\Delta\Phi_e$)/hole ($\Delta\Phi_h$) injection barriers. The experimental (B and C) and theoretical (D) frontier orbital energy diagrams for carbonyl- and dicyanovinylene-functionalized (bis)indenofluorene-based semiconducting small molecules (B and D) and polymers (C), and the major charge carrier polarities. The green regions indicate the OFET devices showing air stability, and the dashed lines indicate the Au-Fermi level and the estimated air-stability threshold.[67] Reprinted with permission from ref. 67. Copyright 2009, American Chemical Society.

The findings that considerably low LUMO energies (<−4 eV) and great electron injection/transport efficiencies could be achieved in quinoidal oligothiophenes and (bis)IFs by using DCV functional groups have been followed in the past decade by the development of new DCV-based acceptors for use in fullerene-free BHJ-OPVs. Today, some of the highest performing (power conversion efficiencies >15%) non-fullerene acceptors include dicyanovinylene end-units (*e.g.*, ITIC, Y6 derivatives)[78,79] as one of the critical parts of their molecular structures.[80,81] With regard to the development of high performance non-fullerene acceptors, dicyanovinylene groups have been crucial for lowering the LUMO energy level, promoting intramolecular charge-transfer, and extending optical absorption.[13] Despite their high performances in OFETs, BHJ-OPVs are yet to be reported with the particular (bis)IF-DCV semiconductors reviewed in this section. This is due to two main reasons: (i) some (bis)IF-DCVs have too low (<−4.1 eV) LUMO energy level to affect open circuit voltage and (ii) (bis)IF-DCVs exhibit strong crystallization behavior in the thin-film phase to form large micron-sized domains exceeding typical exciton diffusion lengths.[82,83]

3.5. Optimization of the alkyl chain position

Recently, Usta and Kim *et al.* reported two new semiconducting molecules, **IF-DCV-5a**[70] and **IF-DCV-5b**[69] (Fig. 10), based on IF-DCV π-acceptor central units. These molecules were solution-processable and exhibited ultralow band gaps ($E_g^{\text{solid-state}}$ = 1.2–1.35 eV). These molecules have D–A–D type π-scaffolds and share the same π-backbone as **IF-DCVs-4a** and **IF-DCVs-4b**, respectively, with the difference of employing alkyl chains at the molecular termini (α,ω-) instead of β-positions. In order to ensure good solubility in common organic solvents, swallow-tailed 2-octyldodecyl substituents were needed instead of typical linear alkyl chains used in β-substituted IF-DCVs. The concentration-dependent (1 → 16 mg mL^{-1}) ^{1}H NMR study for both molecules in chloroform solution indicated strong shielding effects for the aromatic/α-methylene protons upon increasing the concentration, which suggested a strong tendency for molecular stacking, even in solution, *via* intermolecular π–π/donor–acceptor interactions. **IF-DCV-5a** is a liquid crystalline (LC) semiconductor that formed the characteristic fan-shaped texture of a hexagonal columnar LC phase over a wide temperature range (ΔT = 90–130 °C) (Fig. 13). Although both molecules exhibited very low LUMO energies of −4.19 eV (**IF-DCV-5a**) and −4.23 eV (**IF-DCV-5b**), the HOMO level of **IF-DCV-5b** (E_{HOMO} = −5.49 eV) was higher than that of **IF-DCV-5a** (E_{HOMO} = −5.64 eV) as a result of the presence of additional thiophene π-donor end units. Therefore, while **IF-DCV-5a** functioned as an n-channel semiconductor, **IF-DCV-5b** was an ambipolar semiconductor; and the OFETs based on both semiconductors exhibited excellent ambient stabilities.

Spin-coated films of **IF-DCV-5a** exhibit micron-sized (∼0.5–1.0 μm) highly crystalline 2D plate-like grains even upon annealing at a temperature of 50 °C whereas crystallization for **IF-DCV-4a** required far higher temperatures (150 °C). Low-temperature annealed top-contact/bottom-gate OFETs (on an

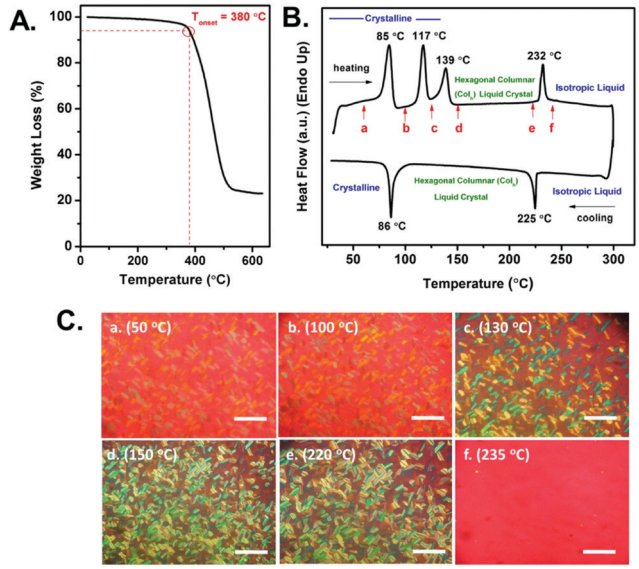

Fig. 13 (A) Thermogravimetric analysis (TGA) and (B) differential scanning calorimetry (DSC) of **IF-DCV-5a** at a temperature ramp of 10 °C min^{-1} under nitrogen. (C) Optical images taken under the conditions of 90° cross-polarization as a function of temperature (a–f); scale bars are approximately 100 μm.[70] Reprinted with permission from ref. 70. Copyright 2017, Wiley-VCH.

n^{++}-Si/SiO$_2$/PS-brush) showed a good electron mobility of 0.11 cm^2 V^{-1} s^{-1} along with high I_{on}/I_{off} ~ 10^7–10^8 and excellent ambient stability. As shown in Fig. 14, LC-state annealing of the **IF-DCV-5a** thin-film decreased the electron mobility by ~10 000× due to unfavorable microstructural/morphological changes in the semiconductor–dielectric interface during cooling from the LC-state. Top-contact/bottom-gate OFETs (on an n^{++}-Si/SiO$_2$/PS-brush) employing solution-sheared **IF-DCV-5b** films exhibited an ambient-stable ambipolar behavior with an electron mobility of 0.13 cm^2 V^{-1} s^{-1} and a hole mobility of 0.01 cm^2 V^{-1} s^{-1} (I_{on}/I_{off} = 10^3–10^4). Complementary-like inverter circuits were also demonstrated to function under ambient conditions with a voltage gain of 30 V/V. Due to the presence of a strong IF-DCV π-acceptor unit and highly coplanar D–A–D type π-electronic structure, **IF-DCV-5b** has still one of the lowest band gaps among all molecular semiconductors reported to date.

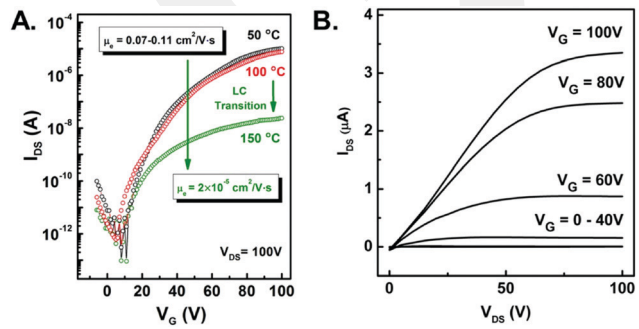

Fig. 14 (A) Transfer curves measured for the top contact/bottom gate OFETs based on the solution-processed thin films of **IF-DCV-5a** annealed at 50, 100, and 150 °C. (B) Output curves of the OFET device fabricated at an annealing temperature of 50 °C.[70] Reprinted with permission from ref. 70. Copyright 2017, Wiley-VCH.

Another family of [1,2-*b*]IF-DCVs (**IF-DCVs-10a** and **-10b** in Fig. 10) with an electron deficient central pyrazine ring instead of a benzene ring and alkyl substituents at 2,8-positions was developed by Yamashita *et al.*[57] While dihexyl-substituted IF-DCV **IF-DCV-10a** was not soluble in organic solvents, its *t*-butyl-substituted counterpart **IF-DCV-10b** could be dissolved in common organic solvents. The cyclic voltammetry data for **IF-DCV-10b** showed a good electron accepting ability with the first half-wave reduction potential of −0.22 V and the corresponding low-lying LUMO level of −4.15 eV. The thin-film XRD analysis of **IF-DCV-10a** showed that the molecules adopt an edge-on orientation relative to the dielectric surface with a 35° tilting angle. The OFETs utilizing vapor-deposited **IF-DCV-10a** thin-films on bare Si/SiO$_2$ showed an initial μ_e of 1.1 × 10^{-2} cm^2 V^{-1} s^{-1} (I_{on}/I_{off} = 10^6 and V_{th} = 25 V) with moderate air stability (μ_e decreases to 1.7 × 10^{-3} cm^2 V^{-1} s^{-1} after 3 hours). However, the thin-films of **IF-DCV-10b** were found to be amorphous, which led to a relatively lower OFET performance (μ_e values of 3.3 × 10^{-4} cm^2 V^{-1} s^{-1} on Si/SiO$_2$/HMDS).

3.6. 2,8-Bis(ethynylation) approach

Although there are no reports on the OFET performance of the unsubstituted IF-DCV molecule **1**, Usta and Kim *et al.* very recently synthesized ethynylated IF-DCV derivative **IF-DCV-6** (Fig. 10) with triisopropylsilyl end-groups.[66] This molecule was substituted along the long molecular axis (2,8-positions), and stabilized (ΔE = 60–200 meV) HOMO/LUMO energies of −5.84/−4.18 eV were obtained as compared with thiophene terminated IF-DCVs (*e.g.*, **IF-DCV-4a** in Fig. 10), reflecting the higher electron deficiency of the new π-backbone (Fig. 8). As shown in Fig. 15, based on the single-crystal structure analysis, DCVs were found to be completely within the IF π-core plane, and the molecules formed a slipped π-stacked (3.47–3.88 Å) one-dimensional (1-D) columnar motif. Strong (Ar)C–H···N contacts (2.458 Å) (10.62% shortened from the van der Waals distance) were identified between neighboring molecules (four close interactions per molecule). Top-contact/bottom-gate OFETs (on an n^{++}-Si/SiO$_2$/PS-brush) fabricated using solution-sheared thin-films exhibited an ambient stable electron mobility of 0.02 cm^2 V^{-1} s^{-1} along with a high I_{on}/I_{off} ratio of 10^7–10^8 and a low threshold voltage of ~2 V, which was three orders of magnitude higher than that of its carbonyl-functionalized counterpart **IF-dione-10** (Fig. 2). These devices were found to be highly stable even after 3 months of ambient storage as a result of a highly stabilized LUMO energy level (< −4.1 eV). **IF-DCV-6** was reported to be the first example of an n-type molecule substituted with (trialkylsilyl)ethynyl groups on its long molecular axes. This study showed again that, when compared with carbonyl functionalities, DCVs on the IF π-backbone could yield more efficient electron transport characteristics.

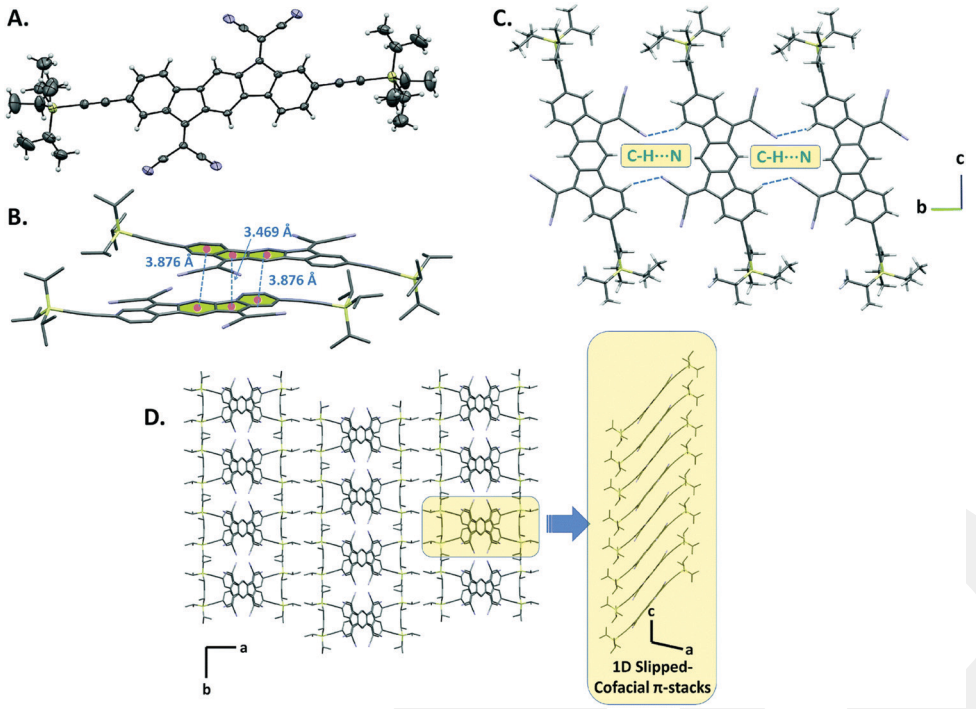

Fig. 15 (A) ORTEP drawing of **IF-DCV-6** (30% probability level) based on the single crystal structure. (B) Intermolecular π-interactions between IFDM cores arranged in a slipped π-stacked fashion and the favorable π···π distances of 3.469/3.876 Å. (C) The continuous π-layer arrangement *via* short CH···N contacts. (D) Perspective views of the molecular packing and one-dimensional slipped cofacial π-stacks along the *c*-direction.[66] Reprinted with permission from ref. 66. Copyright 2018, The Royal Society of Chemistry.

3.7. Dicyanovinylene functionalizations on the [2,1-*b*]IF regioisomer

DCV-functionalization on a completely different IF regioisomer was studied by Jacques and Poriel *et al.* by developing mono- and di-functionalized [2,1-*b*]IF-DCVs **IF-DCVs-8** and **IF-DCVs-9** (Fig. 10).[49] Based on the DFT-optimized geometries, and different than the [1,2-*b*]IF-DCVs, the di-functionalized [2,1-*b*]IF-DCV **IF-DCV-9** adopted a slightly twisted π-backbone with the DCV groups lying out of the IF π-plane (19.8° dihedral angle between DCV π-planes). This was caused by the steric congestion between cyano groups pointing towards each other on the same side of the [2,1-*b*]IF π-core. The DFT-optimized **IF-DCV-8** geometry indicated that when one of the DCV functional groups was replaced with carbonyl the π-backbone became completely planar. The optical band gaps of **IF-DCVs-8** and **IF-DCVs-9** (E_g ~ 2.1–2.2 eV) were found to be much smaller than that of their nonfunctionalized parent compound [2,1-*b*]IF (E_g = 3.62 eV), which was due to significant stabilizations of LUMO and HOMO energies with a larger magnitude in the former. The LUMO energies determined from the electrochemical measurements were −3.93 eV for **IF-DCV-8** and −3.81 eV for **IF-DCV-9**. The semiconducting characteristics of **IF-DCVs-8** and **IF-DCVs-9** were measured in bottom-contact/bottom-gate OFETs (glass/Al(gate)/SU-8(dielectric)/Au(S-D)/semiconductor) by depositing the semiconductor layers *via* thermal evaporation. Both molecules showed n-type charge transports under a nitrogen atmosphere with electron mobilities of 4.6×10^{-6} cm^2 V^{-1} s^{-1} (for **IF-DCV-8**) and 1.02×10^{-3} cm^2 V^{-1} s^{-1} (for **IF-DCV-9**). The low V_{th} (7.2 V), high I_{on}/I_{off} ratio (10^5–10^6), and excellent electrical stress stability allowed the incorporation of **IF-DCV-9**-based n-channel OFETs in an integrated circuit, and pseudo-CMOS inverters were fabricated yielding R_{DSon}/R_{DSoff} of 1.5×10^3.

3.8. IF-TTFs for DSSCs and OFETs

Similar to the DCV-functionalized IFs in which the π-system is extended through the sp^2-hybridized bridge carbons in the lateral molecular direction, the indenofluorene core has also been used as a π-spacer to extend the redox-active tetrathiafulvalene (TTF) π-system, resulting in so-called indenofluorene-extended TTFs (**IF-TTF-1a**, **1b** in Fig. 10). In a very recent study by Nielsen and Freitag *et al.*,[74] this was carried out by positioning two hexylthio-substituted dithiafulvalenes at the IF bridge carbons. These molecular scaffolds were synthesized by a Sonogashira cross-coupling reaction between mono-iodo-functionalized IF-TTF and a benzoic acid acceptor moiety containing a terminal alkyne. While a benzoic acid moiety was used as an acceptor for anchoring the carboxylic acid end-groups onto a TiO_2 electrode of dye-sensitized solar cells (DSSCs), these molecules were synthesized without **IF-TTF-1a** or with **IF-TTF-1b** as an additional benzothiadiazole (BTA) acceptor. Thus, these molecules have a donor–acceptor π-architecture, in which the IF-TTF part acted as a strong donor making these molecules potential π-conjugated sensitizers with strong absorptions in the visible region and two reversible one-electron oxidations.[84–86] According to computational data, IF-TTFs exhibit good coplanarity between their IF-TTF and

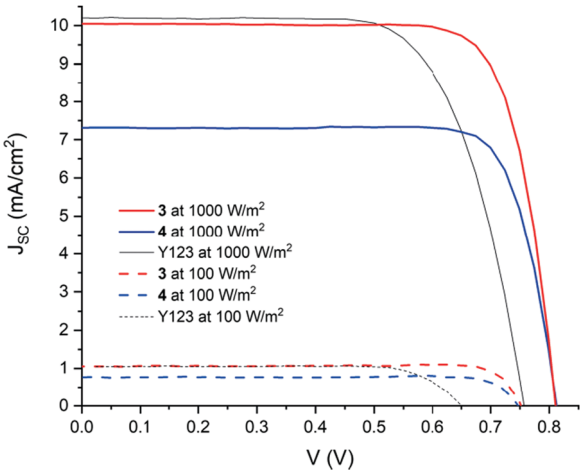

Fig. 16 Current density (J_{sc}) *vs.* applied potential (V) curves of DSSCs (using I^-/I_3^- based electrolyte) fabricated with **IF-TTF-1a** (4 in the figure) and **IF-TTF-1b** (3 in the figure) dyes in comparison to a well-known dye Y123 without the IF π-core under ′AM1.5G illumination.[74] Reprinted with permission from ref. 74. Copyright 2020, Wiley-VCH.

acceptor moieties. Similar to the TTF itself, the ester derivatives of **IF-TTF-1a,b** show two reversible one electron oxidations with the first oxidation peak at 0.32 V. In this study, the authors reported the highest performing IF-based DSSCs in the literature with a power conversion efficiency value of 6.4% (for **IF-TTF-1b** at 100 mW cm^{-2} under ′AM1.5G illumination) along with a V_{oc} of 0.81 V, J_{sc} of 10.1 mA cm^{-2}, and FF of 81% (Fig. 16), which increased to 7.1% at 10 mW cm^{-2} under ′AM1.5G illumination. The molecule without the BTA unit (**IF-TTF-1a**) showed a slightly lower PCE value of 4.8–5.0% (Fig. 16).

This study also demonstrated that mono-iodo-functionalized IF-TTFs are open to Pd-catalyzed coupling reactions rendering these architectures attractive for future structural modifications by allowing facile introduction of diverse acceptors and tuning of optoelectronic properties. We note that these DSSC performances were higher than those previously reported by Lin *et al.* in 2012 with tetraalkyl-substituted dihydro[1,2-*b*]IFs **DH-IF-10a–c** (Fig. 25). In these molecules, DH-IF was used as a π-spacer between diphenylamine donor and cyanoacetic acid acceptor units resulting in a donor–π-spacer–acceptor motif as a potential π-sensitizer for use in DSSCs.[87] The rationale behind this molecular engineering approach is that the DH-IF π-core could provide coplanar bridging and extended π-conjugation, leading to a broad and strong absorption band and efficient communication between donor and acceptor moieties. Thiophene and furan units were also used in **DH-IF-10b,c** to further extend the π-spacer conjugation. The alkyl substitutions at the bridge carbons provided good solubility and processability. These molecules showed optical absorption bands at ∼300 nm stemming from the IF-based localized π–π* transitions, which were accompanied by broader π–π* transitions with charge-transfer characters at 408–430 nm. Molecular orbital computations indicated that there is a spatial separation between the HOMOs mainly residing on the donor–π-spacer part and the LUMOs mainly localized on the π-spacer–acceptor part, leading to a charge-transfer character. The DSSCs fabricated utilizing these sensitizers were all active with the best performance achieved for **DH-IF-10c** (PCE of 4.05%, V_{oc} of 0.71 V, J_{sc} of 8.20 mA cm^{-2}, and FF of 70%).

Tetrathiafulvalene (TTF)-functionalized IFs also offer an electron-rich π-system for hole-transport in OFETs. However, there has been a very limited report on this to date. In the only known report to our knowledge, Dong *et al.*[88] studied the single crystal-based OFETs of a TTF-functionalized IF molecule, **IF-TTF-2** (Fig. 10). This molecule was originally synthesized by Neilsen *et al.*[89] and could be viewed as that the IF π-system is extended through the sp^2-hybridized bridge carbons in the lateral molecular direction. The experimental HOMO and LUMO energies were measured to be −4.64 eV and −2.09 eV, respectively. Similar to TTF itself, **IF-TTF-2** showed crystal polymorphism depending on the solvent used in crystal formation. While α-phase ribbon crystals were obtained from chloroform, β-phase platelet crystals were obtained from toluene. According to the single-crystal structure analysis, in α phase crystals, one **IF-TTF-2** molecule is surrounded by six neighboring molecules *via* strong π···π, S···S, H···H, and C–H···π interactions with an interlayer π···π stacking distance of 3.38 Å. On the other hand, in β phase crystals, one **IF-TTF-2** molecule is surrounded by six neighboring molecules through H···H, and C–H···π interactions with a relatively larger interlayer π···π stacking distance of 3.52 Å. Top-contact/bottom-gate OFETs (on Si/SiO_2/OTS) were fabricated using both single crystal phases, and maximum hole mobility values of 1.44 cm^2 V^{-1} s^{-1} for the α-phase and 0.28 cm^2 V^{-1} s^{-1} for the β phase were achieved under ambient conditions with relatively large I_{on}/I_{off} ratios (10^4–10^5) and threshold voltages below −5 V. The relatively larger hole mobility attained from the α-phase is assigned to the more condensed molecular packing structure in this phase compared to that in the β-phase. Theoretical calculations further confirmed this difference by showing a much larger transfer integral (119.43 meV) for the α-phase, as compared to the β-phase (4.53 and 2.77 meV).

4. Fully conjugated indenofluorenes (π-IFs)

4.1. Brief introduction of an antiaromatic 20 π-electron π-IF system as an electron acceptor

π-Electron rich indenofluorene compounds having sp^2 hybridized methine bridges at the five-membered rings that are in direct conjugation with the IF π-scaffold are classified as fully conjugated indenofluorenes (π-IFs). They have one of the most interesting π-topologies among polycyclic conjugated hydrocarbons (PCHs) with a quinoidal bonding pattern in the central tricyclic indacene subunit. Since indacene is a highly reactive moiety and it could only be kinetically stabilized with bulky substituents (*e.g.*, *t*-butyl),[90] π-IFs developed to date are typically substituted on their bridge methines in the lateral molecular direction. However, one should note that unprotected (*i.e.*, no

substituent on the indacene subunit) π-IF polymers, which could not be prepared with conventional solution-based synthesis, have recently been developed by employing an on-surface synthesis approach on Au(111) substrates.[91,92] Although transistor or solar cell devices were not reported with these polymers, the importance of attaining unprotected IF units with this technique is to investigate in depth the unique electronic properties of fully conjugated IF polymers, especially open-shell *vs.* close-shell configurations, with varied regioisomers for carbon-based spintronic circuits.[93] π-IFs are formally antiaromatic compounds ([4*n*] π-electrons according to Hückel's rule)[94] with 20 π-electrons. This confers them the tendency of accepting electrons, especially on the central six-membered ring, to form a 22 π-electron system having fully aromatic subunits, which yields significant changes in the electronic and crystal structures (Fig. 17A).[95] For example, when **π-IF-4a** (Fig. 18) is reduced with potassium metal in THF-d_8 in the presence of 18-crown-6, the hydrogen atoms located on position 1 (Fig. 17B) showed a significant downfield shift of ~1 ppm (*i.e.* deshielding) indicative of the newly introduced diatropic ring current of the 22 π-electron system of **π-IF-4a**$^{2-}$. In addition, the ^{13}C NMR spectrum confirmed that the methine bridge carbons in **π-IF-4a**$^{2-}$ are significantly shielded (*i.e.*, increased electron density) showing an upfield shift of ~50 ppm compared to its neutral form.

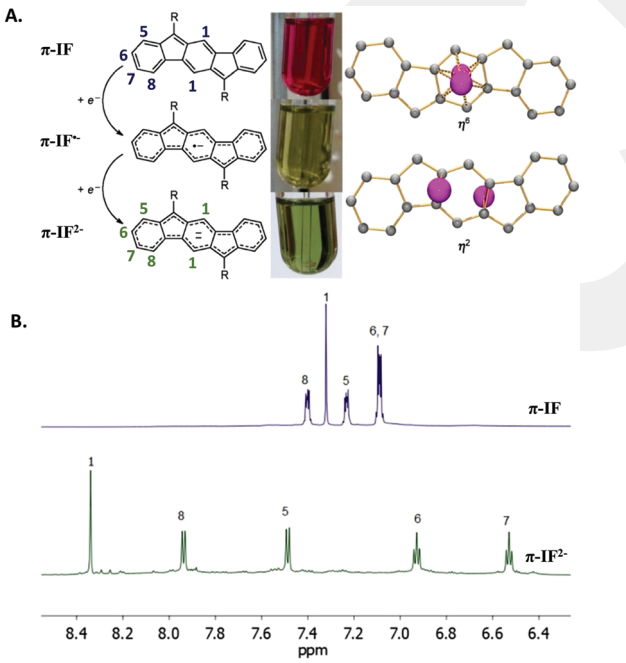

Fig. 17 (A) One- and two-electron reduction processes for a representative **π-IF** core, the corresponding solution colors for neutral (**π-IF**), anion radical (**π-IF**$^{\bullet-}$), and dianion (**π-IF**$^{2-}$) forms, and close-up views of **π-IF**$^{2-}$s in the single-crystal structure with Rb^+ ions (in pink) that are η^2- and η^6-coordinated to the central six-membered ring (hydrogens are omitted for clarity). (B) Partial ^{1}H NMR spectra of neutral **π-IF-4a** and dianion **π-IF-4a**$^{2-}$ in THF-d_8 with assigned hydrogen positions.[95] Reprinted with permission from ref. 95. Copyright 2014, American Chemical Society.

Based on the X-ray structural characterization studies of their neutral and reduced (di)anion structures, π-IFs typically exhibit a highly planar pentacyclic structure with a very small (<0.04 Å) root-mean-square deviation from the average molecular plane, which could yield very effective intramolecular π-delocalization and intermolecular π-interactions in the solid-state. Also, the quinoidal motifs within various π-IFs are typically evident by the strong single–double bond length alteration in their crystal structures. Interestingly, despite being π-electron rich and highly colored molecules, π-IFs are found to be nonemissive, a unique feature observed in polycyclic conjugated hydrocarbons with [4*n*] π-electron systems (*e.g.*, indacenodi(benzothiophene)s,[96] hexabenzoperylene,[97] B_2N_2-dibenzo[*a*,*e*]pentalenes,[98] and dibenzo[*a*,*e*]pentalenes[99]). Detailed photophysical studies revealed that π-IFs exhibit extremely short picosecond time-scale relaxation for $S_1 \rightarrow S_0$ electronic transition [9–12 ps $\ll$ ~1 ns (typical of fluorescence)].[100] Based on the quantum mechanical calculations, this was due to the result of fast $S_1 \rightarrow S_0$ electronic relaxation through conical intersection of potential energy surfaces crossing between the S_0 and S_1 states. This extremely short-lived exciton character in π-IFs may hamper the efficiency of exciton diffusion and charge transfer processes in BHJ solar cells.[82,83] Therefore, a fundamental question arises as to whether the performance improvements in non-fullerene cells could ever benefit from the optical absorption spectrum of π-IF-based acceptors. To the best of our knowledge BHJ solar cells using a π-IF-based acceptor are yet to be fabricated, however, a few studies have investigated the effect of LUMO energy offset, thin-film crystallinity, and side group chemical structures on the formation of charge-transfer exciton and charge photogeneration by using π-IF acceptor molecules **π-IF-4a** and **π-IF-8a** (Fig. 18).[101,102] Thus, considering the small number of studies conducted to date, it is reasonable to conclude that π-IF-based OPV acceptors require further research to understand and reveal their potential in photovoltaics. On the other hand, π-IFs stand out as an important class of quinoidal/antiaromatic molecular semiconductors recently developed for use in OFETs.[103] π-IFs have typically low-to-moderate ($\mu_{e,h}$ = 10^{-3}–10^{-5} cm^2 V^{-1} s^{-1}) charge carrier mobilities, and the good performance (μ_h = 0.44–0.64 cm^2 V^{-1} s^{-1} and μ_e = 0.34 cm^2 V^{-1} s^{-1}) OFETs are based on extended π-IF systems (*i.e.*, **π-IF-13** in Fig. 18).[96,104] Therefore, the development of high performance ($\mu_{e,h} \geq$ 0.5 cm^2 V^{-1} s^{-1}) π-IF semiconductors for OFETs also requires further research efforts.

The chemical structures of the π-IF-based semiconductors reviewed in this section are shown in Fig. 18 with the corresponding optoelectronic properties and device performance metrics listed in Table 3.

4.2. Early examples of π-IFs

When we looked at the synthetic approaches to π-IFs, we realized that they were extremely scarce prior to the early reports in the mid-1990s by Swager *et al.*[42] and Scherf *et al.*[43] As the only known example, Le Berre *et al.* developed π-[2,1-*a*]IF compound **π-IF-5a** (Fig. 18) in 1957, which was highly reactive towards oxygen.[105] In 1994, Swager *et al.* synthesized π-[1,2-*b*]IF compound **π-IF-1** (Fig. 18) as a purple solid *via* the transannular

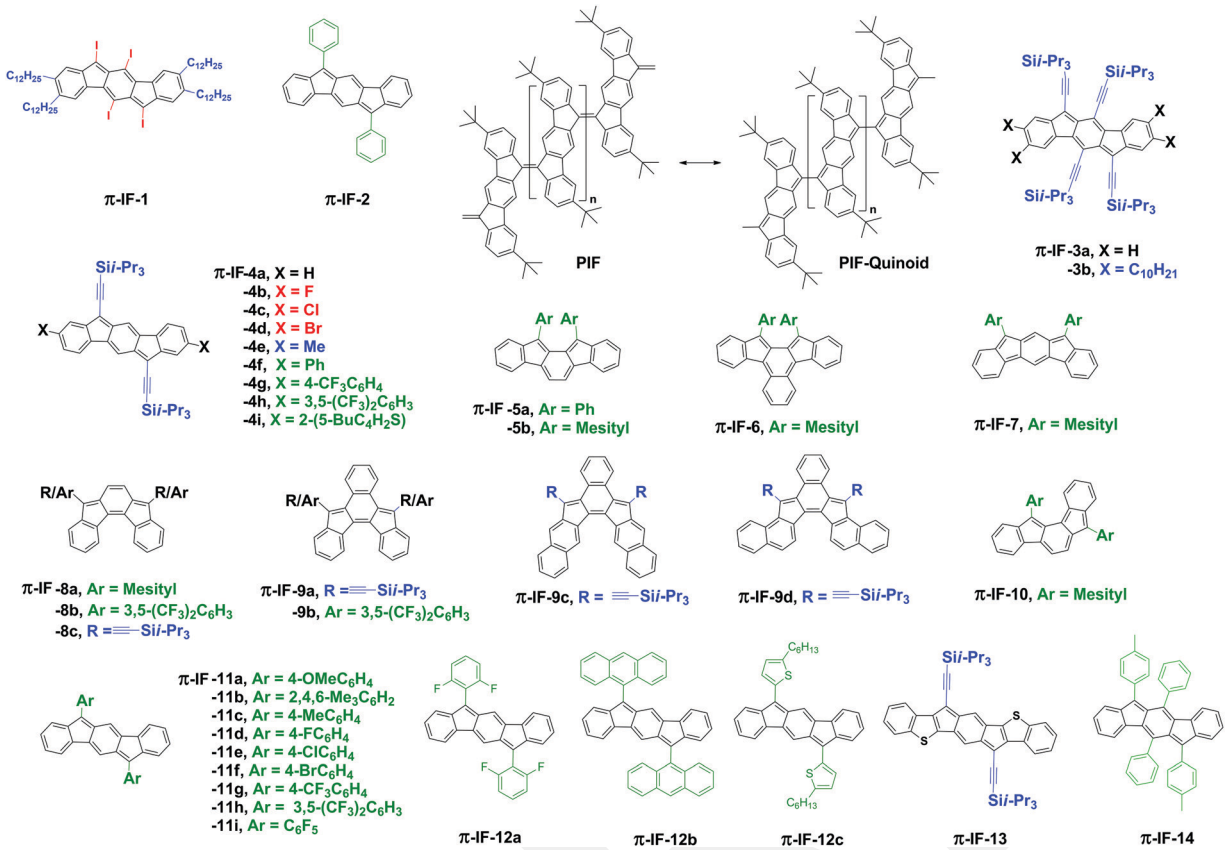

Fig. 18 Chemical structures of fully conjugated indenofluorene (π-IFs)-based semiconductors **π-IFs-1–14** and **PIF/PIF-quinoid**.

Table 3 Summary of experimental HOMO/LUMO energies (or oxidation/reduction potentials (E_{ox}/E_{red})), optical absorption maximum, and optical band gap values for π-IF-based semiconductors, and the (opto)electronic device type and representative organic field-effect transistor (OFET)/bulk-heterojunction organic photovoltaics (BHJ-OPVs) performance values [field-effect mobility for electrons and/or holes (μ_e, μ_h), current on/off ratio (I_{on}/I_{off}), power conversion efficiency (PCE), and open-circuit voltage (V_{oc})] in the corresponding literature

Year	Semiconductor	HOMO/LUMO[a] [eV] or E_{ox}/E_{red}[a] [V]	λ_{max}^{abs} [b] [nm]	E_g^{opt} [c] [eV]	Opto(electronic) device type[d,e]	Performance (μ_e, μ_h [$cm^2\ V^{-1}\ s^{-1}$] (I_{on}/I_{off}) or PCE [%], V_{oc} [V])	Ref.
2012	π-IF-11i	−6.17/−4.00	533	2.20	p/n-OFET (single-crystal)	$\mu_e = 3 \times 10^{-3}$ $cm^2\ V^{-1}\ s^{-1}$ (10^4) $\mu_h = 7 \times 10^{-4}$ $cm^2\ V^{-1}\ s^{-1}$ (10^5)	116
2012	π-IF-2	+0.97/−1.00	542	2.01	p-OFET (thermal evap.)	$\mu_h = 1.6 \times 10^{-5}$ $cm^2\ V^{-1}\ s^{-1}$ (60)	119
	π-IF-12a	+1.18/−0.88 (*vs.* SCE)	529	2.34	p/n-OFET (thermal evap.)	$\mu_e = 8.2 \times 10^{-6}$ $cm^2\ V^{-1}\ s^{-1}$ (10) $\mu_h = 1.9 \times 10^{-5}$ $cm^2\ V^{-1}\ s^{-1}$ (10)	
	π-IF-12b	+1.07/−1.05 (*vs.* SCE)	522	2.20	p/n-OFET (thermal evap.)	$\mu_e = 1.6 \times 10^{-6}$ $cm^2\ V^{-1}\ s^{-1}$ (100) $\mu_h = 1.1 \times 10^{-5}$ $cm^2\ V^{-1}\ s^{-1}$ (30)	
2016	π-IF-13	−5.61/−4.18	682	1.75	p-OFET (spin coat.)	$\mu_h = 0.44$ $cm^2\ V^{-1}\ s^{-1}$ (10^3)	96
2016	π-IF-13	−5.46/−4.27	682	1.19[f]	p/n-OFET (single crystal)*	$\mu_e = 0.34$ $cm^2\ V^{-1}\ s^{-1}$ (10) $\mu_h = 0.64$ $cm^2\ V^{-1}\ s^{-1}$ (10^2)	104
2017	π-IF-14	−5.37/−3.26	557	2.23	BHJ-OPV (thermal evap.)	PCE = 2.91% $V_{oc} = 0.94$ V	123

NR: the corresponding value is not reported in the reference. [a] Measured *via* cyclic voltammetry and estimated based on using the vacuum energy level of the reference electrode. [b] Measured in solution as the low-energy optical absorption maximum. [c] Measured in solution from the low-energy optical absorption edge. [d] Active layer deposition method is given in parentheses. [e] The n-OFET devices measured under ambient conditions are shown with an asterisk (*). [f] Measured *via* cyclic voltammetry.

cyclization reaction (Scheme 1) of a macrocyclic diacetylene molecule **π-IF-1-precursor** with I_2 in benzene in 50–70% yield. Although the chemical stability of **π-IF-1** was relatively good in the solid state, this 20π electron system was found to be highly sensitive to ambient conditions in solution. The solution was oxidized under aerobic conditions (reaction time ~1 h) to produce **IF-dione-2** (Fig. 3) in 60–95% yield (Scheme 1). The other early example of the π-IF molecule, **π-IF-2** (Fig. 18), was

reported by Scherf *et al.* two years later[43] as a model compound for the "quinoid subunit" present in their novel low band gap (E_g = 1.55 eV) polymer polyindenofluorene (**PIF**) (Fig. 18). In this study, the researchers revealed that the quinoid state dominates the electronic ground state of **PIF** and acts as the key chromophore in this polymeric π-system. Although the synthesis of this compound was not disclosed, **π-IF-2** was reported to exhibit an optical band gap of 2.28 eV (λ_{max}^{abs} = 543 nm). Surprisingly, after these two reports, no novel π-IF systems were developed until 2011.

4.3. 6,12-Bis(ethynylation) approach

The early substitution strategy employed for π-IFs to chemically stabilize the indacene subunit was trialkylsilylethynylation at the 6,12-positions. To this end, Haley *et al.* developed the first examples of well-characterized fully conjugated indenofluorene molecules **π-IF-3a**, **π-IF-3b**, and **π-IFs-4a–i** (Fig. 18) in 2011, which were all based on the [1,2-*b*] regioisomeric form.[106,107] In these compounds, additional π-core substitutions at the peripheral positions were also studied. As shown in Scheme 4, synthesis of the π-[1,2-*b*]IF framework in **π-IF-3a**, **π-IF-3b**, and **π-IFs-4a–i** relied on the addition of a lithiated trialkylsilylethynyl reagent to a substituted indeno[1,2-*b*]fluorenedione π-core to afford first a crude diol intermediate (**π-IFs-4a–i-diol** in Scheme 4), which then underwent a subsequent reduction in toluene solution with $SnCl_2$. Changing depending on the substituents, the two-step reaction yield was 31–81% for **π-IFs-4a–i**. Since indeno[1,2-*b*]fluorenedione starting compounds **X_2-IF-dione** with different substituents could be easily prepared in the multigram scale, this route was found to be superior to the transannular cyclization route previously used in the mid-1990s.[42,107]

In their first study, Haley *et al.* developed **π-IF-3a** and **π-IF-3b** to realize a novel fully conjugated semiconductor structure with improved stability to benchmark pentacene derivatives.[108] Thus, **π-IF-3a** and **π-IF-3b** showed optical band gaps of 1.98 eV and 1.91 eV, respectively, which are close to that of TIPS-substituted pentacene (E_g^{opt} = 1.85 eV). However, different than pentacene derivatives, these molecules were non-emissive as a result of their [4*n*] π-system and their solutions were found to be stable in air and ambient light over a few weeks. The single-crystal structure analysis of **π-IF-3a** showed that the π-[1,2-*b*]IF core is planar (deviation rms = 0.013 Å) showing strong C–C bond length alterations (1.44–1.46 Å for single bonds and 1.37–1.39 Å for double bonds) in the central *p*-quinodimethane unit (*i.e.*, the antiaromatic subunit of the central *s*-indacene part) while the peripheral benzene rings have reduced bond length alternation (1.39–1.41 Å). The nucleus independent chemical shift (NICS) calculations were found to coincide well with crystallographic data revealing, for the first time, that π-[1,2-*b*]IF is antiaromatic with a quinoidal structure in the central *s*-indacene subunit and aromatic peripheral benzene rings. **π-IF-3a** exhibited a herringbone arrangement in the solid state with an average packing distance of 3.93 Å, a commonly observed packing motif in unsubstituted acenes.[33] In their second study,[107] Haley *et al.* synthesized a series of **π-IFs-4a–i** ([1,2-*b*] regioisomer) (Fig. 18) having triisopropylsilylethynyl groups at the 6,12-positions and different substituents at the 2,8-positions. These π-[1,2-*b*]IFs were found to be non-emissive and showed a small variation in their optical band gaps (2.08–2.15 eV) with the change of substituents. Cyclic voltammograms in Fig. 19 showed that **π-IFs-4a–i** exhibited quasi-reversible reduction behaviors accepting two electrons. The first reduction half-wave potentials were surprisingly low at −0.52 V to −0.69 V (*vs.* SCE), which indicated a comparable or even greater electron affinities and low-lying LUMOs when compared with well-known electron-acceptors such as [6,6]-phenyl C61 butyric acid methyl ester ($PC_{61}BM$).[109] We note that achieving such strong electron accepting characteristics without having electron withdrawing functional groups or substituents is very unique in the organic semiconductor literature,

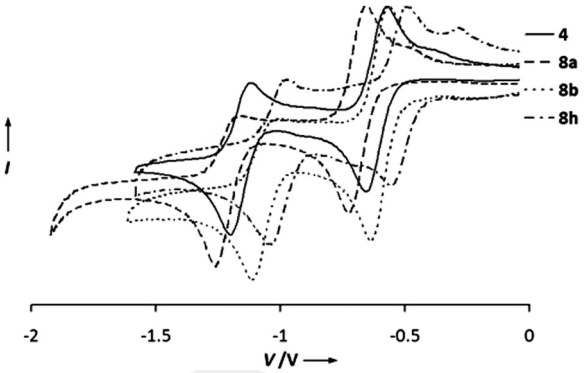

Fig. 19 Cyclic voltammograms of **π-IF-3a** (4 in the figure), **π-IF-4a** (8a in the figure), **π-IF-4b** (8b in the figure), and **π-IF-4h** (8h in the figure) showing normalized reduction peaks.[107] Reprinted with permission from ref. 107. Copyright 2011, Wiley-VCH.

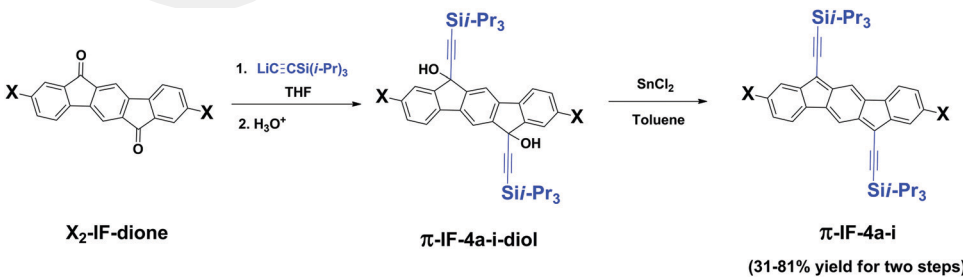

Scheme 4 Synthesis of **π-IFs-4a–i** from the corresponding IF-diones.[107]

and it reflects the strong electronic tendency of these π-[1,2-*b*]IFs to reach [4*n* + 2] ([22] π-electrons) aromatic dianion π-structures. In this study,[107] it was also revealed that the incorporation of electron withdrawing substituents at the 2,8-positions caused the reduction half-wave potentials to be less negative, most likely by stabilizing the dianion reduction products. However, an opposite trend was found for the oxidation half-wave potentials of **π-IFs-4a–i** (1.20–1.35 eV *vs.* SCE), which resulted in the destabilization of the π-[1,2-*b*]IF dication products. Electrochemical band gaps were estimated to be 1.85–1.94 eV, which are in the range of the estimated optical band gaps.

The single-crystal structure analysis of **π-IF-4b** and **π-IF-4h** showed 1D π-stacking arrangements with close C···C contacts of ∼3.4 Å. π-[1,2-*b*]IF fused ring systems in both compounds were essentially planar (deviation rms = 0.017–0.042 Å) and C–C bond length alterations in the central *p*-quinodimethane core due to the quinoidal electronic structure were retained (Fig. 20). On the other hand, the peripheral aryl groups in **π-IF-4h** positioned nearly coplanar with the π-[1,2-*b*]IF core with a slight twist angle of 5.5°.

4.4. [2,1-*a*] π-IF regioisomer

In the same year when **π-IFs-4a–i** (Fig. 18) were developed based on the [1,2-*b*] regioisomer, Tobe *et al.* developed an air-stable fully conjugated IF molecule, **π-IF-5b** (Fig. 18), which was based on the regioisomeric form of π-[2,1-*a*]IF and substituted with dimesityl units at the 11,12-positions.[110] On the basis of the X-ray single crystal analysis, the π-[2,1-*a*]IF core was found to be almost planar and the two mesityl units are twisted out of the IF plane with large dihedral angles of ∼70°. Unlike [1,2-*b*]IFs having *p*-quinodimethane units embedded in the *s*-indacene core, the detailed examination of the crystallographic bond lengths, along with theoretical calculations, suggested that the electronic structure of **π-IF-5b** should be described as a combination of Kekule and singlet biradical canonical structures (Scheme 5). The optical absorption spectrum exhibited low-energy bands at 537 nm/730 nm, indicating a low optical band gap of 1.70 eV. Similar to π-[1,2-*b*]IFs, **π-IF-5b** was also non-emissive. The cyclic voltammogram of this molecule exhibited two reversible redox peaks ($E_{ox}^{1/2}$ = + 0.59 V and $E_{red}^{1/2}$ = −1.51 V (*vs.* Fc/Fc$^+$)).

Tobe *et al.* also developed another fully conjugated IF molecule (**π-IF-6** in Fig. 18) by extending the π-framework of the π-[2,1-*a*]IF in **π-IF-5b** along the lateral molecular axis with an additional benzene ring.[111] Single crystal analysis revealed that the extended backbone of **π-IF-6** was planar and the mesityl units were positioned out of the IF plane with large dihedral angles of ∼70°. Similar to **π-IF-5b**, the electronic structure of **π-IF-6** could be described as a combination of Kekule and singlet biradical canonical structures. As depicted in Scheme 5, on the basis of theoretical calculations, the radical centers could be located at the methylenes of the five-membered rings (singlet biradical structure-1) and on the inner naphthalene ring (singlet biradical structure-2). The optical absorption spectrum exhibited bathochromically shifted low-energy bands at 697 nm/1050 nm, due to its extended π-conjugation and greater singlet biradical character. On the basis of the cyclic voltammogram data, **π-IF-6** underwent easier oxidation and reduction processes than **π-IF-5b** with $E_{ox}^{1/2}$ of 0.38 V and $E_{red}^{1/2}$ of −1.22 V.

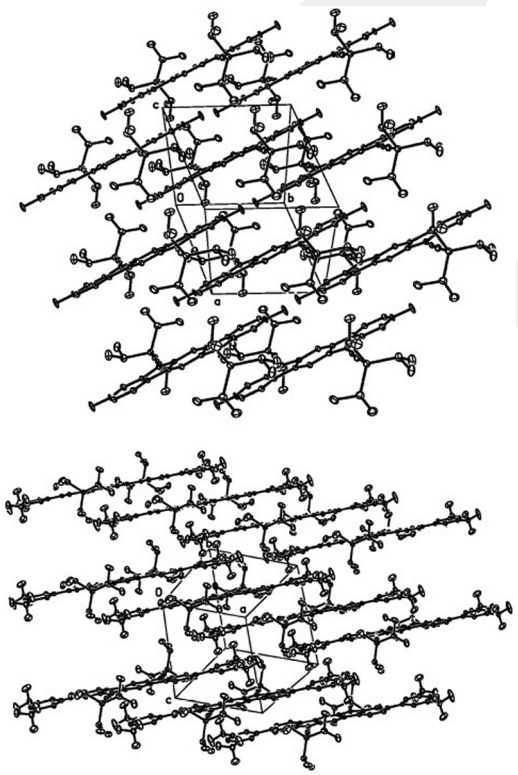

Fig. 20 Single crystal structures and packings of **π-IF-4b** (top) and **π-IF-4h** (bottom) with thermal ellipsoids drawn at the 30% probability level.[107] Reprinted with permission from ref. 107. Copyright 2011, Wiley-VCH.

4.5. [2,1-*b*] and [2,1-*c*] π-IF regioisomers

The same research group also developed [2,1-*b*] regioisomer **π-IF-7** (Fig. 18) having a *m*-quinodimethane unit, which showed a very low-energy optical absorption band at ∼850–2000 nm as a result of its larger singlet biradical character (y = 0.68) when compared with that of π-[2,1-*a*]IF derivatives (y = 0.33) having an *o*-quinodimethane unit.[112] The calculated spin density distribution of the π-[2,1-*b*]IF core indicated large amplitudes at bridge methylenes. The fourth regioisomer of fully conjugated indenofluorenes was developed by Haley *et al.*, which was a π-[2,1-*c*]IF unit substituted with mesityl, 3,5-trifluoromethylphenyl, and triisopropylsilylethynyl groups at the 5,8-positions (**π-IFs-8a-c** in Fig. 18).[113] Similar to the π-[1,2-*b*]IF regioisomer, the formation of the π-[2,1-*c*]IF core requires dearomatization of only one internal benzene ring, and the corresponding IF-dione precursor was readily available in multigram quantities, which enabled the facile synthesis of these molecules. Single crystal analysis of **π-IF-8a** indicated that this molecule possessed a central *p*-quinodimethane unit and homogeneous bond-lengths in the peripheral benzene rings, similar to the [1,2-*b*]IFs.[106,107] The theoretical calculations

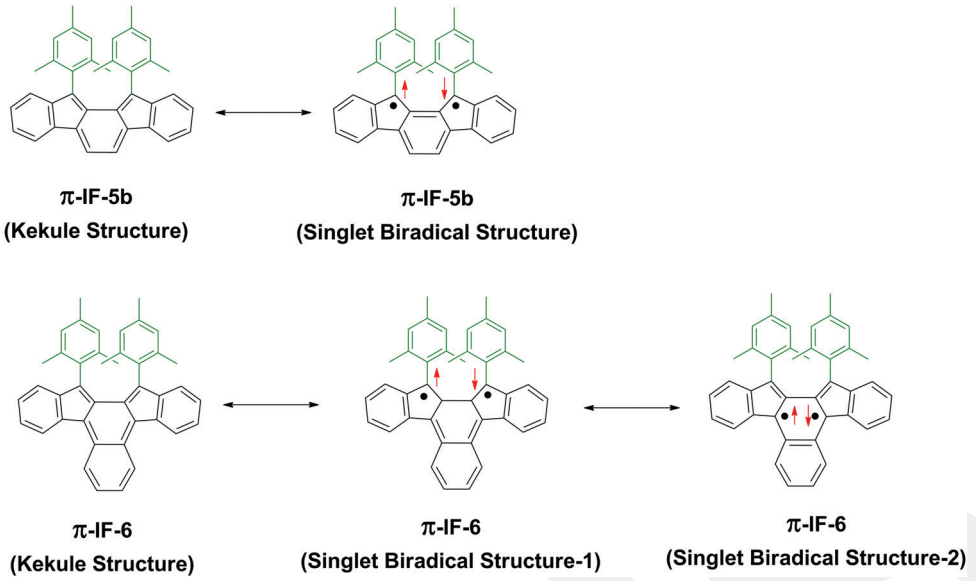

Scheme 5 The canonical resonance structures of **π-IF-5b** and **π-IF-6** showing a combination of Kekule and singlet biradical structures.[110,111]

revealed that the π-[2,1-*c*]IF core exists as a closed shell ground state with a small degree of biradical character. Cyclic voltammetry measurements revealed that these molecules have high electron affinities (E_{LUMO} = −3.63 eV to −4.02 eV) and can undergo reversible two-electron reductions with the first half-wave potentials located at −1.05, −0.71 and −0.66 V, respectively. The HOMO–LUMO and optical band gap for **π-IF-8c** were found to be as low as 1.73 eV and 1.48 eV, respectively. Although all these studies did not report charge transport measurements, they revealed key structural and optoelectronic properties of π-IFs and suggested that π-IFs could be an alternative semiconducting framework to acenes.

Very recently, Haley *et al.* developed four new π-extended derivatives of π-[2,1-*c*]IFs (**π-IFs-9a–d** in Fig. 18) by fusing benzene to the central and peripheral aromatic units.[114] The X-ray single crystal analysis of **π-IF-9a** indicated that this molecule possessed a symmetric helical geometry. The optical absorption spectra of **π-IFs-9a–d** revealed that the positions of benzo-fusion have a direct impact on the electronic properties. That is, the central and linear benzo-fusion in **π-IFs-9a,b** and **9c**, respectively, led to a blue-shifted absorption compared to **π-IFs-8b,c**. On the other hand, the angular benzo-fusion in **π-IF-9d** gave rise to red-shifted low-energy bands. These new molecules were also non-emissive. As is the case with π-[2,1-*c*]IFs, **π-IFs-9a–d** have high electron affinities (E_{LUMO} = −3.5 eV to −4.0 eV) and undergo reversible two-electron reductions. The HOMO–LUMO gap and the optical band gap for **π-IF-9d** were found 1.55 eV and 1.24 eV, respectively, which indicates that this molecule could be utilized as an ambipolar semiconductor. Haley *et al.* recently also synthesized and characterized the last unknown IF regioisomer, namely the fully conjugated indeno[1,2-*a*]fluorene substituted with dimesityl units at 7,12-positions (**π-IF-10** in Fig. 18).[115] This molecule is a highly reactive diradicaloid compound with the largest singlet biradical character of y = 0.80 among all IF regioisomers. The X-ray single crystal analysis of **π-IF-10** was made by converting the molecule into a dianion form, and the crystallographic analysis confirmed that the molecule's carbon connectivity and bond length alternation pattern are in agreement with the computational calculations. The optical absorption spectrum of **π-IF-10** exhibited low-energy bands at 600 nm and 1000 nm. The electrochemically calculated HOMO–LUMO gap and the optical band gap were found to be 1.46 eV and 1.30 eV, respectively.

4.6. 6,12-Diaryl-π-[1,2-*b*]IFs

Following their early studies, Haley *et al.* expanded the structural versatility of π-IFs by arylations at the 6,12-positions.[116] Thus, a series of fully-conjugated 6,12-diaryl-π-[1,2-*b*]IFs (**π-IF-2** and **π-IFs-11a–i** in Fig. 18) were synthesized and characterized in detail. This strategy allowed them to explore various aryl units with different donor and acceptor strengths and their effects on the optoelectronic properties. In contrast to the substitutions at the 2,8-positions in **π-IFs-4a–i**, 6,12-functionalization was found to have profound effects on the optical absorption profiles, electrochemical behaviors, and HOMO–LUMO energies of the 6,12-diaryl-π-[1,2-*b*]IFs, which was attributed to the presence of considerable frontier orbital densities at the 6,12-aryl units. The HOMO–LUMO gaps for **π-IFs-11a–i** were in the range of 1.82–2.17 eV. The LUMO energies of these compounds were between −3.56 eV and −4.00 eV, which are in the range of those of highly performing n-type organic semiconductors in OFETs and electron acceptors in OPVs. In this study, top-contact/bottom-gate OFETs were fabricated by growing micron-scale single-crystals (Fig. 21) of 6,12-di(pentafluorophenyl)-π-[1,2-*b*]IF **π-IF-11i** directly on a surface-treated silicon wafer.

Based on the HOMO (−6.17 eV) and LUMO (−4.00 eV) energies of **π-IF-11i** located symmetrically around the Au work function (~5.1 eV) and its electrochemical behavior showing quasi-reversible reduction and oxidation profiles, the OFETs

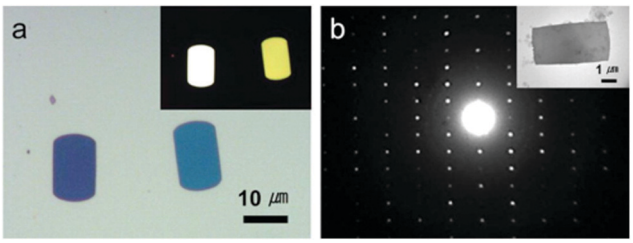

Fig. 21 (a) Optical micrographs (OMs) of the single crystals of **π-IF-11i** from a solvent-exchange method. The inset displays an OM with crossed polarizers. (b) SAED pattern and (inset) bright-field TEM image of a single crystal of **π-IF-11i**.[116] Reprinted with permission from ref. 116. Copyright 2012, American Chemical Society.

(micron-scale single crystals of **π-IF-11i** on p^{++}-Si/SiO_2/OTS) exhibited an ambipolar semiconducting behavior in an inert atmosphere with a hole mobility of 7×10^{-4} cm^2 V^{-1} s^{-1} and an electron mobility of 3×10^{-3} cm^2 V^{-1} s^{-1} (Fig. 22). This study demonstrated not only the first OFET-active π-IF semiconductor in the optoelectronics literature but also one of the rare examples of an ambipolar OFET made from a single crystal.[117,118] Structurally similar π-[1,2-*b*]IFs (**π-IFs-12a–c** in Fig. 18) with different aryl substituents (2,6-difluorophenyl, 9-anthryl, and 5-hexyl-2-thienyl) at the 6,12-positions were synthesized by Yamashita *et al.* in the same year.[119] These compounds showed strong absorptions in the visible spectral region extending to ~500–700 nm and amphoteric redox properties with oxidation and reduction potentials of 0.7–1.2 V and −1.0 V, respectively. The thienyl derivative **π-IF-12c** showed a narrow HOMO–LUMO gap of 1.55 eV, which was explained by the contribution of the biradical resonance form to its electronic structure. The arylation at the 6,12-positions affected not only the dihedral angles between the aryl units and *s*-indacene core (dihedral angle of 76.5° for **π-IF-12b** *vs.* 43.3° for **π-IF-2**) but also the bond alternation in the *s*-indacene core. The quinoid character was found to increase with sterically bulky aryl units at 6,12-positions. Based on DFT calculations and in line with the experimental results, the introduction of five-membered thienyl rings at the 6,12-positions weakened the quinoid character and promoted π-delocalization leading to narrow HOMO–LUMO gaps. OFETs based on **π-IF-2** and **π-IF-12a,b** were fabricated in a bottom-contact/bottom-gate device architecture by thermally evaporating semiconductor films under high vacuum on Si/SiO_2/HMDS substrates. **π-IF-12a** and **π-IF-12b** devices exhibited ambipolar transport with electron/hole mobilities of 8.2×10^{-6}/1.9×10^{-5} cm^2 V^{-1} s^{-1} and 1.6×10^{-6}/1.1×10^{-5} cm^2 V^{-1} s^{-1}, respectively. However, **π-IF-2** devices showed only p-type transport with a hole mobility of 1.6×10^{-5} cm^2 V^{-1} s^{-1}. The low charge carrier mobilities of these molecules were attributed to their amorphous film microstructure.

4.7. Extended π-[1,2-*b*]IFs for high mobility in OFETs

The best performing π-IF semiconductor, **π-IF-13** (Fig. 18), was reported in 2016 by two independent research groups. In this structure, the π-framework of the original π-[1,2-*b*]IF is extended along the long molecular axis by fusing additional thiophene rings between *s*-indacene and terminal benzene units.[96,104] As reported by Haley *et al.*,[96] the synthesis of this semiconductor was performed as reported previously for

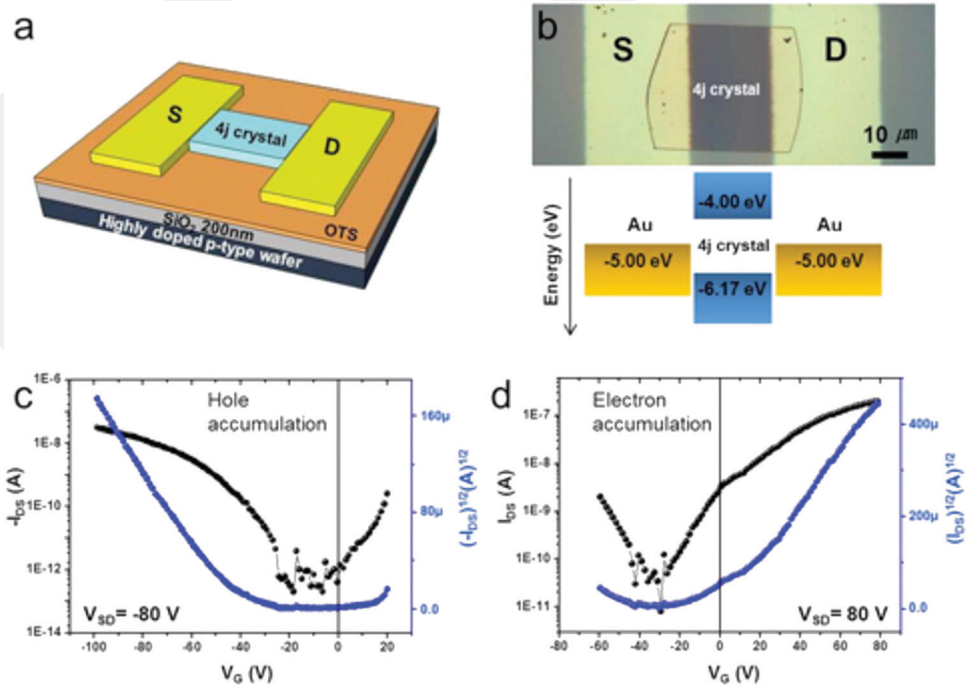

Fig. 22 (a) Illustration of an OFET device with an active channel composed of a **π-IF-11i** (**4j** in the figure) single crystal. (b) Top-view optical micrograph of an OFET and the energy level diagram of Au/**π-IF-11i** crystal/Au (bottom). (c and d) *I*–*V* transfer curves of OFETs with (c) negative and (d) positive drain voltages.[116] Reprinted with permission from ref. 116. Copyright 2012, American Chemical Society.

π-[1,2-*b*]IFs *via* addition of a nucleophile ($(i\text{-}Pr)_3SiC{\equiv}C{:}^-$ in the case of **π-IF-13**) to the corresponding dione intermediate followed by a $SnCl_2$-mediated reductive dearomatization. In this synthesis, rigorous anhydrous and anaerobic conditions were found to be critical for successful $SnCl_2$-mediated reduction. In this study, the authors did not only demonstrate synthesis of ~500 mg of **π-IF-13** in one batch, but also improved the synthesis of the IF-dione precursor to yield multigram quantities without the use of column chromatography. **π-IF-13** showed a low-energy absorption band (λ_{max}^{abs} = 682 nm) in dichloromethane with the absorption onset at 709 nm (E_g^{opt} = 1.75 eV) and underwent (quasi)reversible oxidation and reduction during the cyclic voltammetry measurement. The HOMO and LUMO energies were estimated as −5.61 eV and −4.18 eV, respectively. In this study, the authors found that the replacement of the outer benzene rings with benzothiophenes led to a strong antiaromatic ring current formation in the central *s*-indacene unit. Based on the single-crystal structure, **π-IF-13** was found to pack in 1D slipped-stacked columns in the triclinic lattice with short π–π distances of 3.36 Å and considerable molecular overlaps. The intermolecular electronic couplings (t) for the **π-IF-13** dimer in the triclinic lattice were found to be reasonably large as 50 meV for the HOMO:HOMO and 100 meV for the LUMO:LUMO overlaps (Fig. 23). On the other hand, the electronic band structure for the **π-IF-13** triclinic lattice along various crystallographic directions showed that this semiconductor had an indirect band gap, and the valence and conduction band dispersions were 78 meV and 383 meV, respectively (Fig. 23). In this study, the electronic couplings and band widths are mentioned to be in the range of those for high mobility organic semiconductors, revealing the great potential of **π-IF-13** for efficient charge transport. Bottom-contact/top-gate OFETs (Si/SiO_2/Ti–Au (S–D electrodes)/**π-IF-13**/Cytop/Au (gate electrode)) were fabricated by spin-coating the semiconductor layer and a maximum hole mobility of 0.44 $cm^2\ V^{-1}\ s^{-1}$ (I_{on}/I_{off} ~ 10^3 and V_{th} ~ 1 V) was measured ($\mu_h^{average}$ = 0.14 $cm^2\ V^{-1}\ s^{-1}$) under ambient conditions.

Although electron transport was not observed for these OFETs, another study by Zhu *et al.*[104] in the same year demonstrated ambipolar charge transport characteristics. Different than the above reported synthetic approaches to π-IFs typically involving double intramolecular Friedel–Crafts acylations, the extended π-IF framework in **π-IF-13** was accomplished *via* a double C–H activation cyclization. This new synthetic strategy is very valuable to enhance the structural versatility of π-IFs and their corresponding IF-diones. Top-contact/bottom-gate OFETs (Si/SiO_2/OTS/**π-IF-13**(single crystal)/Au(pasted as foil instead of thermal evaporation)) based on **π-IF-13** single crystals showed high and balanced ambipolar charge transport under ambient conditions with electron and hole mobilities of 0.34 $cm^2\ V^{-1}\ s^{-1}$ (I_{on}/I_{off} ~ 10 and V_{th} ~ 30 V) and 0.64 $cm^2\ V^{-1}\ s^{-1}$ (I_{on}/I_{off} ~ 10^2 and V_{th} ~ -7 V), respectively (Fig. 24e and f). To the best of our knowledge this is one of the best ambipolar devices realized to date with an antiaromatic semiconductor single crystal. In these OFETs, as shown in Fig. 24a–d, **π-IF-13** single crystals were grown directly on Si/SiO_2/OTS using the physical vapor transport method and exhibited short (3.30 Å) π–π stackings along the charge-transport direction. The frontier orbital energies (E_{HOMO} = −5.46 eV and E_{LUMO} = −4.27 eV) measured in this study were very similar to those reported by Haley *et al.*[96] (*vide supra*). Note that, since the LUMO energy level was below −4.0 eV, n-channel OFET measurements mentioned above were performed under ambient conditions.

Finally, although several other structurally modified π-IFs were synthesized by extending the π-conjugation[120] and replacing the outer benzene rings with heterocycles (*i.e.*, thiophene and selenophene),[121,122] their charge transport characteristics were not assessed.

4.8. π-[1,2-*b*]IFs for BHJ-OPVs

The only known example of a BHJ-OPV fabricated with a π-IF donor material was with the fully conjugated 5,6,11,12-tetraarylindeno[1,2-*b*]fluorene derivative **π-IF-14** (Fig. 18), in

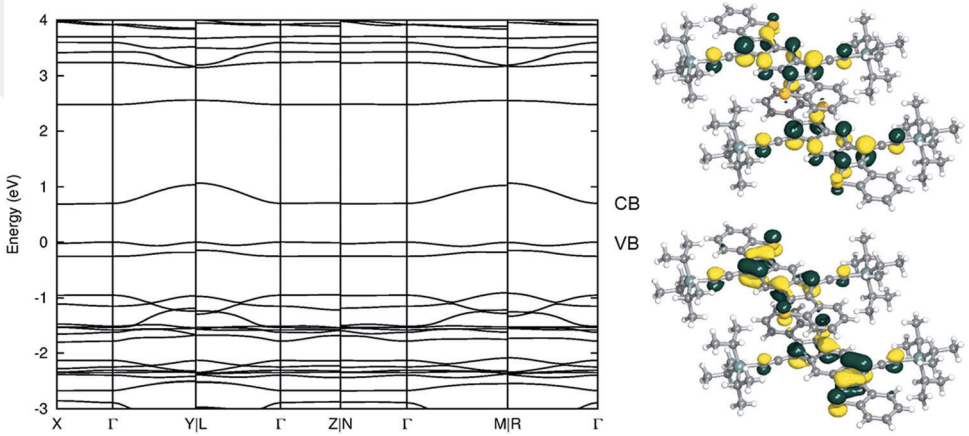

Fig. 23 Computed electronic band structure of **π-IF-13** along various crystallographic directions in the single-crystal triclinic lattice and the pictorial representations of the HOMO (bottom) and LUMO (top) overlaps in the dimer forms. The valence and conduction bands (VB and CB, respectively) are labeled for clarity.[96] Reprinted with permission from ref. 96. Copyright 2016, The Royal Society of Chemistry.

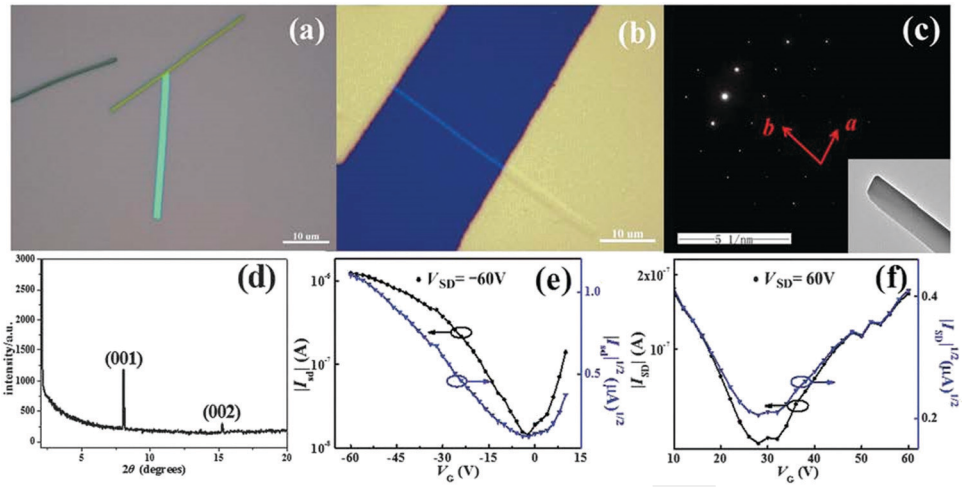

Fig. 24 (a and b) The single crystal optical microscope images of the substrate and along the charge transport direction obtained *via* the PVT method between source–drain electrodes. (c) TEM image matching the SAED pattern. (d) XRD pattern of the single crystals. (e and f) *I*–*V* transfer characteristics for hole and electron transports, respectively.[104] Reprinted with permission from ref. 104. Copyright 2016, The Royal Society of Chemistry.

which peripheral aryl substitutions showed highly twisted conformations ($\theta_{dihedral}$ = 66.8–74.5°) with respect to the π-IF core based on single-crystal analysis.[123] The highly twisted molecular conformation of **π-IF-14** decoupled π-conjugation between π-IF and peripheral aryl substitutions resulting in a blue-shifted optical absorption relative to 6,12-diphenyl-substituted **π-IF-2**. The film of **π-IF-14** showed a low-lying IP (~5.6 eV) and broad absorption up to 700 nm, suggesting that this new molecule has the potential to be used as an electron donor in photovoltaic devices. Furthermore, it was noted that this molecular design imparts good photostability. Because of the low solubility of this molecule, BHJ-OPV devices (ITO/MoO_3/active layer/BCP/Ag) were fabricated *via* vacuum deposition using $PC_{71}BM$ as the acceptor. These devices afforded a high open-circuit voltage of 0.94 V and a power conversion efficiency of 2.91%.

5. (Un)substituted dihydroindenofluorenes (DH-IFs)

5.1. Brief introduction to DH-IFs

Non-functionalized indenofluorene compounds having methylene bridges at the five-membered rings are classified as dihydroindenofluorenes (DH-IFs) and these 18π-electron compounds are the aromatic counterparts of π-IFs. Different than π-IFs, the sp^3 hybridization of the bridge methylenes allows for tetrahedral arrangement of the substituents around this carbon, which affects the crystal packing, solubility, and physicochemical and optoelectronic properties of these compounds. In this section, we will review DH-IF compounds in which methylene bridges are either unsubstituted or substituted with alkyl groups, aryl groups, or halogens. The rationale behind this substitution strategy of DH-IFs has been to attain desirable properties for use in organic optoelectronics. For example, the introduction of alkyl or aryl groups on the bridge methylenes gives rise to more efficient and stable emissive properties in electroluminescent devices, especially in the blue spectral region, by precluding the formation of π-aggregates/excimers.[124–126] The alkyl substituents also increase the solubility of the fused DH-IF π-system. Furthermore, aryl and perfluoroalkyl groups make these compounds less susceptible to ambient oxidation, which in turn suppress long-wavelength emission stemming from ketone defects on the bridge positions.[126–129] On the other hand, halogen substituents in place of hydrogen atoms could be used for lowering the LUMO energy levels to provide electron-transporting materials.[130] It is worth noting that a significant difference between DH-IFs and π-IFs is that DH-IF derivatives are typically emissive. The chemical structures of the (un)substituted DH-IF-based semiconductors reviewed in this section are shown in Fig. 25 with the corresponding optoelectronic properties and device performance metrics listed in Table 4.

5.2. Early examples of DH-IFs

The early examples of DH-IFs (**DH-IF-1** and **DH-IF-2** in Fig. 25) were reported by Deuschel in 1951[37] and by Eglinton *et al.*[131] in 1960, which employed different synthetic procedures to synthesize the [1,2-*b*] regioisomer. The synthetic procedure used by Deuschel for the synthesis of **DH-IF-2** was based on applying a stream of chlorine gas to a neat solution of 1,4-dimethyl-2,5-diphenylbenzene at 185 °C. Later on, the dehalogenation of **DH-IF-2** afforded **DH-IF-1**. On the other hand, Eglinton *et al.* synthesized **DH-IF-1** *via* intramolecular cyclization and aromatization of dehydro[12]annulene fused with benzene. The later studies by Scherf *et al.*[43] in 1996 and Müllen *et al.*[132] in 1999 utilized the dihydro[1,2-*b*]IF core where the hydrogen atoms at the bridge carbon positions were replaced by halogens and alkyl groups (**DH-IF-3** and **DH-IF-4a,b** in Fig. 25, respectively) in order to synthesize novel poly(indenofluorenes) having varied optical properties (**DH-IF-P1** and **DH-IF-P2a,b** in Fig. 25). Scherf *et al.*[43] synthesized **DH-IF-P1** *via* dehalogenation polymerization of the

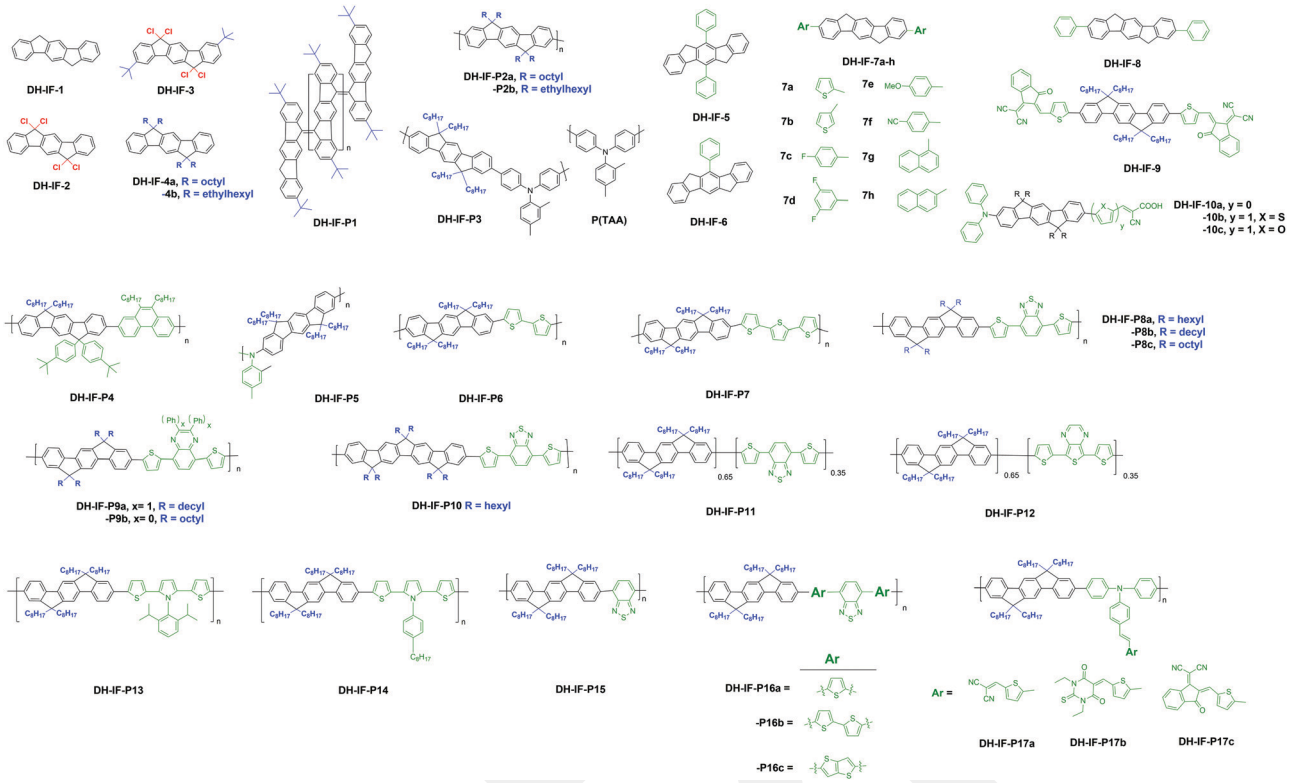

Fig. 25 Chemical structures of (un)substituted dihydroindenofluorene (DH-IF)-based semiconductors **DH-IFs-1–10** and **DH-IFs-P1–P17**.

DH-IF-3 monomer. **DH-IF-P1** was soluble in common organic solvents and showed an optical absorption maximum of 800 nm giving a low band gap of 1.55 eV. Despite the low band gap, **DH-IF-P1** showed excellent chemical stability under ambient conditions. Low band gap polymers, being used as a donor component in BHJ-OPVs, are desirable for absorbing broader solar light[133–136] and, in this respect, **DH-IF-P1** could serve as a framework to design polymers for use in solar cells. In 2003, Meijer *et al.*[137] took advantage of **DH-IF-P1**'s low band gap (1.55 eV), resulting in lower electron/hole charge injection from the same contact, and developed solution-processed ambipolar OFETs ($\mu_{e\,or\,h}$ = 4–5 × 10^{-5} cm^2 V^{-1} s^{-1}) and CMOS-like inverters (gain ~11) (Fig. 26). **DH-IF-P1** was also the first example of an organic polymer employed in a single-component ambipolar OFET.

Müllen *et al.*[132] performed bromination on **DH-IF-4a,b** at the 2,8-positions to yield a monomer, which then underwent Yamamoto polymerization to afford poly-2,8-indenofluorenes **DH-IF-P2a,b** (Fig. 25). These polymers, consisting of tetraalkyl-substituted dihydro[1,2-*b*]IF repeating units, exhibited high molecular weights, excellent thermal stability and good solubility in common organic solvents. While **DH-IF-P2a** showed an absorption maximum at 416 nm and two sharp emission bands at 432 and 479 nm, **DH-IF-P2b** exhibited slightly blue-shifted peaks (*i.e.*, absorption maximum at 408 nm and two sharp emission bands at 428 and 453 nm). This was attributed to the presence of branched alkyl groups (*i.e.*, 2-ethylhexyl) enhancing torsion between dihydro[1,2-*b*]IF repeating units and reducing conjugation along the polymer chain. The luminescence properties of **DH-IF-P2** bridge the gap between blue-light-emitting polyfluorenes[138] and ladder-type poly(*p*-phenylene)s.[139]

5.3. (Hetero)aryl-substituted DH-IFs

Instead of introducing substituents on the bridge methylene positions, there are some examples of DH-IFs in which the central or peripheral benzene rings are functionalized with (hetero)aryl units in order to tune luminescence characteristics. In 2002, Wang *et al.*[54] synthesized 5,11-diphenyl-dihydro[1,2-*b*]-IF and its mono/unsubstituted counterparts (**DH-IF-1**, **DH-IF-5**, and **DH-IF-6** in Fig. 25), which showed similar UV-Vis absorption spectra (λ_{max} ~ 330 nm) and good fluorescence quantum yields of 73–78%. The authors concluded that although the phenyl substituents at the central benzene ring did not affect the absorption maxima and fluorescence quantum efficiency, it resulted in a more conjugated excited state character in **DH-IF-5** and **DH-IF-6** (λ_{PL}^{max} = 375 nm and 364 nm, respectively) relative to **DH-IF-1** (λ_{PL}^{max} = 340 nm). Furthermore, phenyl substituents affected the electrochemical properties of these DH-IFs, leading to much easier reduction processes for **DH-IF-5** and **DH-IF-6** (*i.e.*, the first reduction half-wave potentials of −2.2 and −1.8 V *vs.* SCE, respectively) as compared with **DH-IF-1** (the first reduction half-wave potentials of −2.6 V *vs.* SCE). Besides introducing new luminescent materials to the organic optoelectronics literature, the importance of this study was that it reported, for the first time, the optical and electrochemical properties of the **DH-IF** π-core. In 2005, Py *et al.*[140] synthesized a series of dihydro[1,2-*b*]IFs having the peripheral benzene rings

Table 4 Summary of experimental HOMO/LUMO energies (or oxidation/reduction potentials (E_{ox}/E_{red})), optical absorption maximum, and optical band gap values for (un)substituted DH-IF-based semiconductors, and the (opto)electronic device type and representative organic field-effect transistor (OFET)/bulk-heterojunction organic photovoltaics (BHJ-OPVs) performance values [field-effect mobility for electrons and/or holes (μ_e, μ_h), current on/off ratio (I_{on}/I_{off}), power conversion efficiency (PCE), and open-circuit voltage (V_{oc})] in the corresponding literature

Year	Semiconductor	HOMO/LUMO[a] [eV] or E_{ox}/E_{red}[a] [V]	λ_{max}^{abs} [b] [nm]	E_g^{opt} [c] [eV]	Opto(electronic) device type[d]	Performance (μ_e, μ_h [$cm^2\ V^{-1}\ s^{-1}$] (I_{on}/I_{off}) or PCE [%], V_{oc} [V])	Ref.
2003	DH-IF-P1	NR	799	1.55	p/n-OFET (spin coat.)	$\mu_e = 5 \times 10^{-5}$ $cm^2\ V^{-1}\ s^{-1}$	137
						$\mu_h = 4 \times 10^{-5}$ $cm^2\ V^{-1}\ s^{-1}$	43
2006	DH-IF-7a	−5.1/−2.0	325	2.9	p-OFET (thermal evap.)	$\mu_h = 0.012$ $cm^2\ V^{-1}\ s^{-1}$ (10^5)	141
2009	DH-IF-P3	−5.5/NR	NR	NR	p-OFET (spin coat.)	$\mu_h = 0.04$ $cm^2\ V^{-1}\ s^{-1}$ (10^6)	144
2010	DH-IF-P6	−5.59/−3.21	456	2.38	p-OFET (spin coat.)	$\mu_h = 1.5 \times 10^{-5}$ $cm^2\ V^{-1}\ s^{-1}$ (10^4)	148
	DH-IF-P7	−5.53/−3.43	460	2.10	p-OFET (spin coat.)	$\mu_h = 1.1 \times 10^{-4}$ $cm^2\ V^{-1}\ s^{-1}$ (—)	
2010	DH-IF-P8a	−5.49/−3.46	402	1.97	BHJ-OPV (spin coat.)	PCE = 0.97%	149
						V_{oc} = 0.98 V	
					p-OFET (spin coat.)	$\mu_h = 0.011$ $cm^2\ V^{-1}\ s^{-1}$ (10^3)	
	DH-IF-P9a	−5.45/−3.36	400	2.00	BHJ-OPV (spin coat.)	PCE = 3.04%	
						V_{oc} = 1.00 V	
					p-OFET (spin coat.)	$\mu_h = 0.001$ $cm^2\ V^{-1}\ s^{-1}$ (10^3)	
	DH-IF-P10	−5.45/−3.45	415	1.96	BHJ-OPV (spin coat.)	PCE = 4.50%	
						V_{oc} = 1.04 V	
					p-OFET (spin coat.)	$\mu_h = 0.01$ $cm^2\ V^{-1}\ s^{-1}$ (10^3)	
2010	DH-IF-P8c	−5.64/−3.71	560	1.93	BHJ-OPV (spin coat.)	PCE = 1.70%	150
						V_{oc} = 0.77 V	
					p-OFET (spin coat.)	$\mu_h = 0.001$ $cm^2\ V^{-1}\ s^{-1}$ (2×10^4)	
2010	DH-IF-P13	−5.19/−2.83	465	2.36	BHJ-OPV (spin coat.)	PCE = 1.12%	151
						V_{oc} = 0.67 V	
2011	DH-IF-P16a	−5.60/−3.60	545	1.94	BHJ-OPV (spin coat.)	PCE = 2.05%	152
						V_{oc} = 0.97 V	
2011	DH-IF-P16b	−5.50/−3.86	574	1.77	BHJ-OPV (spin coat.)	PCE = 2.90%	153
						V_{oc} = 0.95 V	
	DH-IF-P16c	−5.54/−3.88	560	1.79	BHJ-OPV (spin coat.)	PCE = 3.13%	
						V_{oc} = 0.95 V	
2011	DH-IF-P17a	−5.32/−3.46	549	1.86	BHJ-OPV (spin coat.)	PCE = 3.10%	154
						V_{oc} = 0.93 V	
2012	DH-IF-P4	−5.8/NR	NR	NR	p-OFET (spin coat.)	$\mu_h = 0.3$ $cm^2\ V^{-1}\ s^{-1}$ (10^8)	146
2012	DH-IF-10a	−5.51/−2.80	408	2.71	DSSC (solution dep.)	PCE = 3.36%	87
						V_{oc} = 0.70 V	
	DH-IF-10b	−5.46/−2.90	426	2.56	DSSC (solution dep.)	PCE = 4.04%	
						V_{oc} = 0.70 V	
	DH-IF-10c	−5.47/−2.83	430	2.64	DSSC (solution dep.)	PCE = 4.05%	
						V_{oc} = 0.71 V	
2014	DH-IF-P5	−4.6/−1.9	443	2.69	p-OFET (spin coat.)	$\mu_h = 0.05$ $cm^2\ V^{-1}\ s^{-1}$ (7×10^4)	147
2017	DH-IF-9	−5.42/−3.85	683	1.82	BHJ-OPV (spin coat.) (used as an acceptor)	PCE = 6.56%	155
						V_{oc} = 0.92 V	

NR: the corresponding value is not reported in the reference. [a] Measured *via* cyclic voltammetry and estimated based on using the vacuum energy level of the reference electrode. [b] Measured in solution as the low-energy optical absorption maximum. [c] Measured in solution from the low-energy optical absorption edge. [d] Active layer deposition method is given in parentheses.

substituted with different aryl and thienyl groups functionalized with donor (*i.e.*, –OMe) or acceptor (*i.e.*, –F or –CN) groups (**DH-IF-7a–h** in Fig. 25). These DH-IF-based molecules were all emissive and exhibited good thermal stability. This study was especially important since it provided a general synthetic route to various DH-IF derivatives to investigate their structure–property relationships. **DH-IF-7a** was used as an emissive layer in OLEDs and reached a high luminance of 1400 cd m^{-2} below 10 V with a whitish yellow emission. In another study by Py *et al.*,[141] **DH-IF-7a** was also used as a semiconducting layer in top-contact/bottom-gate OFETs (vacuum deposited semiconductor on p^{++}-Si/SiO_2/HMDS) exhibiting p-type transport with a hole mobility of 1.2×10^{-2} $cm^2\ V^{-1}\ s^{-1}$ and a threshold voltage of −55 V. Following the synthetic route designed by Py *et al.*,[140] Hümmelgen *et al.*[142] synthesized 2,8-diphenyl-substituted dihydro[1,2-*b*]IF **DH-IF-8** and investigated this molecule to fabricate hybrid permeable-base transistors in a semiconductor/metal/semiconductor architecture (Fig. 27). **DH-IF-8** showed a nearly ideal base transport factor and these transistors operated with holes being the major charge carriers.

5.4. Dialkyl-substituted DH-IF-based polymers for OFETs

Even though DH-IF derivatives have been studied for OLEDs on account of their emissive properties,[50,143] they have also been used as a building block of semiconducting polymers for OFETs. Thus, McCulloch *et al.*[144] developed the solution-processable alternating copolymer **DH-IF-P3** (Fig. 25), which consists of highly planar 6,6,12,12-tetraoctyl-substituted dihydro[1,2-*b*]IF **DH-IF-4a** and triphenylamine repeating units. Bottom-contact/top-gate OFETs fabricated by solution-processing **DH-IF-P3** films showed respectable hole mobilities of 0.04 $cm^2\ V^{-1}\ s^{-1}$ ($I_{on}/I_{off} \sim 10^6$) (Fig. 28b). This performance

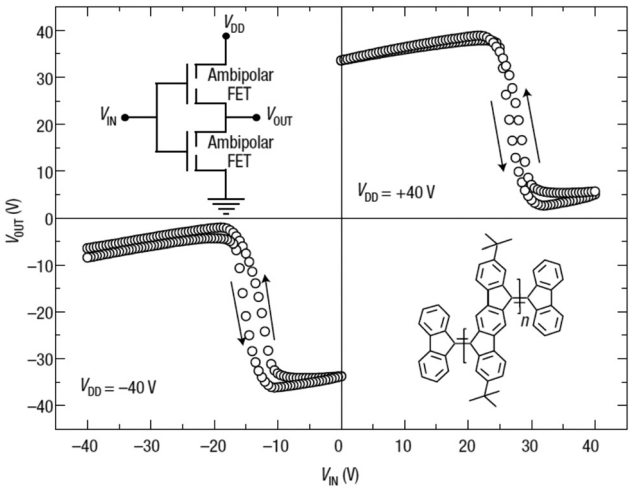

Fig. 26 Transfer characteristics and schematic representation of the electrical connections for a CMOS-like inverter based on two identical **DH-IF-P1**-based ambipolar field-effect transistors. Depending on the polarity of the supply voltage (V_{DD}) the inverter works in the first or the third quadrant.[137] Reprinted with permission from ref. 137. Copyright 2003, Springer Nature.

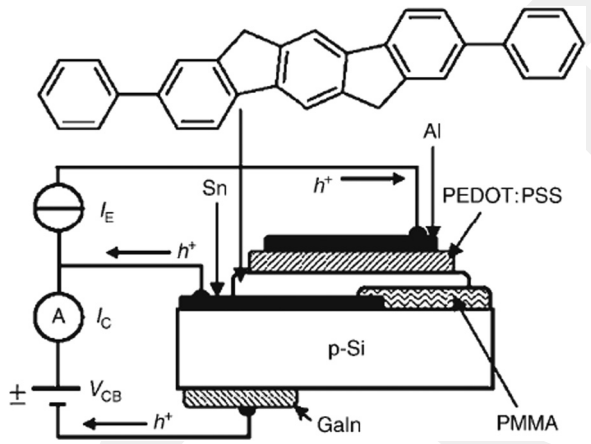

Fig. 27 Schematic of a hybrid permeable-base transistor in the architecture of GaIn/p-Si/Sn/**DH-IF-8**/PEDOT:PSS/Al and the common-base-mode measurement conditions. The chemical structure of **DH-IF-8** is shown on top.[142] Reprinted with permission from ref. 142. Copyright 2006, Wiley-VCH.

was found to be one order of magnitude higher than those fabricated with the parent triarylamine polymer P(TAA) (shown in Fig. 25). **DH-IF-P3** films were found to be amorphous and the improved hole mobility was attributed to the presence of the DH-IF unit, which has an extended conjugation and leads to enhanced intramolecular π-orbital overlap along the polymer backbone. Also, the carbon bridged phenylene units reduced backbone conformation rotational disorder and improved the local structural organization. As a direct result of the lowered HOMO energy level (−5.5 eV), **DH-IF-P3**-based OFETs stored under ambient conditions showed no change in electrical performance over several weeks (Fig. 28a).

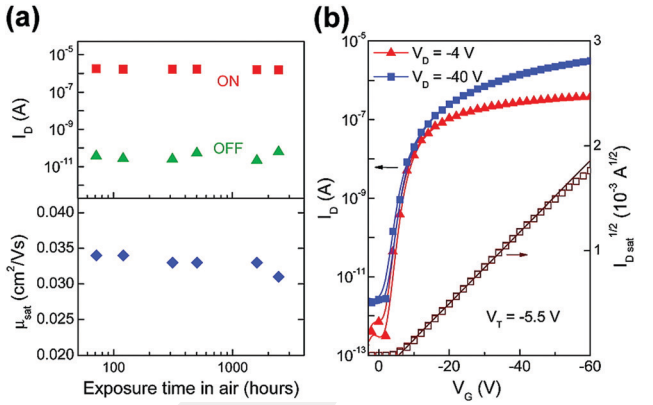

Fig. 28 (a) I_{on}–I_{off} currents (top) and saturated hole mobilities (bottom) measured for **DH-IF-P3**-based OFETs upon storage in air over a period of ~3 months. (b) Transfer characteristics of **DH-IF-P3**-based OFETs (W/L = 1000 μm/30 μm) measured in air.[144] Reprinted with permission from ref. 144. Copyright 2009, American Chemical Society.

Not only is it important to enhance OFET performance for potential commercial use, but also circumventing degradation problems originating from environmental or device-related issues is crucial to improve reliability.[145] Georgakopoulos *et al.*[146] fabricated high performance bottom-contact/top-gate OFETs using solution-processed amorphous **DH-IF-P4** (Fig. 25) films. This amorphous alternating copolymer includes alkyl-/aryl-substituted DH-IF and phenanthrene repeating units, and it displayed great stability against oxidation under ambient conditions due to the high ionization potential (5.8 eV). OFETs based on **DH-IF-P4** displayed an excellent hole mobility of 0.3 $cm^2\,V^{-1}\,s^{-1}$ ($I_{on}/I_{off} \sim 10^8$), which was ascribed to low energetic disorder (σ = 48 meV) at the semiconductor–insulator interface and strong intermolecular coupling (high prefactor mobility = 0.67 $cm^2\,V^{-1}\,s^{-1}$), both obtained by fitting the transistor data to the Gaussian disorder model for charge transport in disordered semiconductors. Also, the **DH-IF-P4**-based FETs exhibited very high I_{on}/I_{off} ratios in excess of 10^7, near zero threshold voltage, and no hysteresis in the I_{SD}–V_G curve. The measured transistor mobility was found to decrease only by ~15% over two months.

Turner *et al.*[147] employed the Buchwald–Hartwig polyamination protocol to modify the backbone of polytriarylamines with (di)indenofluorenes comonomers. As shown in Scheme 6, the polyamination (*i.e.*, (NHC)–Pd catalysed C–N coupling) reactions were performed between the corresponding anilines and dibromo-substituted (bis)indenofluorenes. Among these polymers, the polymer incorporating dihydro[1,2-*b*]IF unit (**DH-IF-P5** in Fig. 25) displayed the highest performance due to its lowest reorganization energy for hole transfer. Bottom-gate/top-contact OFETs based on spin-coated **DH-IF-P5** films (on n^{++}-Si/SiO_2(300 nm)/OTS) exhibited p-type behavior with a good hole mobility and an I_{on}/I_{off} ratio of 0.05 $cm^2\,V^{-1}\,s^{-1}$ and 7×10^4, respectively. This was the highest mobility reported to date for a polytriarylamine semiconductor. Wide angle X-ray scattering (WAXS) of these **DH-IF-P5** films on a silicon substrate showed no reflections indicating an amorphous microstructure. On the other hand, the relatively lower performance

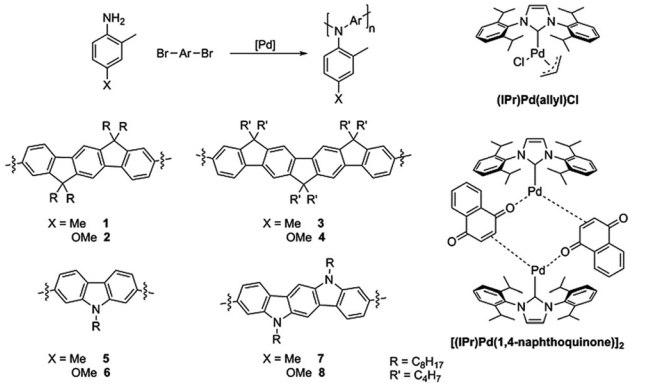

Scheme 6 Buchwald–Hartwig polyamination protocol for the synthesis of (bis)indenofluorenes including **DH-IF-P5** (shown as **1** in the scheme) and the chemical structures of the catalysts (3 mol%) employed in the polymerizations along with 4 equiv. KO*t*-Bu in toluene.[147] Reprinted with permission from ref. 147. Copyright 2014, The Royal Society of Chemistry.

(μ_h = 0.003 $cm^2\ V^{-1}\ s^{-1}$) of more π-extended diindenofluorene copolymers was rationalized by DFT calculations that showed higher reorganization energies for its model oligomers.

Sonar *et al.*[148] reported the synthesis of two alternating copolymers, **DH-IF-P6** and **DH-IF-P7** (Fig. 25), in which the π-conjugated backbones consisted of tetraoctyl-substituted dihydro[1,2-*b*]IF (**DH-IF-4a**) and bi- or ter-thiophene units giving relatively low HOMO energies of ∼−5.6 eV. These copolymers were synthesized *via* Suzuki polycondensations. The authors investigated the optical, electrochemical, and semiconducting properties of these copolymers as well as the film morphologies *via* AFM analysis. The optical band gaps of **DH-IF-P6** and **DH-IF-P7** were measured to be 2.38 and 2.10 eV, respectively, and cyclic voltammograms indicated reversible oxidations with the onset values at 1.19 V (*vs.* Ag/AgCl) and 1.13 V (*vs.* Ag/AgCl), respectively. The lowered band gap and more negative oxidation onset for **DH-IF-P7** reflect longer π-conjugation and more π-electron rich nature of the terthiophene comonomer, as compared with bithiophene. AFM analysis shows that the size of the oligothiophene comonomer governs chain packing in the thin-film morphologies. While the films of **DH-IF-P6** were amorphous with nanometer-sized aggregates, **DH-IF-P7** films displayed a high degree of polymer chain organization (well-defined fibrillar morphology) originating from efficient interchain π–π interactions. Bottom-gate/bottom-contact OFETs (spin-cast on n^{++}-Si/SiO_2(300 nm)/HMDS) showed p-type characteristics with moderate hole mobilities of 1.5 × 10^{-5} $cm^2\ V^{-1}\ s^{-1}$ for **DH-IF-P6** and 1.1 × 10^{-4} $cm^2\ V^{-1}\ s^{-1}$ for **DH-IF-P7**.

5.5. Dialkyl-substituted DH-IF-based polymers for BHJ-OPVs

In 2010, Katz *et al.*[149] reported the first account of using DH-IF units in ladder-type donor polymers for BHJ-OPVs. The authors designed and synthesized three donor–acceptor copolymers, **DH-IF-P8a**, **P8b**, and **P9a** (Fig. 25), in which an alkyl-substituted (hexyl or decyl) dihydro[1,2-*b*]IF was used as an electron-donor building block with 4,7-dithien-2-yl-2,1,3-benzothiadiazole (TBT) or 5,8-dithien-2-yl-2,3-diphenylquinoxaline (DTQ) electron-acceptor units. The design rationale behind these DH-IF copolymers was to create a donor–acceptor π-backbone with deep HOMO energy levels and tuned optical band gaps, both of which are critical to achieve promising photovoltaic performances. All copolymers were prepared by a palladium-catalyzed Suzuki coupling reaction between a dibrominated acceptor and a DH-IF diboronic ester and they were soluble in common organic solvents, thanks to the presence of four solubilizing alkyl chains per DH-IF unit. The alkyl chain variation did not impact the π-conjugation length in this family. The authors pointed that **DH-IF-P8a**, **DH-IF-P8b**, and **DH-IF-P9a** exhibited intense and bathochromically shifted absorption bands as well as greater solubility in organic solvents, when compared with the fluorene containing copolymers having the same acceptor units. The red-shifted absorption band for **DH-IF-P8b** relative to **DH-IF-P9a** indicated that the TBT unit was a stronger acceptor unit than DTQ. The authors also developed a π-extended D–A copolymer, **DH-IF-P10**, which was based on bis-DH-IF donor and TBT acceptor units. The HOMO/LUMO energies and the optical band gaps of these copolymers were *ca.* −5.5 eV/−3.4 eV and 2.0–2.1 eV, respectively, making them suitable for BHJ-OPV fabrication with fullerene-based acceptors. As shown in Fig. 29, all BHJ photovoltaic devices fabricated in a conventional architecture (ITO/PEDOT:PSS/polymer:fullerene/Cs_2CO_3/Al) were active, and the highest photovoltaic performance was achieved for **DH-IF-P10** (for a polymer:$PC_{71}BM$ weight ratio of 1 : 4.0) with a power conversion efficiency of 4.50% and a high open-circuit voltage of 1.04 V. The indenofluorene analogue of this copolymer, **DH-IF-P9a**, showed a power conversion efficiency of 3.04% and an open-circuit voltage (V_{oc}) of 1.00 V. The authors suggested that the optical absorption range in these alkyl-substituted ladder-type (bis)-DH-IF copolymers could be further tuned *via* stronger acceptor units to better match the solar spectrum. These D–A copolymers also exhibited field-effect hole mobilities as high as 0.01 $cm^2\ V^{-1}\ s^{-1}$ in top-contact/bottom-gate OFETs (spin-coated on n^{++}-Si/SiO_2(300 nm)/HMDS).

The same year when the ladder-type DH-IF copolymers were published by Katz *et al.*,[149] Woo *et al.*[150] reported the synthesis and detailed photovoltaic characterization of copolymers having the same π-backbones with the difference of employing octyl chains on the DH-IF unit and without phenylenes on the DTQ acceptor. While two of these copolymers, **DH-IF-P8c** and **P9b** (Fig. 25), include alternating D–A π-backbones, the other copolymers **DH-IF-P11** and **P12** (Fig. 25) were synthesized *via* random Suzuki copolymerization yielding a donor : acceptor ratio of 65 : 35 mol% on the polymer backbone. Varying the content of electron-deficient TBT and DTQ moieties gave rise to different morphological/optical properties, hole mobilities, and eventually different photovoltaic performance. The longer wavelength optical absorption up to 800 nm, a lower LUMO energy level of −3.9 eV, and a lower bandgap of ∼1.6 eV measured for **DH-IF-P9b** and **P12**, as compared to those of **DH-IF-P8c** and **P11** (λ_{abs} up to 650 nm, E_{LUMO} = −3.7 eV, and E_g ∼ 1.9 eV), were attributed to more pronounced quinoid character (a higher degree of coplanarity and enhanced intermolecular interactions) and stronger electron-withdrawing ability of

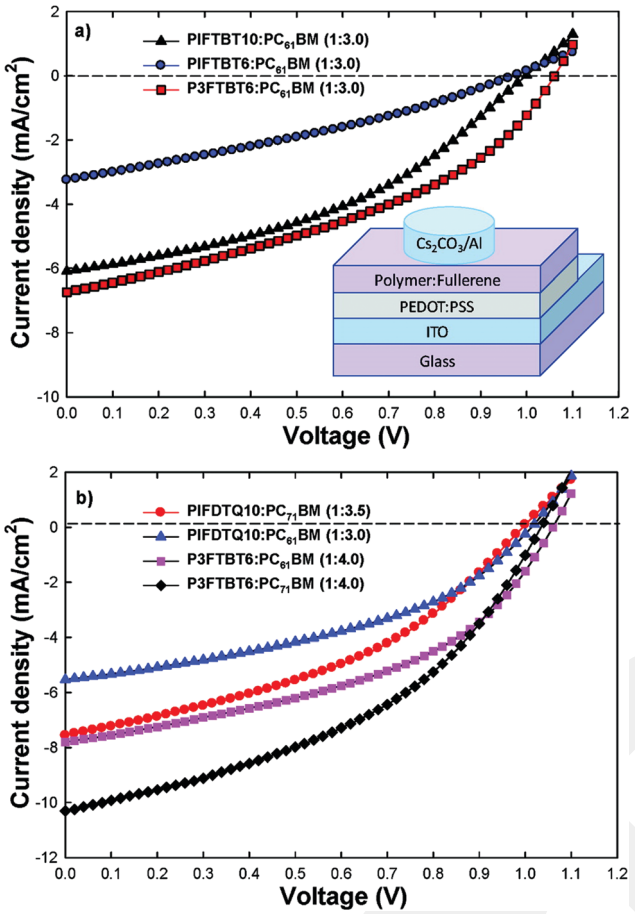

Fig. 29 Current density–voltage (J–V) curves of BHJ-OPV devices based on **DH-IF-P8b** (shown as **PIFTBT10** in the figure), **DH-IF-P8a** (shown as **PIFTBT6** in the figure), and **DH-IF-P10** (shown as **P3FTBT6** in the figure) polymers with $PC_{61}BM$ (a) or $PC_{71}BM$ (b) acceptors under simulated solar light (AM1.5G, 100 mW cm^{-2}, room temperature/ambient conditions). The inset shows the corresponding BHJ-OPV device structure.[149] Reprinted with permission from ref. 149. Copyright 2010, American Chemical Society.

the DTQ unit as compared to TBT. The field effect mobility measurements in OFETs showed a hole mobility of up to 10^{-3} cm^2 V^{-1} s^{-1} for **DH-IF-P8c**. BHJ-OPV devices fabricated in a conventional ITO/PEDOT:PSS/polymer:$PC_{71}BM$/Al architecture with all four copolymers were active and the highest photovoltaic performance was recorded for **DH-IF-P8c** (J_{sc} = 5.50 mA cm^{-2}, V_{oc} = 0.77 V, and PCE = 1.70%).

Tamilavan *et al.*[151] reported the polymerization of the tetraoctyl-substituted dihydro[1,2-*b*]IF π-unit with novel electron-rich comonomers, 2,5-bis(2-thienyl)-*N*-arylpyrroles, that were reported for the first time in this study. *N*-Aryl groups were chosen as 2,6-diisopropylphenyl and 4-octylphenyl, which yielded two copolymers **DH-IF-P13** and **DH-IF-P14** (Fig. 25), respectively. The optical band gaps were found to be ~2.4 eV as measured in chloroform solution, and the HOMO/LUMO energy levels were −5.19/−2.83 eV and −5.20/−2.80 eV, respectively. As seen from the optical/electrochemical characterization, substituents on the *N*-aryl unit did not influence the polymer properties. Bulk heterojunction solar cells were fabricated in ITO/PEDOT:PSS/polymer:$PC_{70}BM$/TiO_x/Al configurations, which afforded power conversion efficiencies of 1.12% and 0.23% for **DH-IF-P13** and **DH-IF-P14**, respectively. The V_{oc} values for these devices were low (~0.6–0.7 V) due to high HOMO energies.

Durrant *et al.*[152] fabricated BHJ solar cell devices in which the photoactive layer consisted of either the **DH-IF-P15** or **DH-IF-P16a** (Fig. 25) copolymer blended with the electron acceptor $PC_{61}BM$. These copolymers include tetraoctyl-substituted dihydro[1,2-*b*]IF units copolymerized with either benzothiadiazole (BT) or dithiophene-benzothiadiazole (TBTT). While **DH-IF-P15**-based devices showed negligible photovoltaic performance, the photovoltaic devices based on the blend of **DH-IF-P16a** with 80 wt% $PC_{61}BM$ exhibited an average PCE of 2.05% with a J_{sc} of 4.86 mA cm^{-2} and a V_{oc} of 0.97 V. Despite the low performance, the importance of this study was that the authors intensively investigated the photophysical properties of these two copolymers in their blended forms with $PC_{61}BM$. As shown in Fig. 30 (top scheme), the negligible photogeneration efficiency for **DH-IF-P15**/$PC_{61}BM$ blend films was attributed to ultrafast efficient Förster energy transfer from **DH-IF-P15** singlet excitons to $PC_{61}BM$. The resulting $PC_{61}BM$ singlet excitons have insufficient free energy to drive charge separation and undergo (non-)radiative decays to the ground state or intersystem crossing to the triplet state. On the other hand, photogeneration of **DH-IF-P16a** singlet excitons leads to charge separation to generate interfacial charge transfer states, which could dissociate into free charge carriers (Fig. 30 (bottom scheme)). Singlet energy transfer from the polymer to $PC_{61}BM$ was not plausible for **DH-IF-P16a** since this polymer exhibited relatively weak and red-shifted photoluminescence. On the basis of their results, the authors stressed to pay attention to energy *versus* electron transfer pathways from donor polymers to acceptor fullerenes during the photoexcitation process of

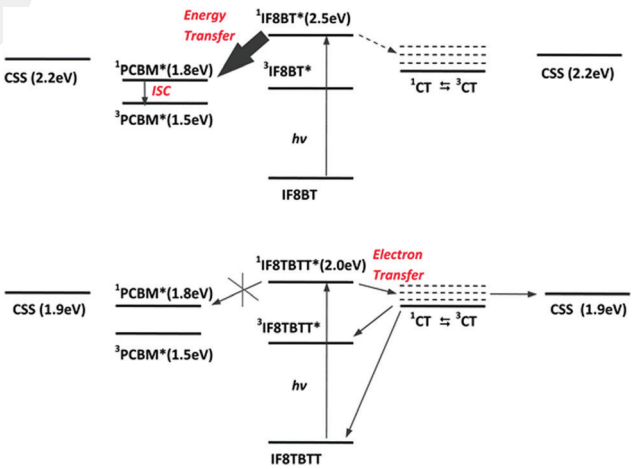

Fig. 30 Schematic illustrations of the photophysical processes upon photoexcitation of the polymer for **DH-IF-P15** (shown as **IF8BT** in the figure)/PCBM and **DH-IF-P16a** (shown as **IF8TBTT** in the figure)/PCBM blend films.[152] Reprinted with permission from ref. 152. Copyright 2011, The Royal Society of Chemistry.

indenofluorenes. Having a similar π-backbone to **DH-IF-P16a**, but employing bithiophene and thienothiophene units instead of a single thiophene, Xia *et al.*[153] reported in the same year the synthesis and photovoltaic characterization of alternating donor polymers **DH-IF-P16b** and **DH-IF-P16c** with narrow bandgaps (Fig. 25). These two dihydro[1,2-*b*]IF-based donor polymers were soluble in common organic solvents. According to UV-Vis absorption measurements, **DH-IF-P16b** and **DH-IF-P16c** show broad absorptions ranging from 350 nm to 700 nm with two absorption maxima for each polymer at 406/535 nm and 426/574 nm, respectively. The optical band gaps were estimated to be ~1.8 eV for both polymers. The HOMO/LUMO energy levels were found to be −5.50/−3.73 eV for **DH-IF-P16b** and −5.54/−3.75 eV for **DH-IF-P16c**, which were suitable for use in BHJ-OPVs with a fullerene acceptor. The BHJ solar cells utilizing **DH-IF-P16b** and **DH-IF-P16c** as donor polymers in a regular device architecture (ITO/PEDOT:PSS/polymer:$PC_{71}BM$/PFN/Al) exhibited the best performances with PCEs of 2.90–3.13% along with a V_{oc} of 0.95 V, J_{sc} values of 6.00–6.34 mA cm^{-2}, and FFs of 41–50%.

Duan *et al.*[154] synthesized three narrow band gap (1.53–1.86 eV) copolymers **DH-IF-P17a-c** (Fig. 25) based on tetraoctyl-substituted dihydro[1,2-*b*]IF and triphenylamine with pendant D–π–A chromophores that were attached by a post-functionalization approach. In this unique design, first aldehyde-containing precursor polymers were prepared and then functionalized with different pendant acceptor groups consisting of malononitrile, 1,3-diethyl-2-thiobarbituric acid, and 2-(1,2-dihydro-1-oxodien-3-ylidene)malononitrile, respectively. All polymers have good solubility in common solvents and excellent thermal stability. Despite being physically distanced from the polymer π-backbone, the introduction of different acceptor groups as pendant chromophores was found to tune the photophysical properties, energy levels, and band gaps. This design strategy made it possible not only to pin the HOMO energy levels of these three copolymers at a relatively deep position (E_{HOMO} ~ −5.35 eV) for large V_{oc} values, but also to tune their LUMO energy levels and band gaps for maximum optical absorption. The increasingly strong electron-withdrawing pendant groups deepened the LUMO energies and narrowed the band gap of dihydro[1,2-*b*]IF-based copolymers. Thus, while the LUMO energy and the optical band gap values in **DH-IF-P17a** were −3.46 eV/1.86 eV, they were further reduced to -3.60 eV/1.76 eV in **DH-IF-P17b** and −3.76 eV/1.53 eV in **DH-IF-P17c**. BHJ solar cells based on **DH-IF-P17a** with a conventional device configuration of ITO/PEDOT:PSS/polymer:$PC_{71}BM$/Ca/Al exhibited the best performance with a PCE of 3.1%, J_{sc} of 7.4 mA cm^{-2} and V_{oc} of 0.93 V.

The dihydro[1,2-*b*]IF π-unit has played a critical role not only in the development of copolymers that function as donors in photovoltaic devices, but also in the investigation of their functionalized π-electron deficient derivatives as small molecular acceptors in fullerene-free BHJ-OPVs. The study done by Gao *et al.*[155] addressed the synthesis of a novel wide bandgap (1.82 eV based on absorption edge of films) electron-acceptor small molecule, **DH-IF-9** (Fig. 25), based on a tetraoctyl-substituted dihydro[1,2-*b*]IF π-core. In the design of this non-fullerene acceptor, the A–D–A π-architecture was constructed by attaching strong electron-acceptor groups (carbonyl/dicyanovinylene-functionalized indenes) at the 2,8-positions of the weak electron-donor dihydro[1,2-*b*]IF. A strong and broad optical absorption ranging from 470 nm to 690 nm, along with suitable HOMO/LUMO energy levels of −5.42/−3.85 eV, was achieved with **DH-IF-9** (Fig. 31). The frontier molecular orbital

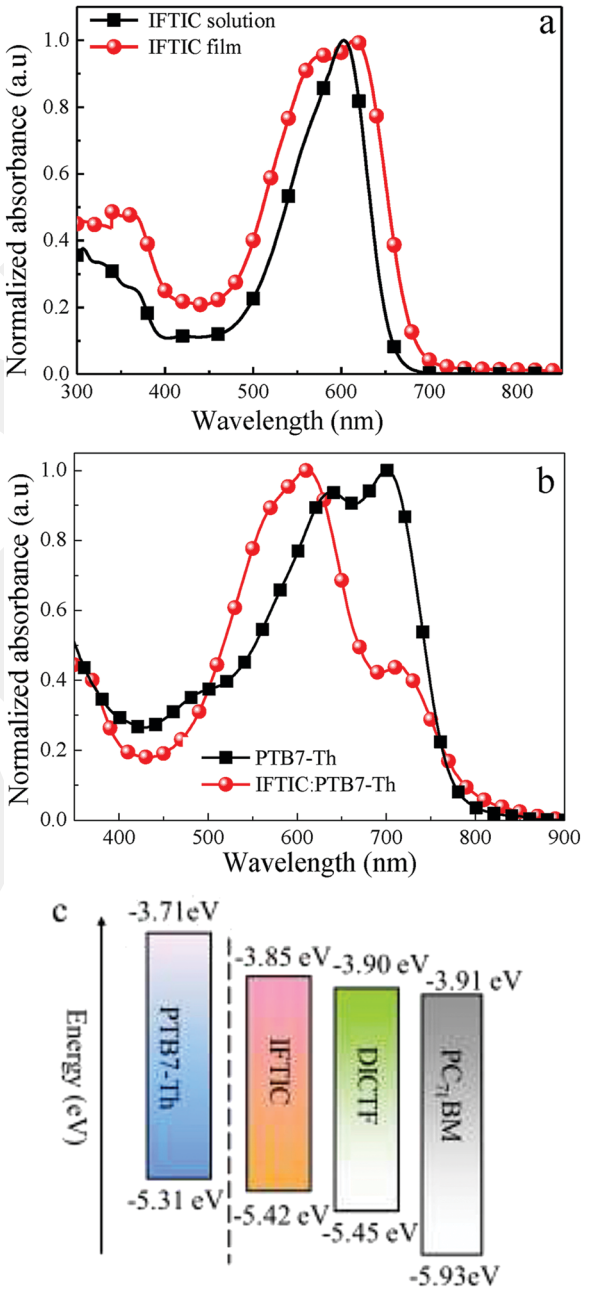

Fig. 31 (a) Normalized optical absorption spectra of the **DH-IF-9** acceptor molecule (shown as **IFTIC** in the figure) in chloroform solution and as thin-film. (b) Normalized optical absorption spectra of **PTB7-Th** donor polymer and **DH-IF-9**:**PTB7-Th** blend films. (c) Energy levels of **PTB7-Th**, **DH-IF-9**, **DICTF** (indenofluorene is replaced with fluorene in the polymer structure of **DH-IF-9**) and **$PC_{71}BM$**.[155] Reprinted with permission from ref. 155. Copyright 2017, Elsevier.

energies of this newly designed electron acceptor matched those of typical low bandgap polymer donor materials. BHJ-OPVs were fabricated using the low-bandgap donor polymer PTB7-Th in an inverted configuration (ITO/ZnO/PFN/PTB7-Th:**DH-IF-9**/MoO_3/Al). These devices exhibited a high PCE of 6.56% with a V_{oc} of 0.92 V and a J_{sc} of 12.71 mA cm^{-2}. This study clearly demonstrated the suitability of alkyl-substituted DH-IF π-structures in the design of novel fullerene-free electron acceptors for use in BHJ-OPV applications.

6. Summary and outlook

As clearly summarized in this review, with over 150 small molecules and polymers, indenofluorenes stand out as an important π-conjugated polycyclic compound enabling great structural and property diversity. The realization of several IF-based π-systems is the result of different 6-5-6-5-6 architectures resulting in five different regioisomers, carbonyl/dicyanovinylene/tetrathiafulvalene functionalizations, alkyl/aryl/halide/ethynyl substitutions, and sp^2 *vs.* sp^3 hybridization of bridge carbons giving different aromaticity/π-delocalization patterns. Although early synthetic accounts to these systems could be found in the late nineteenth century, considerable efforts were initiated at the beginning of the 2000s. Amazingly, advancements in the past two decades have proved that indenofluorene is a promising building block for semiconducting materials for transistor and solar cell applications. Starting from the early IF examples reported before the 2000s, this review has explored recent progress (2003–2021) as summarized in the reported chemical structures shown in Fig. 3, 10, 18, and 25 and optoelectronic properties in Tables 1–4.

As the first subclass, the carbonyl functionalization at the bridge carbons has yielded IF-diones with mid-way HOMO–LUMO energies for favorable electron and/or hole transport characteristics. IF-diones are very interesting among all IFs because all possible semiconductivities (*i.e.*, p-type, n-type, and ambipolar) have been detected. For n-type IF-diones, the lack of hole-transport was rationalized by either the absence of a favorable oxidation process or an extremely deep HOMO level (<-6 eV). However, for p-type IF-diones, the lack of electron-transport could not be directly correlated with the LUMO energy. In other words, a stabilized LUMO does not always guarantee an efficient electron transport in this subclass, thus intermolecular π-orbital overlaps may play a major role. The highest performing p-type ($\mu_h \sim 1.03$ cm^2 V^{-1} s^{-1}) and ambipolar ($\mu_e \sim 0.65$ cm^2 V^{-1} s^{-1} and $\mu_h \sim 0.71$ cm^2 V^{-1} s^{-1}) IF-based semiconductors were reported for IF-dione small molecules substituted along the long molecular axis with electron donating dialkylamino and alkylthio substituents, respectively. Therefore, employing other electron donating substituents such as alkoxy and diarylamino at the same positions should be explored in the future to realize novel IF-dione structures with larger ($\geq$0.5–1 cm^2 V^{-1} s^{-1}) charge carrier mobilities. Despite IF-diones achieved efficient electron transport ($\mu_e \sim$ 0.2–0.7 cm^2 V^{-1} s^{-1}), the limited electron-withdrawing strength of carbonyls could not lower the LUMO energy below 4 eV. Thus, this family did not show thermodynamically ambient-stable electron transport. To our knowledge, there have been no reports to date on photovoltaic devices based on IF-diones. Considering their intermediate π-electron deficiency, which is not as strong as IF-DCVs, IF-dione-based molecules could be interesting non-fullerene electron acceptors enabling high V_{oc} values in BHJ-OPVs. Furthermore, IF-diones with apprpriate molecular size and solubilizing groups might be incorporated as acceptors into donor–acceptor copolymer backbones for use as an electron donor semiconductor. Realizing low optical band gaps ($\sim$1.2–1.6 eV) while keeping a relatively stabilized HOMO (<-5.3 eV) should be achievable for IF-dione based D–A copolymers.

In the second subclass discussed here, IF-DCVs, the IF units become highly π-electron deficient *via* dicyanovinylene functionalization, leading to a family with one of the lowest LUMO energies (-4.3 eV) in the optoelectronics literature. Most of the semiconductors in IF-DCVs are n-type, and a few examples with reasonably high HOMOs (≥ -5.5 eV) and low band gaps ($\sim$1.3–1.5 eV) exhibited ambipolar behavior. Some of the IF-DCVs exhibited ambient-stable electron transport with good electron mobilities ($\mu_e \sim 0.2$ cm^2 V^{-1} s^{-1}) and excellent current modulation characteristics (I_{on}/I_{off} ratios of $\sim 10^8$ and $V_T \sim 0$ V) for OFETs with the semiconductor processed from solution. Interestingly, indenofluorenetetrathiafulvalene (IF-TTF) small molecules were used as π-sensitizers in DSSCs with PCEs of up to 7.1% and, in one report, as a p-type single crystal semiconductor in OFETs with μ_h values of up to 1.44 cm^2 V^{-1} s^{-1}. We note that the majority of the IF-dione, IF-DCV, and IF-TTF structures are based on the [1,2-*b*] regioisomeric form giving linear molecular geometries. Therefore, an interesting future research direction would be exploring other regioisomers. On the other hand, based on some attempts from our research group and the lack of any literature report, it is unlikely that [1,2-*b*]IF-DCVs will perform well as non-fullerene acceptors in BHJ-OPVs despite their substantial electron transport characteristics. This is likely the result of the excessively low LUMO energies (<-4.1 eV) and the tendency to form micron-size crystalline domains, significantly exceeding the exciton diffusion lengths. Thus, the most probable route to address the above issues and to realize high performance non-fullerene acceptors based on DCV-functionalized IFs will likely require the investigation of other regioisomeric forms.

As the third unique subclass, fully π-conjugated IFs exhibit one of the most interesting π-topologies among PCHs with a quinoidal bonding pattern in the central tricyclic indacene subunit. These molecules are antiaromatic (20 π-electrons) and exhibit good electron accepting characteristics. As a result of their small HOMO–LUMO energy separation, π-IFs are typically ambipolar semiconductors, yet with low charge carrier mobilities (μ_e, $\mu_h < 10^{-3}$ cm^2 V^{-1} s^{-1}). Only when the π-system was extended along the long molecular axis *via* thienyl fusion, high electron and hole mobilities (μ_e, $\mu_h \sim$ 0.3–0.6 cm^2 V^{-1} s^{-1}) were realized. Thus, π-IF subclass definitely offers great promise for future designs of ambipolar OFET semiconductors. On

the other hand, photovoltaic performance based on these systems has been disappointing with the best PCE of only 2.9%. Because of the very low optical gap and considering their low LUMOs, it will be difficult to address poor charge dissociation without altering the conjugation pattern that is difficult to foresee at this moment.

As the last but not least subclass, unsubstituted and substituted DH-IFs have found more applications in photovoltaics than other IF subclasses. This is mainly because of the presence of sp^3 hybridized bridge carbons employing alkyl substituents (four alkyl chains per IF unit) which allows for excellent solubility as well as their efficient π-donor ability when copolymerized. The majority of the (un)substituted DH-IFs have been employed in electron donor copolymers leading to low PCEs (up to 4.5%) for the current BHJ-OPV performance standards. However, in one example, a substituted DH-IF π-unit was used in a non-fullerene acceptor molecule, which showed PCEs of up to 6.6%. Also, DSSCs with PCE values of up to 4.04% were demonstrated with substituted DH-IF-based sensitizers. Since (un)substituted DH-IFs are π-electron rich with high LUMO energies, n-channel OFETs have never been reported with DH-IFs, and p-channel OFETs showed decent hole mobilities of up to 0.3 $cm^2 V^{-1} s^{-1}$. Again, almost all of the DH-IFs developed to date are based on the [1,2-*b*]IF π-scaffold; therefore, other regioisomers must be explored for advances in future research.

Despite the great efforts toward novel IFs, when compared with other fused semiconductor families such as linear acenes, thienoacenes, and rylenediimides, it is evident that the number of IFs with high charge carrier mobilities remains very limited. Also, the photovoltaic performances of IF-based materials lag far behind those of the state-of-the-art reports in the literature. For all IF subclasses, one possible future research direction could be ethynylation on the IF's central or peripheral π-rings, which, with the aid of computational modeling, could potentially lead to two dimensional packing motifs and further improve charge transport properties especially for solution-processed films. Also, IF-diones and (un)substituted DH-IFs could find use in organic light-emitting transistor applications based on their great fluorescence properties combined with good charge transport. In particular, it could be quite interesting to explored IF-diones in single- and tri-layer OLETs based on their ambipolar behavior. On the other hand, on the basis of their favorable electrochemical properties, functionalized IFs, especially with carbonyl and dicyanovinylene groups, could find use in n-type electrochemical transistors[23] for the development of a variety of applications ranging from biosensors to artificial synapses. As another unique application for IF-based semiconductors, their micro- and nano-structured films could be prepared *via* modified physical vapor deposition methods and function as surface-enhanced Raman spectroscopy (SERS)-active organic platforms.[156–158] In particular, IF derivatives without alkyl substituents, but fluorinated on the outer phenylene rings, could show ideal structural (large π-density) and electronic (low LUMOs of < -3.0 eV) properties for high Raman signal enhancement.

As thoroughly discussed in this review, IFs have embarked on an exciting journey in the field of organic (opto)electronics during the past two decades and future rational designs could be guided by the goal of realizing state-of-the-art performances for several (opto)electronic devices. While still requiring further improvements both in terms of device performance and a deeper understanding of structure–property relationships, on the basis of what is discussed in this review, the remaining challenges represent an exciting opportunity to develop novel IF-based semiconductors and optoelectronic devices in the next decade.

Conflicts of interest

The authors declare no competing financial interest.

Acknowledgements

H. U. acknowledges support from the Turkish Academy of Sciences and The Science Academy through the Young Scientist Award Programs (TUBA-GEBIP-2015 and BAGEP-2014), the AGU-BAP (Abdullah Gül University-Scientific Research Projects Funding Program) (FYL-2018-115 and FYL-2016-65), and The Scientific and Technological Research Council of Turkey (TUBITAK-113C021).

References

1 C. Wang, H. Dong, W. Hu, Y. Liu and D. Zhu, *Chem. Rev.*, 2012, **112**, 2208–2267.
2 S. E. Root, S. Savagatrup, A. D. Printz, D. Rodriquez and D. J. Lipomi, *Chem. Rev.*, 2017, **117**, 6467–6499.
3 H. Usta, A. Facchetti and T. J. Marks, *Acc. Chem. Res.*, 2011, **44**, 501–510.
4 A. Facchetti, *Chem. Mater.*, 2011, **23**, 733–758.
5 J. C. Yang, J. Mun, S. Y. Kwon, S. Park, Z. Bao and S. Park, *Adv. Mater.*, 2019, **31**, 1904765.
6 P. de Echegaray, M. J. Mancheño, I. Arrechea-Marcos, R. Juárez, G. López-Espejo, J. T. López Navarrete, M. M. Ramos, C. Seoane, R. P. Ortiz and J. L. Segura, *J. Org. Chem.*, 2016, **81**, 11256–11267.
7 Y. Wang, H. Guo, S. Ling, I. Arrechea-Marcos, Y. Wang, J. T. López Navarrete, R. P. Ortiz and X. Guo, *Angew. Chem., Int. Ed.*, 2017, **56**, 9924–9929.
8 K. Zhou, H. Dong, H. Zhang and W. Hu, *Phys. Chem. Chem. Phys.*, 2014, **16**, 22448–22457.
9 G.-S. Ryu, Z. Chen, H. Usta, Y.-Y. Noh and A. Facchetti, *MRS Commun.*, 2016, **6**, 47–60.
10 V. Figà, C. Chiappara, F. Ferrante, M. P. Casaletto, F. Principato, S. Cataldo, Z. Chen, H. Usta, A. Facchetti and B. Pignataro, *J. Mater. Chem. C*, 2015, **3**, 5985–5994.
11 H. Shirakawa, E. J. Louis, A. G. MacDiarmid, C. K. Chiang and A. J. Heeger, *J. Chem. Soc. Chem. Commun.*, 1977, 578.

12 H. Usta and A. Facchetti, *Large Area and Flexible Electronics*, Wiley-VCH Verlag GmbH & Co. KGaA, Weinheim, Germany, 2015, pp. 1–100.
13 G. Zhang, J. Zhao, P. C.-Y. Chow, K. Jiang, J. Zhang, Z. Zhu, J. Zhang, F. Huang and H. Yan, *Chem. Rev.*, 2018, **118**, 3447–3507.
14 G.-H. Lee, H. Moon, H. Kim, G. H. Lee, W. Kwon, S. Yoo, D. Myung, S. H. Yun, Z. Bao and S. K. Hahn, *Nat. Rev. Mater.*, 2020, **5**, 149–165.
15 A. Riaño, P. Mayorga Burrezo, M. J. Mancheño, A. Timalsina, J. Smith, A. Facchetti, T. J. Marks, J. T. López Navarrete, J. L. Segura, J. Casado and R. Ponce Ortiz, *J. Mater. Chem. C*, 2014, **2**, 6376.
16 R. Li, W. Hu, Y. Liu and D. Zhu, *Acc. Chem. Res.*, 2010, **43**, 529–540.
17 O. Ostroverkhova, *Chem. Rev.*, 2016, **116**, 13279–13412.
18 D. Fazzi, S. Fabiano, T.-P. Ruoko, K. Meerholz and F. Negri, *J. Mater. Chem. C*, 2019, **7**, 12876–12885.
19 J. L. Bredas, J. P. Calbert, D. A. da Silva Filho and J. Cornil, *Proc. Natl. Acad. Sci. U. S. A.*, 2002, **99**, 5804–5809.
20 V. Coropceanu, J. Cornil, D. A. da Silva Filho, Y. Olivier, R. Silbey and J.-L. Brédas, *Chem. Rev.*, 2007, **107**, 926–952.
21 A. A. Virkar, S. Mannsfeld, Z. Bao and N. Stingelin, *Adv. Mater.*, 2010, **22**, 3857–3875.
22 K. Takimiya, S. Shinamura, I. Osaka and E. Miyazaki, *Adv. Mater.*, 2011, **23**, 4347–4370.
23 H. Sun, J. Gerasimov, M. Berggren and S. Fabiano, *J. Mater. Chem. C*, 2018, **6**, 11778–11784.
24 M. Massetti, F. Jiao, A. J. Ferguson, D. Zhao, K. Wijeratne, A. Würger, J. L. Blackburn, X. Crispin and S. Fabiano, *Chem. Rev.*, 2021, **121**, 12465–12547.
25 Y. Cui, H. Yao, J. Zhang, T. Zhang, Y. Wang, L. Hong, K. Xian, B. Xu, S. Zhang, J. Peng, Z. Wei, F. Gao and J. Hou, *Nat. Commun.*, 2019, **10**, 2515.
26 Y. Cui, H. Yao, L. Hong, T. Zhang, Y. Xu, K. Xian, B. Gao, J. Qin, J. Zhang, Z. Wei and J. Hou, *Adv. Mater.*, 2019, **31**, 1808356.
27 G. Zhang, J. Zhao, P. C.-Y. Chow, K. Jiang, J. Zhang, Z. Zhu, J. Zhang, F. Huang and H. Yan, *Chem. Rev.*, 2018, **118**, 3447–3507.
28 A. Listorti, B. O'Regan and J. R. Durrant, *Chem. Mater.*, 2011, **23**, 3381–3399.
29 A. Facchetti, *Mater. Today*, 2013, **16**, 123–132.
30 K. Takimiya, I. Osaka, T. Mori and M. Nakano, *Acc. Chem. Res.*, 2014, **47**, 1493–1502.
31 B. A. Jones, A. Facchetti, T. J. Marks and M. R. Wasielewski, *Chem. Mater.*, 2007, **19**, 2703–2705.
32 H. Hopf, *Classics in Hydrocarbon Chemistry: Syntheses, Concepts, Perspectives*, Wiley-VCH, 2000.
33 J. E. Anthony, *Chem. Rev.*, 2006, **106**, 5028–5048.
34 M. Sawamoto, M. J. Kang, E. Miyazaki, H. Sugino, I. Osaka and K. Takimiya, *ACS Appl. Mater. Interfaces*, 2016, **8**, 3810–3824.
35 C. K. Frederickson, B. D. Rose and M. M. Haley, *Acc. Chem. Res.*, 2017, **50**, 977–987.
36 S. Gabriel, *Ber. Dtsch. Chem. Ges.*, 1884, **17**, 1389–1396.
37 W. Deuschel, *Helv. Chim. Acta*, 1951, **34**, 2403–2416.
38 L. Chardonnens, B. Laroche and W. Sieber, *Helv. Chim. Acta*, 1974, **57**, 585–599.
39 L. Chardonnens and R. Ritter, *Helv. Chim. Acta*, 1955, **38**, 393–396.
40 A. G. Fix, D. T. Chase and M. M. Haley, *Polyarenes I. Topics in Current Chemistry*, Springer, Berlin, Heidelberg, 2012, vol. 349, pp. 159–195.
41 W. Frank and R. Gompper, *Tetrahedron Lett.*, 1987, **28**, 3083–3086.
42 Q. Zhou, P. J. Carroll and T. M. Swager, *J. Org. Chem.*, 1994, **59**, 1294–1301.
43 H. Reisch, U. Wiesler, U. Scherf and N. Tuytuylkov, *Macromolecules*, 1996, **29**, 8204–8210.
44 J. Zaumseil and H. Sirringhaus, *Chem. Rev.*, 2007, **107**, 1296–1323.
45 A. Hagfeldt, G. Boschloo, L. Sun, L. Kloo and H. Pettersson, *Chem. Rev.*, 2010, **110**, 6595–6663.
46 J. M. Cole, G. Pepe, O. K. Al Bahri and C. B. Cooper, *Chem. Rev.*, 2019, **119**, 7279–7327.
47 B. J. Jung, N. J. Tremblay, M.-L. Yeh and H. E. Katz, *Chem. Mater.*, 2011, **23**, 568–582.
48 H. Usta, A. Facchetti and T. J. Marks, *Org. Lett.*, 2008, **10**, 1385–1388.
49 M. Romain, M. Chevrier, S. Bebiche, T. Mohammed-Brahim, J. Rault-Berthelot, E. Jacques and C. Poriel, *J. Mater. Chem. C*, 2015, **3**, 5742–5753.
50 C. Poriel, J.-J. Liang, J. Rault-Berthelot, F. Barrière, N. Cocherel, A. M.-Z. Slawin, D. Horhant, M. Virboul, G. Alcaraz, N. Audebrand, L. Vignau, N. Huby, G. Wantz and L. Hirsch, *Chem. – Eur. J.*, 2007, **13**, 10055–10069.
51 Y. Miyata, T. Minari, T. Nemoto, S. Isoda and K. Komatsu, *Org. Biomol. Chem.*, 2007, **5**, 2592–2598.
52 T. Nakagawa, D. Kumaki, J. Nishida, S. Tokito and Y. Yamashita, *Chem. Mater.*, 2008, **20**, 2615–2617.
53 H. Usta, A. Facchetti and T. J. Marks, *J. Am. Chem. Soc.*, 2008, **130**, 8580–8581.
54 S. Merlet, M. Birau and Z. Y. Wang, *Org. Lett.*, 2002, **4**, 2157–2159.
55 D. Vak, B. Lim, S. H. Lee and D. Y. Kim, *Org. Lett.*, 2005, **7**, 4229–4232.
56 J. Jacob, S. Sax, T. Piok, E. J.-W. List, A. C. Grimsdale and K. Müllen, *J. Am. Chem. Soc.*, 2004, **126**, 6987–6995.
57 J. Nishida, H. Deno, S. Ichimura, T. Nakagawa and Y. Yamashita, *J. Mater. Chem.*, 2012, **22**, 4483–4490.
58 Y.-I. Park, J. S. Lee, B. J. Kim, B. Kim, J. Lee, D. H. Kim, S. Oh, J. H. Cho and J. Park, *Chem. Mater.*, 2011, **23**, 4038–4044.
59 Y. Cho, H. R. Lee, A. Jeong, J. Lee, S. M. Lee, S. H. Joo, S. K. Kwak, J. H. Oh and C. Yang, *ACS Appl. Mater. Interfaces*, 2019, **11**, 40347–40357.
60 J. E. Anthony, J. S. Brooks, D. L. Eaton and S. R. Parkin, *J. Am. Chem. Soc.*, 2001, **123**, 9482–9483.
61 M. M. Payne, S. R. Parkin, J. E. Anthony, C.-C. Kuo and T. N. Jackson, *J. Am. Chem. Soc.*, 2005, **127**, 4986–4987.
62 B. D. Rose, D. T. Chase, C. D. Weber, L. N. Zakharov, M. C. Lonergan and M. M. Haley, *Org. Lett.*, 2011, **13**, 2106–2109.

63 J. E. Anthony, D. L. Eaton and S. R. Parkin, *Org. Lett.*, 2002, **4**, 15–18.
64 B. D. Rose, P. J. Santa Maria, A. G. Fix, C. L. Vonnegut, L. N. Zakharov, S. R. Parkin and M. M. Haley, *Beilstein J. Org. Chem.*, 2014, **10**, 2122–2130.
65 C. K. Frederickson and M. M. Haley, *J. Org. Chem.*, 2014, **79**, 11241–11245.
66 R. Ozdemir, S. Park, İ. Deneme, Y. Park, Y. Zorlu, H. A. Alidagi, K. Harmandar, C. Kim and H. Usta, *Org. Chem. Front.*, 2018, **5**, 2912–2924.
67 H. Usta, C. Risko, Z. Wang, H. Huang, M. K. Deliomeroglu, A. Zhukhovitskiy, A. Facchetti and T. J. Marks, *J. Am. Chem. Soc.*, 2009, **131**, 5586–5608.
68 M. Ozdemir, D. Choi, G. Kwon, Y. Zorlu, H. Kim, M.-G. Kim, S. Seo, U. Sen, M. Citir, C. Kim and H. Usta, *RSC Adv.*, 2016, **6**, 212–226.
69 R. Ozdemir, D. Choi, M. Ozdemir, G. Kwon, H. Kim, U. Sen, C. Kim and H. Usta, *J. Mater. Chem. C*, 2017, **5**, 2368–2379.
70 R. Ozdemir, D. Choi, M. Ozdemir, H. Kim, S. T. Kostakoğlu, M. Erkartal, H. Kim, C. Kim and H. Usta, *ChemPhysChem*, 2017, **18**, 850–861.
71 Z.-P. Fan, X.-Y. Li, X.-E. Luo, X. Fei, B. Sun, L.-C. Chen, Z.-F. Shi, C.-L. Sun, X. Shao and H.-L. Zhang, *Adv. Funct. Mater.*, 2017, **27**, 1702318.
72 J. Ferraris, D. O. Cowan, V. Walatka and J. H. Perlstein, *J. Am. Chem. Soc.*, 1973, **95**, 948–949.
73 H. Alves, A. S. Molinari, H. Xie and A. F. Morpurgo, *Nat. Mater.*, 2008, **7**, 574–580.
74 J. Mogensen, H. Michaels, R. Roy, L. Broløs, M. D. Kilde, M. Freitag and M. B. Nielsen, *Eur. J. Org. Chem.*, 2020, 6127–6134.
75 S. Handa, E. Miyazaki, K. Takimiya and Y. Kunugi, *J. Am. Chem. Soc.*, 2007, **129**, 11684–11685.
76 D. M. de Leeuw, M. M.-J. Simenon, A. R. Brown and R. E.-F. Einerhand, *Synth. Met.*, 1997, **87**, 53–59.
77 B. A. Jones, M. J. Ahrens, M.-H. Yoon, A. Facchetti, T. J. Marks and M. R. Wasielewski, *Angew. Chem.*, 2004, **116**, 6523–6526.
78 Y. Lin, J. Wang, Z.-G. Zhang, H. Bai, Y. Li, D. Zhu and X. Zhan, *Adv. Mater.*, 2015, **27**, 1170–1174.
79 Y. Lin, F. Zhao, Q. He, L. Huo, Y. Wu, T. C. Parker, W. Ma, Y. Sun, C. Wang, D. Zhu, A. J. Heeger, S. R. Marder and X. Zhan, *J. Am. Chem. Soc.*, 2016, **138**, 4955–4961.
80 W. Zhao, D. Qian, S. Zhang, S. Li, O. Inganäs, F. Gao and J. Hou, *Adv. Mater.*, 2016, **28**, 4734–4739.
81 S. Li, Z. Zhang, M. Shi, C.-Z. Li and H. Chen, *Phys. Chem. Chem. Phys.*, 2017, **19**, 3440–3458.
82 S. M. Menke and R. J. Holmes, *Energy Environ. Sci.*, 2014, **7**, 499–512.
83 O. V. Mikhnenko, P. W.-M. Blom and T.-Q. Nguyen, *Energy Environ. Sci.*, 2015, **8**, 1867–1888.
84 J. F. Petersen, C. K. Frederickson, J. L. Marshall, G. E. Rudebusch, L. N. Zakharov, O. Hammerich, M. M. Haley and M. B. Nielsen, *Chem. – Eur. J.*, 2017, **23**, 13120–13130.
85 O. Hammerich and M. B. Nielsen, *J. Mater. Chem. C*, 2019, **7**, 2809–2822.
86 M. A. Christensen, C. R. Parker, T. J. Sørensen, S. de Graaf, T. J. Morsing, T. Brock-Nannestad, J. Bendix, M. M. Haley, P. Rapta, A. Danilov, S. Kubatkin, O. Hammerich and M. B. Nielsen, *J. Mater. Chem. C*, 2014, **2**, 10428–10438.
87 S. Chaurasia, Y.-C. Chen, H.-H. Chou, Y.-S. Wen and J. T. Lin, *Tetrahedron*, 2012, **68**, 7755–7762.
88 L. Feng, H. Dong, Q. Li, W. Zhu, G. Qiu, S. Ding, Y. Li, M. A. Christensen, C. R. Parker, Z. Wei, M. B. Nielsen and W. Hu, *Sci. China Mater.*, 2017, **60**, 75–82.
89 M. A. Christensen, C. R. Parker, T. J. Sørensen, S. de Graaf, T. J. Morsing, T. Brock-Nannestad, J. Bendix, M. M. Haley, P. Rapta, A. Danilov, S. Kubatkin, O. Hammerich and M. B. Nielsen, *J. Mater. Chem. C*, 2014, **2**, 10428–10438.
90 K. Hafner, B. Stowasser, H.-P. Krimmer, S. Fischer, M. C. Böhm and H. J. Lindner, *Angew. Chem., Int. Ed. Engl.*, 1986, **25**, 630–632.
91 M. Di Giovannantonio, K. Eimre, A. V. Yakutovich, Q. Chen, S. Mishra, J. I. Urgel, C. A. Pignedoli, P. Ruffieux, K. Müllen, A. Narita and R. Fasel, *J. Am. Chem. Soc.*, 2019, **141**, 12346–12354.
92 M. Di Giovannantonio, J. I. Urgel, U. Beser, A. V. Yakutovich, J. Wilhelm, C. A. Pignedoli, P. Ruffieux, A. Narita, K. Müllen and R. Fasel, *J. Am. Chem. Soc.*, 2018, **140**, 3532–3536.
93 M. Di Giovannantonio and R. Fasel, *J. Polym. Sci.*, 2022, 1–13.
94 V. I. Minkin, M. N. Glukhovtsev and B. Y. Simkin, *Aromaticity and Antiaromaticity: Electronic and Structural Aspects*, John & Wiley Sons Inc., New York, USA, 1994.
95 B. D. Rose, N. J. Sumner, A. S. Filatov, S. J. Peters, L. N. Zakharov, M. A. Petrukhina and M. M. Haley, *J. Am. Chem. Soc.*, 2014, **136**, 9181–9189.
96 J. L. Marshall, K. Uchida, C. K. Frederickson, C. Schütt, A. M. Zeidell, K. P. Goetz, T. W. Finn, K. Jarolimek, L. N. Zakharov, C. Risko, R. Herges, O. D. Jurchescu and M. M. Haley, *Chem. Sci.*, 2016, **7**, 5547–5558.
97 X.-Y. Wang, M. Richter, Y. He, J. Björk, A. Riss, R. Rajesh, M. Garnica, F. Hennersdorf, J. J. Weigand, A. Narita, R. Berger, X. Feng, W. Auwärter, J. V. Barth, C.-A. Palma and K. Müllen, *Nat. Commun.*, 2017, **8**, 1948.
98 X.-Y. Wang, A. Narita, X. Feng and K. Müllen, *J. Am. Chem. Soc.*, 2015, **137**, 7668–7671.
99 J. Wilbuer, D. C. Grenz, G. Schnakenburg and B. Esser, *Org. Chem. Front.*, 2017, **4**, 658–663.
100 B. D. Rose, L. E. Shoer, M. R. Wasielewski and M. M. Haley, *Chem. Phys. Lett.*, 2014, **616–617**, 137–141.
101 M. J. Kendrick, A. Neunzert, M. M. Payne, B. Purushothaman, B. D. Rose, J. E. Anthony, M. M. Haley and O. Ostroverkhova, *J. Phys. Chem. C*, 2012, **116**, 18108–18116.
102 K. Paudel, B. Johnson, M. Thieme, M. M. Haley, M. M. Payne, J. E. Anthony and O. Ostroverkhova, *Appl. Phys. Lett.*, 2014, **105**, 043301.
103 Y. Sun, Y. Guo and Y. Liu, *Mater. Sci. Eng. R: Rep.*, 2019, **136**, 13–26.
104 L. Ren, C. Liu, Z. Wang and X. Zhu, *J. Mater. Chem. C*, 2016, **4**, 5202–5206.

105 A. Le Berre, *Ann. Chim.*, 1957, **13**, 371–379.
106 D. T. Chase, B. D. Rose, S. P. McClintock, L. N. Zakharov and M. M. Haley, *Angew. Chem., Int. Ed.*, 2011, **50**, 1127–1130.
107 D. T. Chase, A. G. Fix, B. D. Rose, C. D. Weber, S. Nobusue, C. E. Stockwell, L. N. Zakharov, M. C. Lonergan and M. M. Haley, *Angew. Chem., Int. Ed.*, 2011, **50**, 11103–11106.
108 I. Kaur, W. Jia, R. P. Kopreski, S. Selvarasah, M. R. Dokmeci, C. Pramanik, N. E. McGruer and G. P. Miller, *J. Am. Chem. Soc.*, 2008, **130**, 16274–16286.
109 J. A. Mikroyannidis, A. N. Kabanakis, S. S. Sharma and G. D. Sharma, *Adv. Funct. Mater.*, 2011, **21**, 746–755.
110 A. Shimizu and Y. Tobe, *Angew. Chem., Int. Ed.*, 2011, **50**, 6906–6910.
111 H. Miyoshi, S. Nobusue, A. Shimizu, I. Hisaki, M. Miyata and Y. Tobe, *Chem. Sci.*, 2014, **5**, 163–168.
112 A. Shimizu, R. Kishi, M. Nakano, D. Shiomi, K. Sato, T. Takui, I. Hisaki, M. Miyata and Y. Tobe, *Angew. Chem., Int. Ed.*, 2013, **52**, 6076–6079.
113 A. G. Fix, P. E. Deal, C. L. Vonnegut, B. D. Rose, L. N. Zakharov and M. M. Haley, *Org. Lett.*, 2013, **15**, 1362–1365.
114 T. Jousselin-Oba, P. E. Deal, A. G. Fix, C. K. Frederickson, C. L. Vonnegut, A. Yassar, L. N. Zakharov, M. Frigoli and M. M. Haley, *Chem. – Asian J.*, 2019, **14**, 1737–1744.
115 J. J. Dressler, Z. Zhou, J. L. Marshall, R. Kishi, S. Takamuku, Z. Wei, S. N. Spisak, M. Nakano, M. A. Petrukhina and M. M. Haley, *Angew. Chem., Int. Ed.*, 2017, **56**, 15363–15367.
116 D. T. Chase, A. G. Fix, S. J. Kang, B. D. Rose, C. D. Weber, Y. Zhong, L. N. Zakharov, M. C. Lonergan, C. Nuckolls and M. M. Haley, *J. Am. Chem. Soc.*, 2012, **134**, 10349–10352.
117 R. W.-I. de Boer, A. F. Stassen, M. F. Craciun, C. L. Mulder, A. Molinari, S. Rogge and A. F. Morpurgo, *Appl. Phys. Lett.*, 2005, **86**, 262109.
118 T. Takahashi, T. Takenobu, J. Takeya and Y. Iwasa, *Appl. Phys. Lett.*, 2006, **88**, 033505.
119 J. Nishida, S. Tsukaguchi and Y. Yamashita, *Chem. – Eur. J.*, 2012, **18**, 8964–8970.
120 H. Sharma, P. K. Sharma and S. Das, *Chem. Commun.*, 2020, **56**, 11319–11322.
121 B. S. Young, D. T. Chase, J. L. Marshall, C. L. Vonnegut, L. N. Zakharov and M. M. Haley, *Chem. Sci.*, 2014, **5**, 1008–1014.
122 J. L. Marshall, G. E. Rudebusch, C. L. Vonnegut, L. N. Zakharov and M. M. Haley, *Tetrahedron Lett.*, 2015, **56**, 3235–3239.
123 Y.-C. Lo, H.-C. Ting, Y.-Z. Li, Y.-H. Li, S.-W. Liu, K.-W. Huang and K.-T. Wong, *Org. Chem. Front.*, 2017, **4**, 675–681.
124 D. Marsitzky, J. C. Scott, J.-P. Chen, V. Y. Lee, R. D. Miller, S. Setayesh and K. Müllen, *Adv. Mater.*, 2001, **13**, 1096–1099.
125 A. C. Grimsdale, P. Leclère, R. Lazzaroni, J. D. MacKenzie, C. Murphy, S. Setayesh, C. Silva, R. H. Friend and K. Müllen, *Adv. Funct. Mater.*, 2002, **12**, 729–733.
126 J. Jacob, J. Zhang, A. C. Grimsdale, K. Müllen, M. Gaal and E. J.-W. List, *Macromolecules*, 2003, **36**, 8240–8245.
127 P. E. Keivanidis, J. Jacob, L. Oldridge, P. Sonar, B. Carbonnier, S. Baluschev, A. C. Grimsdale, K. Müllen and G. Wegner, *ChemPhysChem*, 2005, **6**, 1650–1660.
128 J. P. Amara and T. M. Swager, *Macromolecules*, 2006, **39**, 5753–5759.
129 Y. Ie, M. Nitani and Y. Aso, *Chem. Lett.*, 2007, **36**, 1326–1327.
130 Y. Ie, Y. Umemoto, M. Nitani and Y. Aso, *Pure Appl. Chem.*, 2008, **80**, 589–597.
131 O. M. Behr, G. Eglinton, A. R. Galbraith and R. A. Raphael, *J. Chem. Soc.*, 1960, 3614–3625.
132 S. Setayesh, D. Marsitzky and K. Müllen, *Macromolecules*, 2000, **33**, 2016–2020.
133 R. Kroon, M. Lenes, J. C. Hummelen, P. W.-M. Blom and B. de Boer, *Polym. Rev.*, 2008, **48**, 531–582.
134 T. Xu and L. Yu, *Mater. Today*, 2014, **17**, 11–15.
135 S. Rasmussen, in *Encyclopedia of Polymeric Nanomaterials*, ed. S. Kobayashi and K. Müllen, Springer Berlin Heidelberg, Berlin, Heidelberg, 2021, pp. 1–13.
136 E. Preis and U. Scherf, *Macromol. Rapid Commun.*, 2006, **27**, 1105–1109.
137 E. J. Meijer, D. M. de Leeuw, S. Setayesh, E. van Veenendaal, B. H. Huisman, P. W.-M. Blom, J. C. Hummelen, U. Scherf and T. M. Klapwijk, *Nat. Mater.*, 2003, **2**, 678–682.
138 M. Kreyenschmidt, G. Klaerner, T. Fuhrer, J. Ashenhurst, S. Karg, W. D. Chen, V. Y. Lee, J. C. Scott and R. D. Miller, *Macromolecules*, 1998, **31**, 1099–1103.
139 U. Scherf and K. Muellen, *Macromolecules*, 1992, **25**, 3546–3548.
140 T. Hadizad, J. Zhang, Z. Y. Wang, T. C. Gorjanc and C. Py, *Org. Lett.*, 2005, **7**, 795–797.
141 C. Py, T. C. Gorjanc, T. Hadizad, J. Zhang and Z. Y. Wang, *J. Vac. Sci. Technol., A*, 2006, **24**, 654–656.
142 J. P.-M. Serbena, I. A. Hümmelgen, T. Hadizad and Z. Y. Wang, *Small*, 2006, **2**, 372–374.
143 C. Poriel and J. Rault-Berthelot, *Acc. Chem. Res.*, 2018, **51**, 1818–1830.
144 W. Zhang, J. Smith, R. Hamilton, M. Heeney, J. Kirkpatrick, K. Song, S. E. Watkins, T. Anthopoulos and I. McCulloch, *J. Am. Chem. Soc.*, 2009, **131**, 10814–10815.
145 H. Sirringhaus, *Adv. Mater.*, 2009, **21**, 3859–3873.
146 S. Georgakopoulos, Y. Gu, M. M. Nielsen and M. Shkunov, *Appl. Phys. Lett.*, 2012, **101**, 213305.
147 R. S. Sprick, M. Hoyos, M. S. Wrackmeyer, A. V. Sheridan Parry, I. M. Grace, C. Lambert, O. Navarro and M. L. Turner, *J. Mater. Chem. C*, 2014, **2**, 6520–6528.
148 P. Sonar, L. Oldridge, A. C. Grimsdale, K. Müllen, M. Surin, R. Lazzaroni, P. Leclère, J. Pinto, L.-L. Chua, H. Sirringhaus and R. H. Friend, *Synth. Met.*, 2010, **160**, 468–474.
149 Q. Zheng, B. J. Jung, J. Sun and H. E. Katz, *J. Am. Chem. Soc.*, 2010, **132**, 5394–5404.
150 J. Kim, S. H. Kim, I. H. Jung, E. Jeong, Y. Xia, S. Cho, I.-W. Hwang, K. Lee, H. Suh, H.-K. Shim and H. Y. Woo, *J. Mater. Chem.*, 2010, **20**, 1577–1586.

151 V. Tamilavan, P. Sakthivel, Y. Li, M. Song, C.-H. Kim, S.-H. Jin and M. H. Hyun, *J. Polym. Sci. Part A: Polym. Chem.*, 2010, **48**, 3169–3177.
152 Y. W. Soon, T. M. Clarke, W. Zhang, T. Agostinelli, J. Kirkpatrick, C. Dyer-Smith, I. McCulloch, J. Nelson and J. R. Durrant, *Chem. Sci.*, 2011, **2**, 1111–1120.
153 Y. Xia, Z. He, J. Tong, B. Li, C. Wang, Y. Cao, H. Wu, H. Y. Woo and D. Fan, *Macromol. Chem. Phys.*, 2011, **212**, 1193–1201.
154 C. Duan, W. Cai, C. Zhong, Y. Li, X. Wang, F. Huang and Y. Cao, *J. Polym. Sci. Part A: Polym. Chem.*, 2011, **49**, 4406–4415.
155 J. Zhang, B. Zhao, Y. Mi, H. Liu, Z. Guo, G. Bie, W. Wei, C. Gao and Z. An, *Dyes Pigm.*, 2017, **140**, 261–268.
156 M. Yilmaz, E. Babur, M. Ozdemir, R. L. Gieseking, Y. Dede, U. Tamer, G. C. Schatz, A. Facchetti, H. Usta and G. Demirel, *Nat. Mater.*, 2017, **16**, 918–924.
157 G. Demirel, R. L.-M. Gieseking, R. Ozdemir, S. Kahmann, M. A. Loi, G. C. Schatz, A. Facchetti and H. Usta, *Nat. Commun.*, 2019, **10**, 5502.
158 I. Deneme, G. Liman, A. Can, G. Demirel and H. Usta, *Nat. Commun.*, 2021, **12**, 6119.